1973

Scour hole profiles in granular material below deflector buckets.

Teliang. Kung
University of Windsor

SCOUR HOLE PROFILES IN GRANULAR MATERIAL BELOW DEFLECTOR BUCKETS

A Thesis

Submitted to the Faculty of Graduate Studies through the Department of Civil Engineering in Partial Fulfillment of the Requirements for the Degree of Doctor of Philosophy at the University of Windsor

by

Teliang Kung

Windsor, Ontario

1973

ABSTRACT

The characteristics and problems of scour holes formed by jets from deflector buckets were studied.

The equations for predicting the profiles of scour holes were derived using the theories of wall jet and submerged diffusion jet with the aid of experimental observations.

In addition to the formula derived for profiles of scour holes, a set of dimensionless equations were developed to describe the three-dimensional configuration of scour holes.

The dimensions of stable and economical plunge basins below flip buckets were also obtained and found to conform well with field information.

ACKNOWLEDGEMENTS

The author wishes to express his profound gratitude to his supervisor, Dr. S.P. Chee, for his valuable suggestions and advice offered during the course of this research. The comments of the members of this thesis committee at the time of the comprehensive examination were also appreciated.

Acknowledgement is extended to the Department of Civil Engineering in the University of Windsor for the opportunity of carrying out this research.

Finally, the author would like to thank his wife and family for their moral support during this project.

TABLE OF CONTENTS

LIST OF FIGURES

LIST OF TABLES

CHAPTER I

INTRODUCTION

The flip bucket device is used as an energy dissipator when tailwater depth in the stilling basin is not enough to form a hydraulic jump or the tailwater depth cannot be predicted accurately. The bucket deflects the high velocity flow as a free jet which dissipates energy partly in the air and lands at a distance downstream where riverbed scour will not endanger the spillway structure. This method of dissipating energy is more economical than the deep and expensive hydraulic jump stilling basin and especially suitable if the downstream riverbed is not easily erodible. This type of energy dissipator is often operated under high head.

At the point of impact with the bed material, the plunging jet is deflected horizontally downstream creating drag forces on the riverbed. If there is no artificial protective surface on the downstream erodible riverbed, the bed material will be transported downstream and a dish shaped scour hole will gradually be formed. The scour hole deepens until equilibrium is reached between the lift and drag forces of the material. The volume and depth of scour hole depend on the jet velocity, tailwater depth and the characteristics of the bed material.

There has not been much theoretical work done on local scour below flip buckets. Some experimental formulae were derived by Rurkov (10), Chee et al. (13,14,15), Schoklitsch (54), and U.S.B.R. (68).

In the present studies, the longitudinal profiles of scour holes are derived applying the theories of the wall jet and the submerged diffusion jet.

The cross-sectional profiles are derived mathematically using the tractive force method.

The maximum and intermediate depths of scour and radius vector length of scour hole have also been found empirically using dimensional analysis.

The location of the deepest point of the scour hole is predicted by the principles of a freely falling jet.

Objective

This thesis deals with the investigation of local scour on downstream riverbed composed of granular materials below flip buckets. The purposes of this investigation are:

a) To establish formulae for predicting the contour pattern of the scour hole, the depth, and the location of maximum scour for varying hydraulic conditions, such as, discharge, head, tailwater depth, flip bucket angle, and the characteristics of downstream riverbeds;

b) To extend the theories developed in the case of scour below flip bucket to the case of scour below weirs;

c) To recommend the most economical shape of plunge basin.

CHAPTER II

REVIEW OF LITERATURE

The deflector-bucket type of energy dissipator was first designed by Andre Coyne(20) and constructed at the 330 feet high Mereges Dam in France. Since then similar types of engergy dissipators have been used in a number of dams, such as, Glen Canyon Dam in Arizona, Grand Coulee Dam in Washington, Yellowtail Dam in Montana, Yanhee Dam in Thailand , Wu-Sheh Dam in Taiwan (50), and Grand Rapid Dam and Cattle Rapid Dam in Manitoba.

2.1 Maximum Depth of Scour

In the past, various empirical equations for maximum depth of scour have been derived from model tests.

Veronese (68) has developed an equation for limiting scour depth when a freely falling overflow nappe drops vertically into a pool in a river bed as follows:

$$D_m = 1.32\, q^{0.54}\, H^{0.225} \qquad (2.1)$$

where D_m = the maximum depth of scour below tailwater in feet,

H = the head from the reservoir to tailwater level in feet, and

q = the discharge in second-feet per foot of width.

But, the size of bed material is not used as a variable in Eq.(2.1).

Schoklitsch (54) has suggested the following equation based on his experimental data to estimate the maximum depth of scour:

$$D_m = \frac{3.15\, q^{0.57}\, H^{0.2}}{d_{m.m.}^{0.32}} \qquad (2.2)$$

where $d_{m.m.}$ = mean bed material size in m.m.

The results of Schoklitsch indicated that a doubling of unit discharge increases the maximum depth of scour by approximately fifty percent and that an increase in head H of about six times would have to be affected to create the same increase in the depth of scour. Doddiah, Albertson, and Thomas (19) showed that scour depths calculated from Eq.(2.2) by Schoklitsch were generally low; a possible explanation suggested was that equilibrium conditions were not reached.

Gunko et al.(10) conducted experiments related to the hydraulic regime and local scour of rock bed below spillways of high head dams with a flip bucket at the toe and have derived equations for maximum depth of scour and length of scour pit. The equation for determining the length of scour pit

will be described in next section. The equation for maximum depth of scour was derived as:

$$\frac{D_m - h}{h} = \frac{3.7\,K_1}{F_1}\left(C_v \frac{H_o}{d}\right)^{0.75}\left(C_v^2 \frac{D_T}{h} - (1 - C_v^2)\right)^{1.33} \qquad (2.3)$$

where h = tailwater depth,

D_T = vertical distance between maximum pool elevation and the bucket lip,

$F_1 = V_1^2 / (g\,h)$, (2.4)

g = gravity acceleration,

V_1 = velocity of jet at the bucket lip,

H_o = total head - velocity head ,

C_v = velocity coefficient, and

K_1 = empirical coefficient.

The velocity coefficient C_v is ranged from 0.60 to 0.94 which can be determined by graphs prepared by Gunko et al. for given values of unit discharge and spillway length. The coefficient K_1 is related to the entrance angle of jet, the disruption and aeration of jet, the shape of bed material and the dip and extention of bed. The value of K_1 is ranged from 0.4 to 0.8 from the experiments.

Khosla (34) developed an equation for depth of scour below river barrages and around bridge piers with sandy bed

for which the mean bed material size is 0.4 m.m. Khosla suggested

$$D_m = K_2 \frac{0.9\, q^{0.67}}{f^{0.33}} \qquad (2.5)$$

where f = silt factor $= 8\, d^{0.5}$,

d = mean diameter of bed material expressed in inches, and

K_2 = empirical coefficient ranged from 1.5 to 2.1. A mean value of 1.8 for K_2 is often used.

Essentially Eq(2.5) is a contraction equation derived from the following two Lacey (35) regime equations,

$$B_s = P = 2.67\, Q^{0.5} \qquad (2.7)$$

$$R_h = 0.473\, Q^{0.33} / f^{0.33} \qquad (2.8)$$

where P = wetted perimeter(ft),

B_s = surface water width (ft),

Q = discharge (cfs), and

R_h = hydraulic radius (ft).

Eq.(2.5) has been extended to erosion below stilling basin with a proper choice of the coefficient K_2.

Yuditsky (10), by the help of laboratory investigation, studied the effect of a water jet issuing from a flip bucket

on the joint blocks located where the jet struck the riverbed. The studies also made it possible to compute the maximum depth of erosion.

If the maximum actual tearing load exceeds the submerged weight of joint block, the block will be taken out of a state of rest and under the action of the first high pulsation impulse, the joint block will be lifted off.

The least ultimate values of tearing load T^* and increased averaged load P^* may be determined by the following equation derived by Yudisky :

$$P^*_{ult} = T^*_{ult} = 1.1\, d\, \frac{\gamma_s - 1}{\gamma} \cos\phi \qquad (2.9)$$

where d = size of block,

γ_s = specific weight of bed material,

γ = specific weight of water, and

ϕ = angle between horizontal and possible direction of expelling of the joint block.

The tearing loads gradually decrease as the scour pit depth increases. Graphs characterizing the decreasing values of T^* and P^* with an increase in the depth of scour were drawn. The ultimate values of P^*_{ult} and T^*_{ult} are computed using equation (2.9). Using the graphs, the scour pit depth can be determined corresponding to the ultimate values of the tearing load and the averaged increased load.

Chee and Padiyar (14) had obtained the following equation to determine the maximum depth of scour under the effect of a jet issuing from the circular shaped flip bucket with exit angle 30 degrees.

$$D_m = \frac{1.235\ q^{0.67}\ H^{0.18}}{d^{0.063}} \qquad (2.10)$$

A singular similarity between equations (2.5) and (2.10) is the values of the exponents of q which are identical.

Strelchuk (61) conducted the experiments for investigation of local scour at the base of flip bucket with the exit angle of 45 degrees. He found the depth of scour calculated by all equations (2.1), (2.2), and (2.5) were lower than the observed values from his experiments. A possible explanation suggested is the omission of the flip-bucket angle as a variable in all three equations (2.1), (2.2), and (2.5).

2.2 Jet Trajectory Length

The length of the jet trajectory determines the location of the scour pit. This length depends on the energy of the flow available at the bucket lip, the exit angle of the bucket, the height of the bucket lip with respect to the bucket invert, and the height of bucket from the riverbed. As the water jet falls freely through the air, there will be losses in energy due to areation and jet will not carry as far as an unareated jet. The Principal fac-

tors which determine the jet trajectory length are exit angle and head. The lip height should be set sufficiently high so that the jet will be projected well beyond the structure without interference from the tailwater.

If V_o is the velocity of the jet as it leaves the bucket and α is the angle of the bucket to the horizontal, then the length of the jet measured horizontally assuming that the buchet is set at or near river bed is (41)

$$L = V_o^2 \operatorname{Sin} 2\alpha / g \qquad (2.11)$$

Gunko (10) et al studied the distance of jet deflection related to the scour bed below flip-bucket spillways.

If the bucket is set at any other elevation relative to the river bed, then the length L is calculated by the relationship for a freely flying body as

$$L = 2 C_v^2 (H - B_o - \Delta h) \operatorname{Cos}\alpha \left(\operatorname{Sin}\alpha + \sqrt{\operatorname{Sin}^2\alpha + \frac{(D_T+h)+B_o/2\operatorname{Cos}\alpha}{C_v^2(H-B_o-\Delta h)}} \right) \qquad (2.12)$$

where Δh = difference between lip elevation and bucket invert elevation

$$= R_b (1 - \operatorname{Cos}\alpha) \qquad (2.13)$$

R_b = radius of bucket, and

B_o = jet thickness at bucket lip.

The symbols C_v, H, D_T, h, and α are the same as previously defined.

2.3 Area of Influence of Bed Material

White (71) has attempted to analyze the threshold condition by considering the equilibrium of a single typical grain. It is assumed that the bed shear is an average compound from the drag forces on a number of grains which are more exposed or prominent than others in the bed. The number of these exposed grains per unit area of the bed will clearly vary as $1 / d^2$, and is assumed equal to r_p / d^2, where r_p is a packing factor which will be less than unity. This is another way of saying that there is, corresponding to each prominent grain, an area of influence, a, equal to d^2 / r_p, as in Fig. 2.1.

If F_d is the drag force on each prominent grain, the average shear stress is equal to

$$\tau = \frac{F_d}{\text{area of influence}} = \frac{F_d \; r_p}{d^2} \qquad (2.14)$$

where $$F_d = \tau \, d^2 / r_p \qquad (2.15)$$

and the threshold condition is described by equating this force to the resistence force, equal to the effective weight of the grain times the effective coefficient of friction, the tangent of the angle of repose of the grain.

It follows from Eq(2.15) that

$$\tau\, d^2 / r_p = \frac{\pi d^3}{6} \gamma (S_s - 1) \operatorname{Tan} \theta \qquad (2.16)$$

i.e. $$\tau = \frac{\pi}{6} r_p \gamma d (S_s - 1) \operatorname{Tan} \theta \qquad (2.17)$$

where θ is the angle of repose of the bed material, and S_s is the specific gravity of the bed material.

Shield (56) expressed the threshold of movement of bed material in terms of bed shear stress arranged in a dimensionless combination. This approach may be explained by his plot of entrainment function F_s against particle Reynolds number R_e^* as shown in Fig. 2.2. The entrainment function and particla Reynolds number are given by

$$F_s = \frac{\tau}{\gamma (S_s - 1) d} \qquad (2.18)$$

and $$R_e^* = \frac{V^* d}{\nu} \qquad (2.19)$$

respectively, where ν = kinematic viscosity,

V^* = shear velocity = $\sqrt{\tau/\rho}$ (2.20)

and ρ = density of the fluid.

It is interesting to note that Eq(2.16) contains Shields' entrainment function, for it can be rewritten

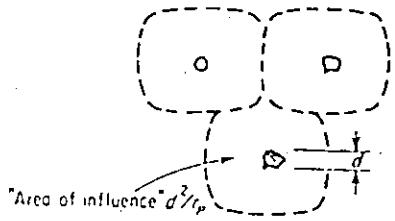

FIG. 2.1 DISTRIBUTION OF PROMINENT GRAINS, AFTER WHITE(71).

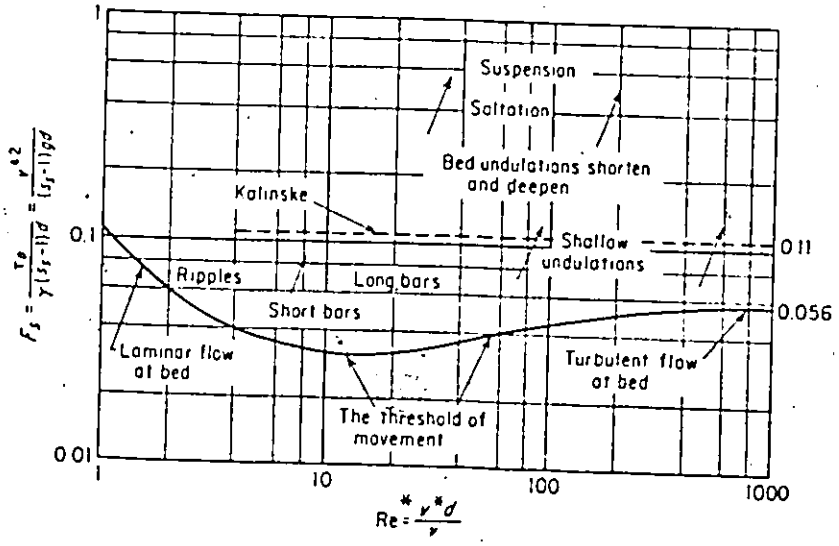

FIG.2.2 THE ENTRAINMENT FUNCTION, AFTER SHIELD (56)

$$F_s = \frac{\tau}{\gamma d (S_s - 1)} = \frac{r_p \pi \tan\theta}{6} \qquad (2.21)$$

It is noted from Fig. 2.2 that the coefficient F_s is substantially constant when the flow is under the condition of fully developed turbulence. Taking this constant as 0.056, it follows from Eq.(2.21) for sand and gravel

$$r_p = 0.107 / \tan\theta \qquad (2.22)$$

2.4. Wall Jet

The wall jet is described as a jet of fluid which impinges onto a wall at an angle from 0 to 90 degrees. The name wall-jet seems to have been ascribed by Glauert (23) , although the terms partially open jet, surface jet, and submerged jet have been used by Forthmann (22), Zerbe and Selna (72), and Poreh and Cermak (44). This flow is of the self-preserving class of shear flows such as jets, wakes, and free-mixing layers.

There are many applications of wall jet flows, such as : study of the ground effect of vertical-take-off and landing aircrafts, design of steel making furnaces, window de-icers, welding torches, paper drying, and design of various spraying devices. The water jet issuing from the hydraulic outlet works and from bucket type spillway impinges the downstream riverbed may also be analysed as a

wall jet. Even though there are many situations in hydraulic engineering which are basically wall-jets, but of special nature due to the boundary conditions, there have been few application of wall-jet principles towards their understanding. In the present studies, the wall jet theory [redacted] applied to determine the shear stress along the scour hole for deriving the longitudinal profiles of scour holes below flip buckets.

A sketch of wall jet is shown in Fig. 2.3 , which indicates a fully developed profile .

Forthmann (22) was the first person to undertake an experimental study of the plane, two dimensional wall jet. In his study, the transverse velocity distribution in the region of developed flow was worked out.

According to Forthmann, beyond twenty-slot widths downstream of the jet slot the flow reached a fully developed or self-preserving state as in the case of free jets and wakes. This was moderately short distance downstream (between 20 to 33 slot widths) and for a range of Reynolds number of from 91,000 to 113,000. He defined the Reynolds number on the basis of the maximum velocity as well as the width from the wall to the half maximum velocity point. On the basis of his experimental data, he defined the similarity velocity profiles as

$$u = x^b (y / x^c) \qquad (2.23)$$

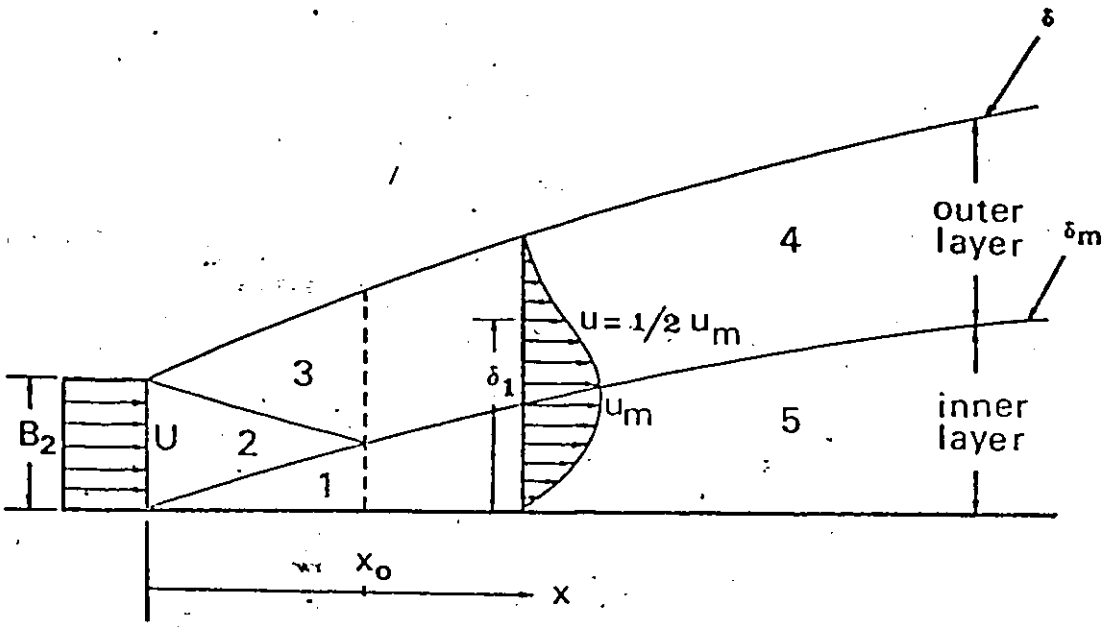

1,5: Inner or wall layer-- assumed to behave like a plate boundary layer

2: Uniform core -- region where $u = U$

3,4: Free jet region or outer layer -- assumed to behave like free jet mixing

FIG.2.3. DEFINITION SKETCH FOR WALL JET

in which u = velocity,

x = longitudinal distance,

and y = transverse distance.

The constants b and c are adjustable according to the type of flow considered. Because the maximum velocity, u_m, was found to vary as x^b and a characteristic lateral dimension δ_1 was found to vary as x^c, the velocity profile took the similarity form of

$$\frac{u}{u_m} = f\left(\frac{y}{\delta_1}\right) \qquad (2.24)$$

where δ_1 represents the distance from the wall to the location which the velocity of the jet relative to the free stream is one-half of the maximum velocity difference in the flow. His conclusion was that for the range investigated $b = -0.5$ and c was near unity. Further, he determined from his experimental data that the velocity in the inner layer varied as the one-seventh power of the distance from the wall.

Zerbe and Selna (72) invetigated experimentally the problem of heat transfer in a wall jet in a still medium and verified the assumption that $b = -0.5$.

Forthmann also used the momentum-integral method to

obtain the shear distribution normal to the flat surface but did not show the variation along the longitudinal distance.

Glauert's (23) work with the laminar and turbulent wall jet, is the primary work on the wall jet. He predicted that the inner part and the outer part of the flow could not possibly have the same similarity form. Therefore, he divided the flow into two regions: an outer region which is characterized by the features of free turbulent flows, and an inner region where the effect of the wall is apparent. Glauert obtained solutions for both regions under the assumptions that the variation of the mean shear stress in the inner layer is the same as in turbulent pipe flow described by Blasius (53) and the eddy viscosity is proportional to $R_e^{3/4}$, and the eddy viscosity in the outer region is a constant across the layer and varying with R_e, the Reynolds number, as described by Prandtl's hypothesis. The Blasius empirical equation of shear stress is

$$\tau / \rho = 0.0225\, u_m^2 \left(u_m \delta_m / \nu \right)^{-0.25} \qquad (2.25)$$

where δ_m is the thickness of boundary layer when $u = u_m$. Glauert's solutions for both inner and outer regions were matched at the point of maximum mean velocity, where the shear stress was assumed to be zero, giving a combined dimensionless velocity profile which depends on a single pa-

rameter P_s. The resultant velocity field is approximately similar, as P_s depends on the local Reynolds number and varies with the distance. The variation of P_s is very small, however. The deviation of Glauert's solution from similarity is exhibited by the different rate of change of length and velocity scales of the two regions. As the outer region is much larger, on the basis of Glauert's analysis, the thickness of the entire jet should grow proportionally to the distance. He postulated correctly that because the wall jet flow is comprised of a boundary layer and a free mixing flow, and both of these flows mix differently, there could not be a unique similarity equation for the entire flow. However, if the flow divided into inner and outer parts, and if each part was treated separately, then similarity conditions could be achieved. Each part was found to have separate values of b and c, the exponents in the growth process as shown in Eq.(2.23). It was found by Glauert that $b = -0.615$ and $c = 0.923$ for the inner profile, while $b = -0.667$ and $c = 1.0$ for the outer profile. An averaged estimate for the values of b and c for entire flow could be taken as $b = -0.641$ and $c = 0.963$.

The velocity distribution of the turbulent radial wall jet and the variation of velocity and length scales with downstream position was measured by Bakke (4). He found that the velocity scale, u_m, varied as a power of x with exponent -1.12 ± 0.03 and the length scale as 0.94

$\pm$ 0.02 . The velocity profiles showed a self-preserving character in both the inner and outer layers. His measurements indicate that the flow at different radial portions is similar, and that the dimensionless velocity profile is in good agreement with Glauert's (23) profiles. However , Bakke's experimental results indicate that the length scale of the wall jet δ_1 , does not follow Glauert's prediction. Glauert predicted the length scale varying as a power of x with exponent 1.02.

The measurements of shear stress in a wall jet was done by Sigalla (58) by using the method of Preston. His data was correlated in a manner analogous to that of a turbulent boundary layer on a plate. The measurement range was from 15 to 60 slot widths with a Reynolds number 60,000. He found experimentally that the boundary layer thickness varied linearly with the distance x. Further, he found that the velocity scale varied as a power of x with an exponent of minus one-half. The velocity was seen to remain constant for about ten nozzle widths from exit and then decayed somewhat in the same manner for a freely expanding plane jet. The formulae fitted to his data were given as:

$$\frac{u_m}{u} = 3.45 \left(\frac{x}{B_2} \right)^{-0.5} \qquad (2.26)$$

and $$\delta_1 / B_2 = 0.5 + 0.065\, x / B_2 \qquad (2.27)$$

Sigalla's experimental investigation of the distribution of skin friction along the wall shows that it is possible to describe the variation of skin friction coefficient by a formula similar to the Blasius formula, Eq.(2.25), which is based on experimental results of turbulent pipe flow. This is simply achieved by considering the inner layer of fluid between the wall and the position where the velocity is a maximum as a boundary layer with an outer uniform free stream and velocity equal to the local maximum velocity. Sigalla also found that $C_f (u_m \cdot \delta_m / \nu)^{1/4}$ was nearly constant, where C_f is the coefficient of friction, for x/ B_2 greater than about 20 and that this constant was approximately equal to 0.0555. For smaller values of x / B_2 the coefficient appeared to decrease to 0.045.

Bradshaw and Gee (9) obtained some experimental shear stress results for the wall jet with an external stream. They find friction factors that are about six percent higher than Sigalla's. Further, it is noted that the Reynolds shear stress is not zero at the plane of maximum velocity.

Schwarz and Cosart (62) measured the mean velocity with a hot-wire anemometer for distances between 25 slot widths to 70 slot widths. The Reynolds number based on the maximum velocity and the thickness of the boundary layer varied from 22,000

to 106,000. They obtained the wall shearing stress information by applying momentum integral techniques to their measured velocity profiles. It was shown theoretically that length scale δ_1 varied as x, the velocity scale u_m varied as x^b. The exponent b was empirically determined and, as an average, b = -0.555 within their experimental range. Using the similarity arguments and experimental data, they found that

$$u_m / U = 5.395 (x / B_2 + 11.2)^{-0.555} \qquad (2.28)$$

and

$$\delta_1 / B_2 = 0.0678 (x / B_2 + 11.2) \qquad (2.29)$$

Further, it was found that in a large portion of the wall layer, the velocity distribution followed the one fourteenth power law. Their data also showed no effect of Reynolds number upon the velocity decay.

It is noted that the results of Schwarz and Cosart (62) are in agreement with those of Bradshaw and Gee (9), and Forthmann (22) in concerning decay of the maximum velocity and growth of the jet. But the shear stress measurements of Schwarz and Cosart were about twice those found by Sigalla.

The turbulent diffusion of a two dimensional plane wall jet in a moving free-stream with a zero pressure gradient was invetigated by Eskinzi and Kruka (21). Four different flow

ratios of the jet velocity U to the free-stream velocity u_s of 2.06, 3.65, 10.0, and 18.4 were used in their experiments. It was found that the wall jet had to be divided into a boundary layer region and a free mixing region and the velocity distribution in each was similar. The length scale δ_1 grows linearly with the distance travelled by the jet relative to the free stream x_s .

$$\delta_1 = C_1 x_s^c \qquad (2.30)$$

The values of C_1 was found to equal to 0.0737 and c = 1. The value c = 1 which coincides with the value found by Schwarz and Cosart (62) and is close to the value determined by Forthmann, 0.997. The maximum velocity excess $\Delta u_m = u_m - u_s$ varied with x_s as Δu_m is proportional to x_s^b . It was determined experimentally for $U / u_s = 18.4$ that b = -0.496 for the inner profile and b = -0.536 for the outer profile, thus supporting Glauert's theoretical prediction. The latter value is close to the values determined by other investigators for the no-free-stream case. It was also found that the similarity conditions were applicable to all values of U / u_s . Further, Eskinzi and Kruka noted that the boundary shear stress followed the Blasius type of relation as shown in Eq.(2.25).

The mean velocity, turbulence intensities, and the wall friction in a radial wall jet formed by an impinging circular

jet on a smooth flat plate were measured by Poreh, Tsuei, and Cermark (45). Their data showed that the velocity field of the radial wall jet was approximately similar and only slightly dependent on the overall Reynolds number of the flow. The measured non-dimensional velocity profile was quite close to the curve predicted by Glauert (23) with the single parameter $P_s = 1.3$ and to that obtained experimentally by Bakke (4). The flow was found to depend on the distance between the origin of the impinging jet and the wall, even at large radial distance from the stagnation point. The rate of decay of radial velocities was discovered to be larger than those in a free-radial jet. Their measurements of turbulent intensities indicated that the turbulence level in the wall jet was higher than in boundary layers and pipe flow. It may be suggested that eddies from the outer part of the jet penetrate deep into the inner boundary layer increasing in the manner the skin friction acting on the wall.

A thorough study of the development, the velocity profiles, and the wall shearing stress in a two-dimensional, incompressible, turbulent wall jet was undertaken by Myers, Schauer and Eustis (39). They predicted the maximum velocity decay, jet thickness, and the shearing stress analytically by momentum- integral methods. Their wall shear results were obtained by a hot-film technique and covered a more extensive range of variables. Experimental data were

extended to 180 slot widths and the slot Reynolds number range was from 7,100 to 56,500. The shear variation along the wall surface was also obtained. The complete similarity between the inner and outer layers of the wall jet was not assumed in their analysis.

It is noted that the variation of u_m in the analysis of Myers et al. is the same for the plane free jet. This is a reasonable result in view of the fact that the assumption of infinite eddy viscosity in the outer layer was made. Physically, this means that the free jet portion, or the outer layer, of the flow plays a determining role in the wall jet. Bradshaw and Gee (9) also noted this fact.

The maximum velocity decay was given experimentally by Myers et al. as

$$u_m / U = 3.45 (x / B_2)^{-0.49} \qquad (2.31)$$

The length scale was found to have a slight dependence on the jet Reynolds number.

The analysis of Myers et al. indicates the shear to vary as $x^{-1.10}$ which agrees with Schwarz and Cosart's result of $x^{-1.11}$. The data of Myers et al. are 15 percent higher than Sigalla's. Smith and Walker (40) found that Preston's method used by Sigalla gave results about 12 to 14 percent below accepted data. After using this information,

Sigalla's data would be only 2 percent less than the data of Myers et al.

Myers et al. also found that a 2 percent error in the value of the exponent for the velocity decay would introduce a 20 percent error in the friction factor.

More details of the shear analysis of Myers et al. will be given in the next chapter.

The diffusion of a stream issuing from a sluice gate in a rectangular channel under high submergence was treated by Rajaratnam (47) as a problem of the plane turbulent wall jet. He found experimentally that the velocity distribution in the region of fully developed flow, the variation of the velocity and length scales agreed with the corresponding characteristics of a plane turbulent wall jet issuing into stagnant surroundings on a smooth wall under zero pressure gradient.

2.5 Submerged Diffusion Jet

If the flow is deeply submerged, the decay of the maximum velocity as well the shear stress is considerably retarded. For developing safe but economical designs of energy dissipators, a good knowledge of at least the mean diffusion characteristics of the flow is necessary.

The approximate characteristics of the mean flow pattern of the submerged diffusion jet have been derived

analytically by Albertson et al.(3), with the exception of a single empirical constant C_s, through assumptions that: (a) the pressure is hydrostatically distributed throughout the flow; (b) the diffusion process is dynamically similar under all conditions; and (c) the longitudinal component of velocity within the diffusion region varies according to the normal probability function at each cross section. The constant C_s was obtained by their experimental data. A greater detail for the derivation of the submerged diffusion flow pattern will be shown in the next chapter.

2.6 Tractive Force Method

The drag force on the wetted area of the channel is named tractive force. The method, based on using this force as a criterion for the design of erodible channels, is known as the tractive force method. This method is studied comprehensively by the U.S.B.R. (67).

The detail for the developing of this method is given in Chapter 3.

CHAPTER III

THEORETICAL ANALYSIS OF THE LONGITUDINAL AND CROSS-SECTIONAL PROFILES OF SCOUR HOLES

Scour in the erodible bed below the flipbucket is greatly influenced by the characteristics of the water jet issuing from the upstream reservoir and the properties of the material forming the riverbed. For the theoretical approach, the water jet is considered as a submerged diffusion jet when it enters the tailwater until it strikes the riverbed. When it impinges the bed, the jet is treated as a wall jet. Based on the theories of the submerged diffusion jet and the wall jet, the longitudinal profiles of scour holes are derived. The cross-sectional profiles of scour holes are derived analytically using the principles of tractive force method.

3.1. Longitudinal Profiles of Scour Holes

3.1.1 Mean Flow Pattern of Submerged Diffusion Jet

The mean flow pattern of the submerged diffusion jet were studied by Albertson et al.(3) with the assumptions of hydrodynamic pressure, dynamic similarity of the diffusion process, and normal-probability variation of the velocity.

According to the work of Albertson et al. ,the submerged jet was divided into two parts; the zone of flow establish-

ment and the zone of established flow.

The definition sketch is shown in Fig. 3.1.

In the zone of flow establishment, the maximum velocity, V_{max} , for the cross-section is equal to the initial velocity of the jet, V_1 .

The flow pattern in the zone of established flow was obtained analytically through the assumptions of Albertson et al. From the assumption that the longitudinal component of the velocity within the diffusion region varies according to the normal-probability function, then

$$V_x / V_{max} = \text{exp.} (- y^2 / 2\sigma^2) \qquad (3.1)$$

where v =the velocity, and

σ = the standard deviation.

The subscript x denotes the position with distance x from the origin of the submerged jet.

Under the condition of dynamic similarity of the diffusion process at all sections,

$$\sigma / x = C_s \qquad (3.2)$$

where C_s is a constant.

By the conservation of momentum flux, the momentum flux must be constant for all sections of a given flow

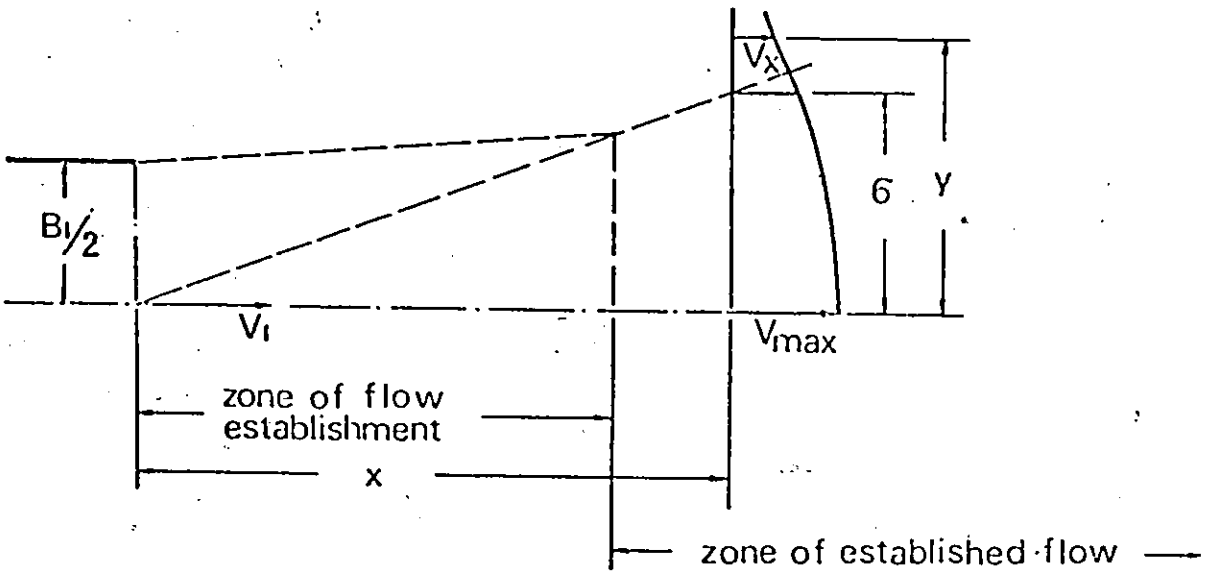

FIG.3.1 DEFINITION SKETCH FOR SUBMERGED DIFFUSION JET

pattern,

$$\frac{M_x}{M_1} = \frac{\int_o^\infty V_x^2 \, d A_c}{V_1^2 \, (A_c)_1} = 1 \qquad (3.3)$$

where A_c = the area of the cross-section, and

M = the momentum flux.

The subscript 1 denotes the starting position of the submerged jet.

Substituting Eq.(3.1) into Eq.(3.3), then the unit momentum flux becomes,

$$M_x = \int_o^\infty V_{max} \exp. (- y^2 / 2 \sigma^2) \, d y$$

$$= V_1^2 \cdot B_1 / 2 \qquad (3.4)$$

where B_1 is the jet thickness at the starting position of the submerged jet.

Substituting Eq.(3.2) into Eq.(3.4), the velocity V_{max} is obtained,

$$\frac{V_{max}}{V_1} = \sqrt{\frac{1}{\sqrt{\pi} \, C_s} \frac{B_1}{x}} \qquad (3.5)$$

Albertson et al. determined the single constant C_s =

0.109 by experimental observations. The velocity V_{max} can be expressed as

$$V_{max} = 2.28\, V_1 \sqrt{B_1 / x} \qquad (3.6)$$

3.1.2 Shear Stress of Water Jet

Myers et.al.(39) applied the momentum method to obtain a prediction for the wall shear stress. They solved the problem by dividing it into two parts,

a) the starting length problem where the maximum jet velocity had not yet begun to decay, and

b) the region where the maximum velocity was decreasing.

In solving each of these two parts, the flow was divided into two regions. The region next to the wall, termed inner layer, was assumed to behave similarly to a turbulent boundary layer. The region away from the wall, or outer layer, was assumed to behave like a free jet.

Fig. 2.3 describes the varis areas and the terms to be used.

In each region, the momentum boundary layer equation was used,

$$\frac{1}{\rho}\frac{\partial \tau}{\partial y} = u\, \partial u / \partial x + v\, \partial u / \partial y \qquad (3.7)$$

where τ is the shear stress.

The continuity equation was also used,

$$\partial u / \partial x + \partial v / \partial y = 0 \qquad (3.8)$$

where u and v denote the velocity components with x and y directions respectively.

In the wall layer, the Blasius (53) relation was used,

$$\tau_w / \rho = 0.0225 \, u_m^2 \left(u_m \, \delta_m / \nu \right)^{-0.25} \qquad (3.9)$$

where τ_w is the shear stress of the wall jet. The terms ρ, u_m, ν and δ_m are defined in Chapter II.

In the free jet layer, the shear stress was assumed using Prandtl's theory (53),

$$\tau / \rho = n \, u_m \left(\delta - \delta_m \right) \partial u / \partial y \qquad (3.10)$$

where δ = boundary layer thickness, and

n = constant.

In the inner layer, Eq.(3.7) was integrated from y = 0 to $y = \delta_m$ with Eqs. (3.8) and (3.9). The boundary conditions were $\tau(\delta_m) = 0$, $u = v = 0$ at $y = 0$, and $u = u_m = U$

at $y = \delta_m$. This gave

$$0.0225 \frac{\nu^{0.25} u_m^2}{u_m^{0.25} \delta_m^{0.25}} = u_m \frac{d}{dx} (\delta_m - u_m) \int_0^1 E(\eta)\, d\eta - \frac{d}{dx} (u_m^2 \delta_m) \int_0^1 E^2(\eta)\, d\eta \qquad (3.11)$$

where

$$\eta = y / \delta_m \qquad (3.12)$$

and

$$E = u / u_m \text{ in the inner layer.} \qquad (3.13)$$

In the outer layer, Eq. (3.7) was integrated from $y = \delta_m$ to $y = \delta$ using Eqs.(3.8) and (3.10) with the boundary conditions $\tau(\delta_m) = \tau(\delta) = 0$, $u(\delta_m) = u_m$ and $u(\delta) = 0$. This resulted in the following relation,

$$\int_0^1 F^3(\zeta)\, d\zeta \frac{d}{dx} \{ u_m^3 (\delta - \delta_m) \} + \int_0^1 P(\eta)\, d\eta\, u_m^2 \frac{d}{dx} (\delta_m u_m) + 2 n u_m^3 \int_0^1 F'^2(\zeta)\, d\zeta = 0 \qquad (3.14)$$

where $\zeta = (y - \delta_m) / (\delta - \delta_m)$ (3.15)

and $F = u / u_m$ in the outer layer. (3.16)

After solving Eqs.(3.11) and (3.14), Myers et al. obtained the following equations to predict the shear stress,

$$C_f R_e^{1/5} = C_2 t^2 m^{-1/4} \quad (3.17)$$

where C_f = friction factor $= 2 \tau_w / \rho U^2$, (3.18)

R_e = Reynolds number $= U B_2 / \nu$, (3.19)

$$t = u_m / U = \left(\sqrt{1 + 0.381 \left(x / 7B_2 \right) - 1} \right)^{-1} \quad (3.20)$$

$$m = (0.523 t^{10} + 0.477 t^{-1})^{4/5}, \quad (3.21)$$

and C_2 = constant.

The initial velocity U and jet thickness B_2 are defined in Chapter II.

3.1.3 Analytical Development of Longitudinal Profiles of Scour Holes

Referring to Fig. 3.3, the equation for balancing the forces acting on a particle at the tangential direction of

the scour hole can be expressed as

$$a\ \tau_w - W_s \sin\phi - F_R = 0 \qquad (3.22)$$

where F_R = resistant force of a particle

$$= (W_s \cos\phi - a\ \tau_L) \tan\theta \qquad (3.23)$$

τ_L = lift force, and

ϕ = angle between the tangent of scour profile and the horizontal level.

Combining Eqs.(3.17), (3.18) and (3.19), the shear stress can be written as ,

$$\tau_w = C_2\ \rho\ t^2\ m^{-1/4}\ R_e^{-1/5}\ U^2 / 2 \qquad (3.24)$$

Substituting Eqs.(3.23) and (3.24) into Eq.(3.22), then,

$$C_2\ a\ (\rho\ U^2 / 2)\ t^2\ m^{-1/4}\ R_e^{-1/5} - W_s \sin\phi$$

$$= (W_s \cos\phi - a\ \tau_L) \tan\theta \qquad (3.25)$$

The area of influence, a, can be determined by

$$a = d^2 / r_p \qquad (3.26)$$

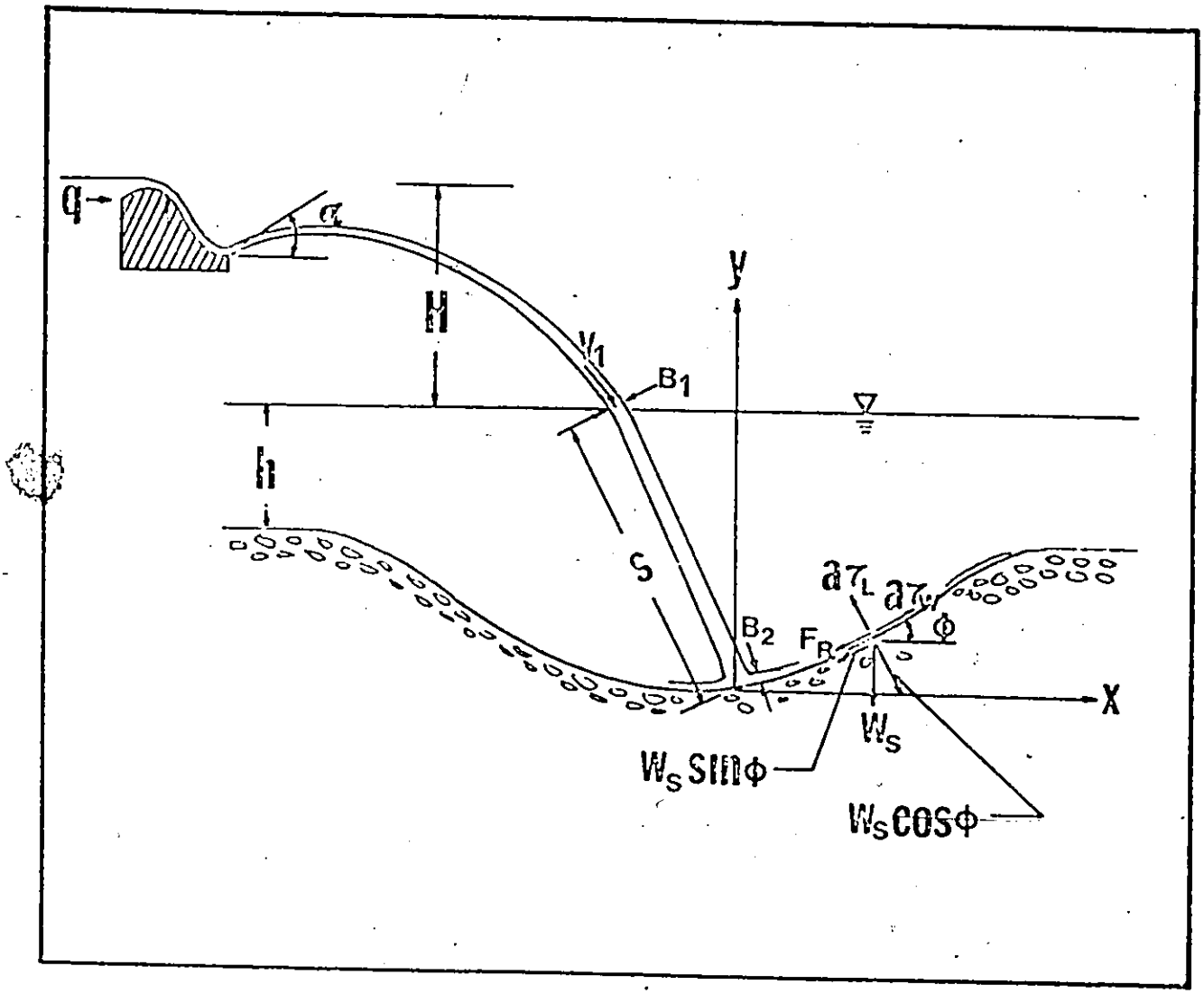

FIG.3.2 DEFINITION SKETCH FOR THE LONGITUDINAL PROFILE OF SCOUR HOLE

and $$r_p = 0.107 / \text{Tan}\,\theta \qquad (3.27)$$

which were suggested by White (71) using Shield's (56) entrainment function as discussed in Chapter II. In Eq.(3.26), d is the mean diameter of the bed material.

The lift stress is expressed as

$$\tau_L = C_L (\rho u_m^2 / 2) \qquad (3.28)$$

where C_L is the lift constant.

Substituting Eqs.(3.26), (3.27), (3.28) and $\text{Tan}\,\phi = dy / dx$ into Eq.(3.25), thus,

$$C_2\, a\, (\rho U^2 / 2)\, t^2\, m^{-1/4}\, R_e^{-1/5}$$

$$- W_s\, (dy/dx)\, (\sqrt{1 + (dy / dx)^2}\,)^{-1}$$

$$- \left\{ W_s (\sqrt{1 + (dy/dx)^2}\,)^{-1} - a(\rho C_L u_m^2\, t^2)/2 \right\} \text{Tan}\,\theta = 0 \qquad (3.29)$$

In the equation above, the wall jet velocity U can be obtained by

$$U = 2.28\, V_1\, (B_1 / s)^{1/2} \qquad (3.30)$$

where $s = D_m / \sin\beta$ (3.31)

and β = angle between the tailwater level and jet projectile.

Therefore, the theoretical longitudinal profiles of scour hole can be predicted by Eq.(3.29) after the constants C_L and C_2 are determined from the experimental data.

3.2. Cross-sectional Profiles of Scour Hole

3.2.1 Tractive Force Ratio and Tractive Force Method

The tractive force method was studied by U.S.B.R. (17).

Consider a particle resting on the sloping side of a channel as shown in Fig. 3.3. Two forces tend to cause the particle to move; the force $a\tau_s$ and the component of gravity force $W_s \sin\phi$. The symbols used are

τ_s = unit tractive force on the side of channel,

ϕ = the side slope of channel,

W_s = weight of the particle of bed material, and

a = area of influence of the particle.

The resultant force tending to move the particle is

$$(W_s^2 \sin^2\phi + a^2 \tau_s^2)^{1/2} \qquad (3.32)$$

The force resisting the motion is

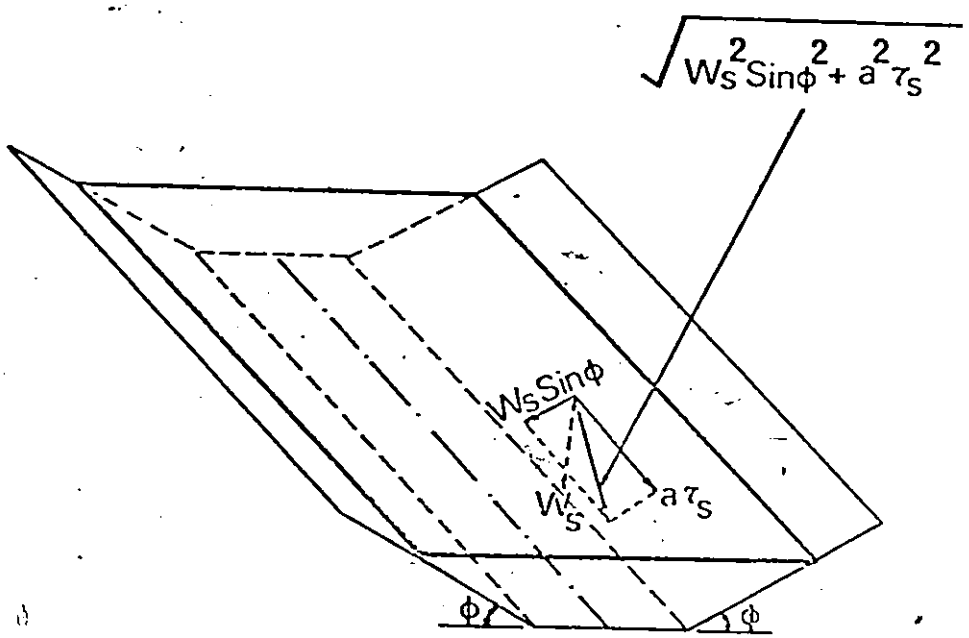

FIG.3.3 FORCES ACTING ON A PARTICLE RESTING ON THE SIDE OF A CHANNEL.

$$W_s \cos\phi \tan\theta \qquad (3.33)$$

where θ is the angle of repose of the material.

At the equilibrium condition, the forces mentioned above in Eqs.(3.32) and (3.33) must be the same,

$$(W_s \sin^2\phi + a^2 \tau_s^2)^{1/2} = W_s \cos\phi \tan\theta \qquad (3.34)$$

Then, the tractive force can be solved by Eq.(3.34),

$$a \tau_s = W_s \tan\theta \cos\phi (1 - \tan^2\phi / \tan^2\theta)^{1/2} \qquad (3.35)$$

The tractive force at the bed surface is

$$a \tau_b = W_s \tan\theta \qquad (3.36)$$

Then, the tractive force ratio is obtained as

$$K_t = \tau_s / \tau_b = \cos\phi (1 - \tan^2\phi / \tan^2\theta)^{1/2} \qquad (3.37)$$

3.2.2 Theoretical Considerations of the Cross-sectional Profiles of Scour Hole

Referring to Fig. 3.4, the tractive force can be expressed as

$$\tau_s = W_w (y + h) S_e \cos\phi \qquad (3.38)$$

and

$$\tau_b = W_w (y_o + h) S_e \qquad (3.39)$$

where S_e = energy slope,

W_w = weight of water,

y_o = vertical distance from the original bed to the maximum scour point, and

τ_b = unit tractive force that causes impending motion on the bottom of the scour hole.

The tractive force ratio was recommended by the U.S.B.R. (17) as

$$K_t = \tau_s / \tau_b = \cos\phi \left(1 - \tan^2\phi / \tan^2\theta \right)^{1/2} \qquad (3.37)$$

However, the tractive force ratio can also be obtained from Eqs.(3.38) and (3.39),

$$K_t = \tau_s / \tau_b = \cos\phi (y + h) / (y_o + h) \qquad (3.40)$$

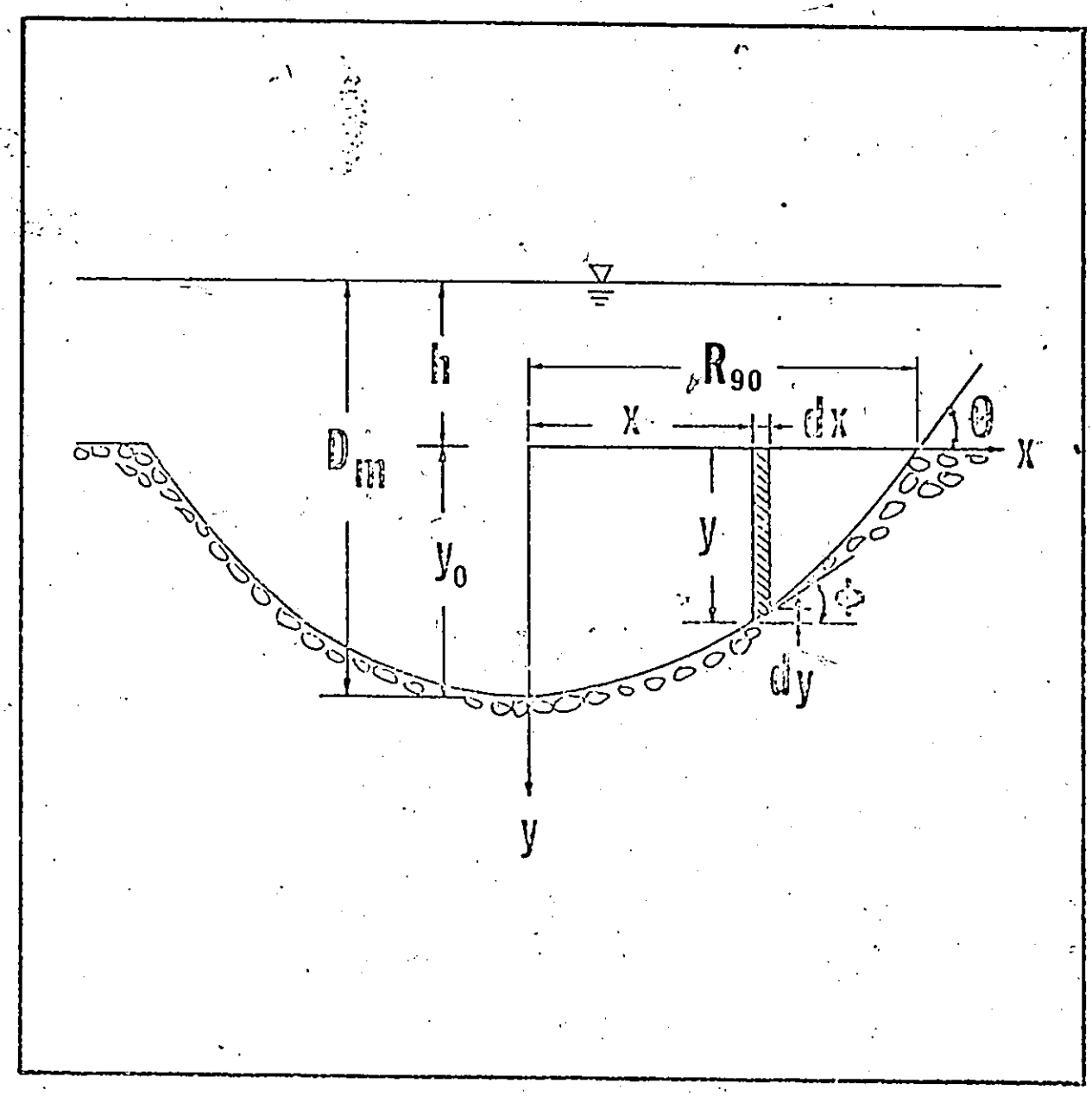

FIG.3.4 DEFINITION SKETCH FOR THE CROSS-SECTIONAL PROFILE OF THE SCOUR HOLE

Equating Eqs.(3.37) and (3.40), then,

$$(1 - \mathrm{Tan}^2 \phi / \mathrm{Tan}^2 \theta)^{1/2} = (y + h) / (y_o + h) \qquad (3.41)$$

Substituting $\mathrm{Tan}\,\phi = - dy / dx$ into Eq.(3.41),

$$1 - (- dy / dx)^2 / \mathrm{Tan}^2 \theta = (y + h)^2 / (y_o + h)^2 \qquad (3.42)$$

or

$$\frac{dy}{dx} = - \mathrm{Tan}\theta \sqrt{1 - \left(\frac{y + h}{y_o + h} \right)^2} \qquad (3.43)$$

Integrating Eq.(3.43),

$$\int \frac{dy}{\sqrt{(y_o+h)^2-(y+h)^2}} = - \frac{\mathrm{Tan}\,\theta}{y_o + h} \int dx \qquad (3.44)$$

Solving for Eq.(3.44)

$$\mathrm{Sin}^{-1} \frac{y + h}{y_o + h} = - \frac{\mathrm{Tan}\,\theta\, x}{y_o + h} + C_i \qquad (3.45)$$

Using the boundary condition that $x = R_{90}$ at $y = 0$, the constant C_i can be solved as

$$C_i = \text{Sin}^{-1} \frac{h}{y_0 + h} + \frac{\text{Tan}\,\theta \; R_{90}}{y_0 + h} \qquad (3.46)$$

where R_{90} = length of radius vector at the angle $\theta_b = 90^o$ measured to the rim of the scour hole, and

θ_b = angle measured clockwise and anticlockwise from the reference radius vector.

Therefore, the solution of Eq. (3.42) will give the cross-sectional profiles of scour holes, thus,

$$\frac{y + h}{y_0 + h} = \text{Sin}\left(\frac{-\text{Tan}\theta \; x}{y_0 + h} + \text{Sin}^{-1} \frac{h}{y_0 + h} + \frac{\text{Tan}\,\theta \; R_{90}}{y_0 + h} \right) \qquad (3.47)$$

CHAPTER IV

EMPIRICAL EQUATION OF LOCAL SCOUR BELOW FLIP BUCKETS AND SHARP-EDGED WEIRS

The scour below flip buckets is also studied experimentally. The empirical equations are obtained using dimensional analysis with the aid of statistical methods. The scour hole profile is assumed as a parabola with the empirical costants determined by observed data. The equation to determine the maximum depth of scour below a flip bucket is extended to the case of scour below sharp-edged weirs. Instead of the principles of a freely falling jet used in the case of scour below flip buckets, the Blaisdell's (7) empirical equation is used in determining the jet velocity in the case of local scour below sharp-edged weirs.

4.1 Maximum Depth of Scour

The maximum depth of scour below flip buckets is studied under two cases.

Case 1. Without scour hole formation. In this case, the maximum depth of scour at equilibrium is simply the tail-water depth.

Case 2. With scour hole formation. In this case, the maximum depth of scour is the vertical distance from the

tailwater to the maximum scour point when the bed material reaches equilibrium after the scour hole formation.

The definition sketchs are shown in Figs. 4.1 and 4.2.

4.1.1 Without Scour Hole Formation

Concrete blocks were used as idealized bed material in most of the investigations.

The important variables which influence the maximum depth of scour, D_m, are V_m, S_s, d, z, g and β. These parameters can be expressed functionally as,

$$D_m = f (V_m, S_s, d, z, g, \beta) \qquad (4.1)$$

where V_m = velocity of submerged jet at the center of the block, or the bed material, and can be calculated by the theory of the submerged diffusion jet(3).

$$= 2.28 V_1 (B_1 / s)^{1/2} \qquad (4.2)$$

V_1 = velocity at the position where the jet enters the tailwater

$$= (2gH)^{1/2} \qquad (4.3)$$

B_1 = thickness of the jet at the point where the jet strikes the tailwater

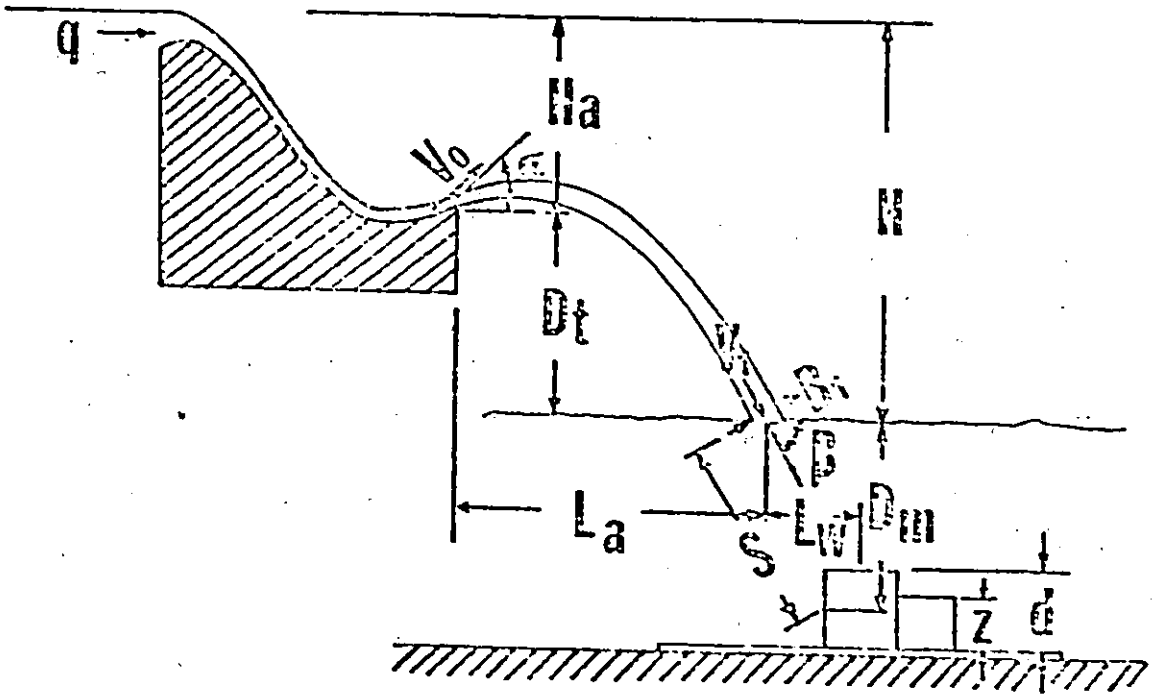

FIG. 4.1 DEFINITION SKETCH FOR SCOUR BELOW FLIP BUCKET IN THE CASE WITHOUT SCOUR HOLE FORMATION

$$B_1 = q / V_1 \quad , \tag{4.4}$$

$$S = D_m / \text{Sin}\,\beta \tag{4.5}$$

β = angle between tailwater level and V_1

$$= \text{Tan}^{-1} \left(\frac{g L_a}{V_o^2 \text{Cos}^2 \alpha} - \text{Tan}\,\alpha \right) , \tag{4.6}$$

L_a = the horizontal distance from the lip of bucket to the position where jet enters the tailwater,

S_s = specific gravity of blocks or of bed material,

d = size of blocks or of bed material, and

z = height of the obstruction to the block.

The terms of α, g, H, q, and V_o are the same as previously defined.

Using Buckingham's threorem of dimensional analysis, the functional relationship can be represented as follows,

$$D_m / d = f \left[V_m^2 / gd \, , \; 1 / (S_s - 1), \; 1/(1+ z/d), \; \beta \right] \tag{4.7}$$

Therefore, an empirical equation can be written as,

$$D_m / d = C_3 \left(V_m^2/gd \right)^{K_3} \left(\frac{1}{S_s - 1} \right)^{K_4} \left(\frac{1}{1+z/d} \right)^{K_5} \beta^{K_6} \tag{4.8}$$

where C_3, K_3, K_4, K_5, and K_6 are empirical costants determined from experimental observations in conjunction with statistical method.

4.1.2 With Scour Hole Formation

The dimensionless terms, V_m^2/gd, $1/(S_s-1)$, $1/(1+z/d)$ and β are selected as the governing parameters for the determining the ratio of depth of maximum scour, D_m, to the bed material size, d. Therefore, the same type of equation as shown in Eq.(4.8) is used in this case. The exponential constant of the term $1/(1+z/d)$ is selected as the same as the one used in the case without any scour hole formation. Then, the value of the the equivalent z/d, based on the one used in Case 1, can be determined from the experimental observations for any specific bed material.

4.2. Scour Hole Configuration

The contours of the scour hole are symmetrical about the longitudinal axis passing through the maximum scour point. The point on the bed level directly above the maximum scour is used as the origin in this analysis.

The difinition sketch is shown in Fig. 4.3.

4.2.1 Radius Vector Length at Bed Level

The most significant variables affecting the radius

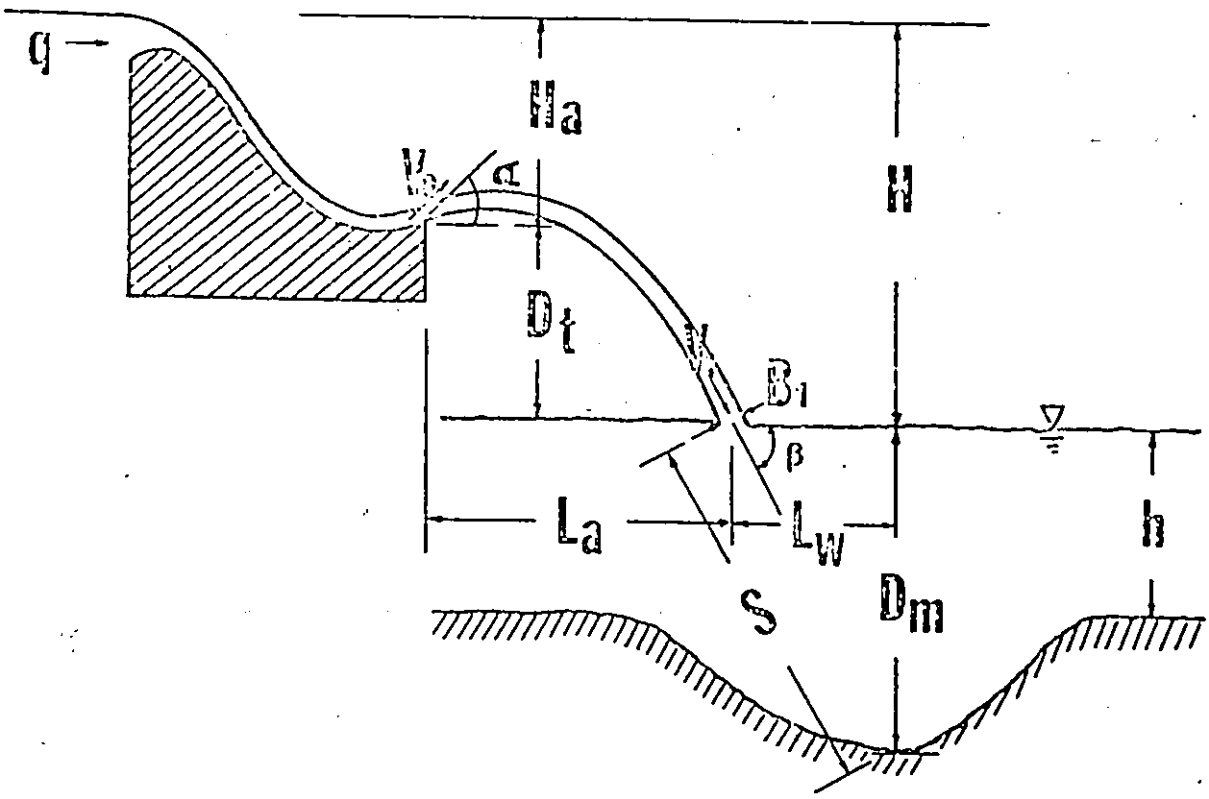

FIG. 4.2 DEFINITION SKETCH FOR SCOUR BELOW FLIP BUCKET IN THE CASE WITH SCOUR HOLE FORMATION

vector lengths are presented in the following relationships.

$$R_\theta = f (R_o, \theta_b) \qquad (4.9)$$

and

$$R_o = f (D_m, h) \qquad (4.10)$$

where R_θ = length of radius vector at the angle of θ_b measured to the rim of the scour hole, and

R_o = reference radius vector pointing in the downstream direction when the rim of scour is closest to the origin.

The symbols h, D_m, and θ_b are defined previously.

Then, the equation for radius vector length can be introduced in the following forms,

$$R_\theta = R_o (1 + C_4 \theta_b^{K_7}) \qquad (4.11)$$

and

$$R_o = C_5 (D_m - h)^{K_8} \qquad (4.12)$$

where C_4, C_5, K_7, K_8 are constants which can be determined from experimental results.

4.2.2 Intermediate Depths of Scour

The intermediate depth of scour, D, is defined as the depth at any point along a radius vector measured from

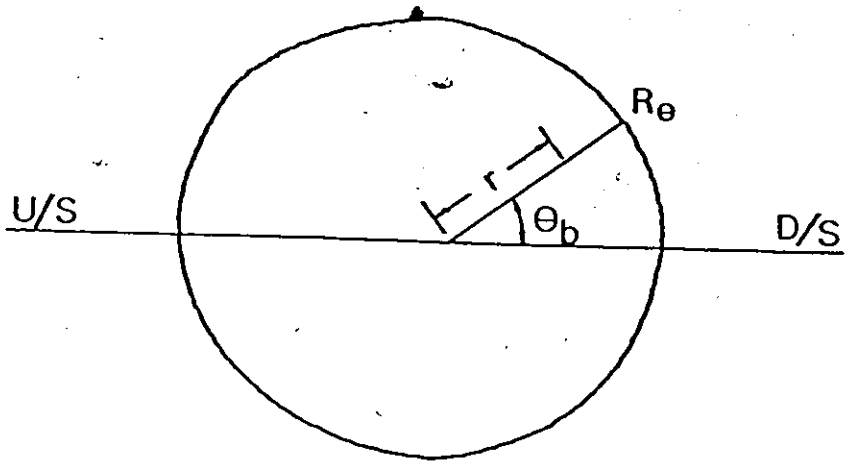

(A) RADIUS VECTOR LENGTH AT BED LEVEL

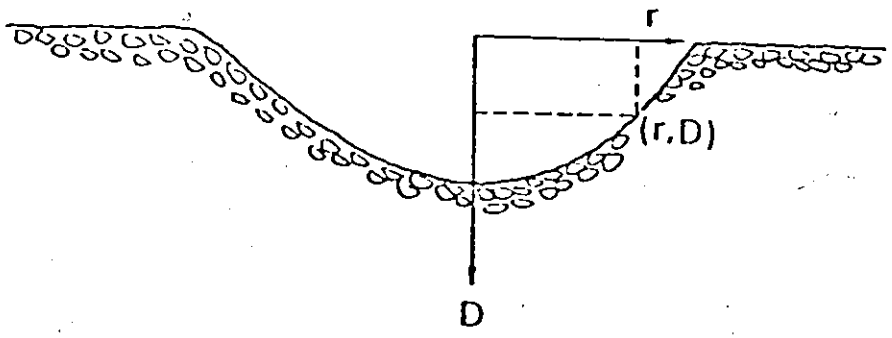

(B) INTERMEDIATE DEPTH OF SCOUR

FIG.4.3 DEFINITION SKETCH FOR SCOUR HOLE CONFIGURATION

the scour hole bottom to the original bed.

The terms of D_m, h, r, and R are selected as the governing factors to determine the intermediate depth of scour.

Assuming any scour hole profile is a parabola with the vertex at (0, $-D_m+h$) and origin at point of maximum scour, the important variables can be related as

$$D = (D_m - h) (1 - r^2/R^2) \qquad (4.13)$$

where r = distance at any point along a radius vector, and R = length of radius vector measured to the rim of the hole.

4.3 Maximum Scour Depth below Sharp-edged Weirs

The concrete blocks were also used as the idealized bed material in this part of the study. In this study, the maximum depth of scour is simply the depth of tailwater.

The definition sketch is shown in Fig. 4.4.

The dimensionless parameter of V_m^2/gd, $1/(S_s-1)$, β and $1/(1+z/d)$ selected for studying the local scour below flip bucket are again used in this case. Therefore, the same kind of equation as shown in Eq.(4.8) is used, but the empirical constants are determined again.

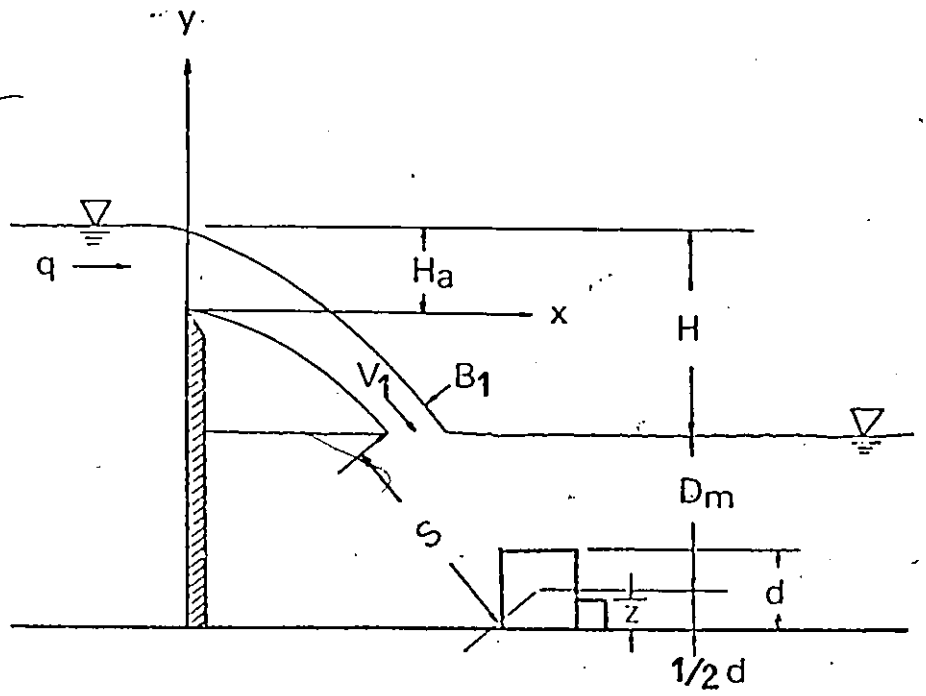

FIG.4.4 DEFINITION SKETCH FOR SCOUR BELOW WEIR

The shape of the flow nappe over a sharp-edged weir is needed for determining the velocity of the submerged jet, V_m. Blaisdell (7) suggested the following equation to determine this shape of the flow nappe,

$$y/H_a = C_6 (x / H_a)^2 + C_7 (x / H_a) + C_8 \qquad (4.14)$$

where H_a is the difference in elevation between the upstream level and the edge of the weir. He also determined the constants C_6, C_7, C_8 by experiments,

$$C_6 = -0.425,$$
$$C_7 = 0.055, \text{ and} \qquad (4.15)$$
$$C_8 = 0.430.$$

From Eqs.(4.14) and (4.15), the derivation of y with respect to x can be expressed as

$$dy / dx = 0.85 x / H_a - 0.055 \qquad (4.16)$$

Thus, the velocity of submerged diffusion jet, V_m, can be calculated by Eqs.(4.2), (4.3), (4.4), (4.5) and

$$\beta = \text{Tan}^{-1} (dy / dx) \quad \text{at } y = -H \qquad (4.17)$$

where dy / dx is determined by Eq.(4.16).

4.4. Jet Trajectory Distance

The jet trajectory distance, L , is the horizontal length measured from the downstream edge of the spillway to the position of maximum scour as shown in Figs. 4.1 and 4.2. It is made up of two components as

a) the horizontal flight distance, L_a , from the lip of the bucket to the point where the jet enters the tailwater;

b) the horizontal length, L_w , which the submerged jet travels from the latter position to the point of maximum scour.

The first part of trajectory distance is calculated using the theory of the simple projectile. The second part of the distance is determined assuming the submerged jet continues on a path tangent to its trajectory in air until it intersects the point of maximum bed scour.

Applying the principle of the simple projectile, it is assumed that when the jet leaves the spillway it acts as a freely falling body following a parabolic path with a constant horizontal velocity and a vertical gravity-accelerating velocity under the situation that the effect of air resistance is neglected.

The point of exit of the jet from the spillway lip is taken as the origin of the coordinate axes. The upward direction is assumed as the positive ordinate. Then, the equation for the trajectory of the free falling nappe is

$$y = \frac{-g}{2 V_o^2 \cos^2 \alpha} x^2 + x \tan \alpha \qquad (4.18)$$

where the jet velocity at the bucket lip, V_o , can be calculated by applying Bernoulli's equation to the upstream tank reservoir and at the lip of the flip bucket as

$$V_o = (2 g H_a)^{1/2} \qquad (4.19)$$

the symbol H_a means the difference in elevation between upstream level and bucket lip.

At the point where jet enters the tailwater,

$$x = L_a \quad \text{and} \quad y = D_T \qquad (4.20)$$

Substituting Eq.(4.20) into Eq.(4.18), the distance L_a can be solved as

$$L_a = \frac{V_o^2 \cos^2 \alpha}{g} \left(\tan \alpha + \sqrt{\tan^2 \alpha + \frac{2 D_T g}{V_o^2 \cos^2 \alpha}} \right) \qquad (4.21)$$

After the jet enters the tailwater, the horizontal distance from the point of entry to the maximum scour is

$$L_w = D_m / \tan \beta \qquad (4.22)$$

where both the values of D_m and Tan β are assumed to be positive.

Taking the derivative of y with respect to x in Eq. (4.18) at point (L_a, $-D_T$),

$$\frac{dy}{dx} = -\frac{g\, L_a}{V_o^2 \cos^2\alpha} + \text{Tan}\,\alpha = -\text{Tan}\,\beta \qquad (4.23)$$

Substituting Eq.(4.23) into Eq.(4.22),

$$L_w = \frac{D_m}{\frac{g\, L_a}{V_o^2 \cos^2\alpha} - \text{Tan}\,\alpha} \qquad (4.24)$$

All the terms of g, α , D_T and β used in section are the same as previously defined.

Then, the total horizontal trajectory distance is

$$L = L_a + L_w \qquad (4.25)$$

where L_a and L_w are given by Eqs. (4.21) and (4.24) respectively.

CHAPTER V

EXPERIMENTAL PROGRAM

The main objectives of the experimental studies of local scour below flip buckets for this thesis are:

a) To verify the cross-sectional profiles of the scour holes derived by Eq.(3.47).

b) To determine the constants C_2 and C_L used in Eq. (3.29), and to obtain the longitudinal profiles of the scour holes.

c) To determine the empirical constants used in Chap. IV to establish the formulae for predicting the maximum scour depth and scour hole configuration.

d) To verify the jet trajectory length derived in Eqs. (4.21), (4.24), and (4.25) for locating the position of maximum scour.

5.1 Experimental Apparatus

The apparatus used for the experimental studies of this thesis is shown in Figs. 5.1 and 5.2.

A 1'-9" x 4' x 4' head tank made of steel plates was used. The water entered the head tank by a 6" diameter supply pipe. A circular orifice 2 1/2" in diameter was provided at the base of the tank to drain the water.

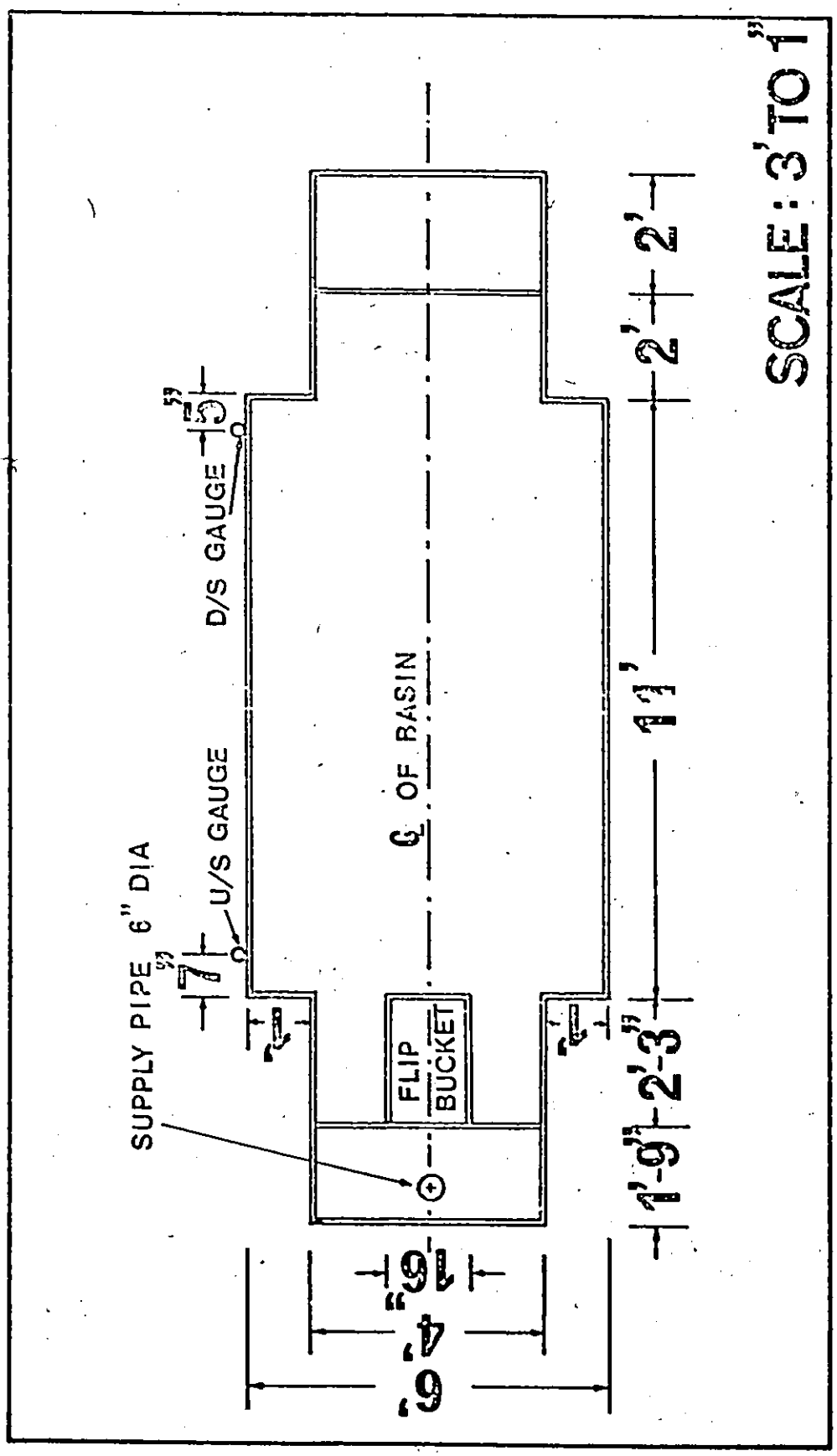

FIG.5.1 PLAN OF EXPERIMENTAL APPARATUS

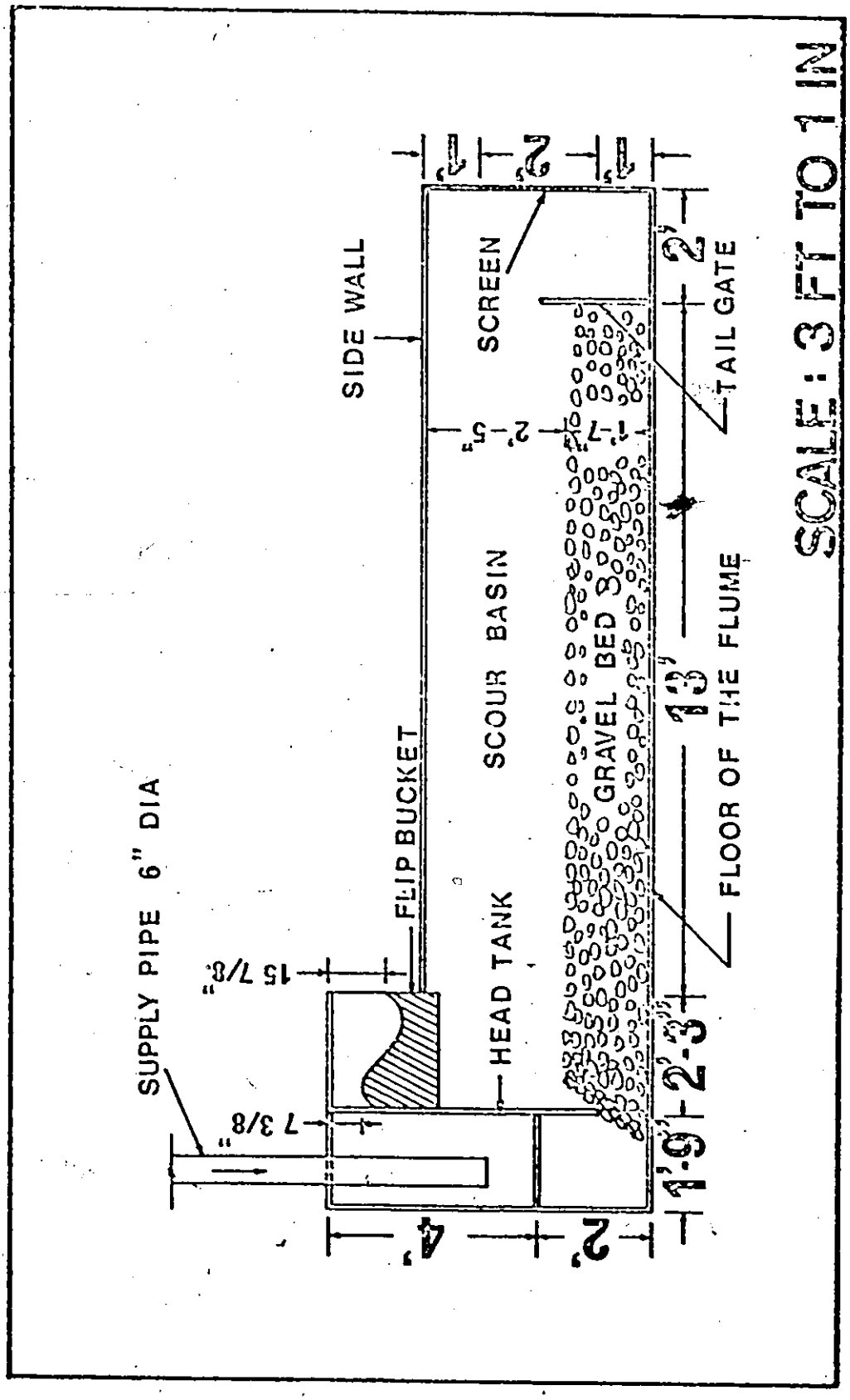

FIG.5.2 ELEVATION OF EXPERIMENTAL APPARATUS

The downstream scour basin, 11' x 6" in plan with 4' high sidewalls, was made of timber. This basin was provided with a 1' - 7" thick bed made up of granular material. A tailwater control gate was installed at the downstream end. A filter was provided at the outlet end.

Five circular flip buckets were used in the experiments; four of them are 16" wide with 8" radius and having different exit angles of 15°, 30°, 45° and 60°. Another one is 2' wide, 12" radius and with 30° exit angle.

The measurements of water levels were made by using manometers gauges and point gauges, the positions of which are shown in Figs. 5.1 and 5.2. The discharge was measured by an electronic flow meter.

5.2 Experimental Investigation

The whole experimental program was investigated under two different cases.

Case 1. Experiments conducted to observe the local scour with the scour hole formation in granular materials.

Case 2. Experiments conducted to observe the incipient motion of the bed material.

5.2.1 Maximum Depth and Configuration of Scour Hole

In this portion of investigation, two different

granular bed materials were used with nominal sizes of 1/4" and 3/4", and specific gravities of 2.55 and 2.25 respectively. The discharges used from 0.385 cfs to 3.41 cfs. In the experiments the flow was varied from the lowest value would cause a measurable amount of scour in the downstream basin to the highest value, within the model limitations, to produce the maximum amount of scour. As the scour hole formed, the scoured material deposited directly downstream from the scour hole was removed.

The experimental procedures were adopted as follows.

a) Each experiment was started with the bed levelled.

b) The initial readings were taken.

c) The head tank filled with water and the jet was allowed to plunge into the basin.

d) The test was run for a minimum period of two hours.

e) The discharge of flow and the corresponding head tank water level, upstream tailwater levels were recorded.

f) The water was drained from the basin.

g) Strings were placed around the scour hole at 1" or 2" intervals to mark the scour hole contours.

h) The water drained until the bottom of the scour hole was seen.

i) The maximum scour point was marked.

j) The maximum depth of scour was measured by a point gage.

5.2.2 Maximum Depth of Scour without Scour Hole Formation

In this part of the investigations, the concrete blocks were used as the idealized bed material. The sizes of blocks used in the experiments ranged from 1" to 6", and their specific gravities ranged from 1.06 to 4.14. The discharges during the invetigations ranged from 0.23 cfs to 2.36 cfs.

The 3/4" wide and 2' long wooden strips were used as obstructions to the movement of the blocks. The values of z of the obstruction represented by the heights of the wooden strips ranged from 1" to 4 1/2". Ratios of z/d of 0, 1/4, 1/2, and 3/4 were used.

The first two experimental procedures adopted were the same as mentioned as (a) and (b) in section 6.2.1. Then a 2' x 3' x 3/8" steel plate was placed on the bed in the area of the jet impingement and a concrete block of known size and specific gravity was placed without or with the strip for a z/d value on the plate at the center where the jet struck the plate. The head tank filled with water and the jet was allowed to plunge into the basin. The minimum discharge which would move the block was found; the corresponding head tank water level, upstream and downstream tailwater levels were recorded.

5.3 Experimental Errors

The possible errors which may be introduced during the experimental investigations are as follows.

a) The instrumental errors relating to the electronic flow meter and its degree of accuracy. Since the flow recorded was graduated to read directly to 50 U.S. gallons per minute, the discharge could be read only to an accuracy of 10 U.S. gallons per minute. During the whole investigations the maximum and minimum discharges read about 1250 and 250 U.S. g.p.m. respectively. Thus, the minimum possible error in reading the discharge is 0.8 % and the maximum is 4%.

b) Due to the fluctuations in the gages, the water levels observed could be subject to an error of ± 1/8". The maximum and minimum observed water levels were about 58" and 4.5" respectively. Therefore, the minimum possible error in reading the water level is 0.21% and the maximum is 2.8%.

c) The jet trajectory length was measured to the accuracy of 1/8". The maximum and minimum length measured were 63.5" and 36.125" respectively. Then, the possible maximum and minimum errors are 1.97% and 0.35% respectively.

CHAPTER VI

RESULTS AND DISCUSSION

This chapter compares the theoretical profiles of scour holes and the calculated jet trajectory length with the corresponding experimental ones. Based on the experimental data, the empirical equations are also obtained for predicting the maximum depth of scour and scour hole configuration. The equation used for calculating the maximum depth of scour below flip buckets is extended to the case of scour below sharp-edged weirs. The effect of time on the scour development is discussed too. Finally, the practical and economical shape of the plunge basin below the deflector buckets is recommended. This shape is also verified by experiments with a large range of hydraulic variables.

6.1 Time Factor for Development of Maximum Scour Condition

An important consideration for the development of maximum depth of scour is whether or not the model has operated for a length of time sufficient for its formation. Two tests were conducted for observing this scour development with varying time. The forty-five degree flip bucket and two different bed materials with nominal sizes of 3/4" and 3/8"

were used in these tests. The scour depths of five different positions in each scour hole were measured. Both tests were run for a period of twenty four hours. The results are shown in Figs. 6.1 and 6.2, and Tables B.1 and B.2.

Because the space between curves of points 1 and 2 is limited, the curves of points 3 and 4 are not shown on Figs. 6.1 and 6.2.

The maximum depth of scour in a non-cohensive bed material occurs when the drag force caused by the horizontal deflection of the jet by the bed is in equilibrium with the resisting force of the bed material. It is noted that after a model running time of approximately one half hour the maximum depth of scour is formed. At the point of equilibrium, the drag forces may keep some of the bed material in suspension but are not sufficient to transport them away from the scour pit. It is found that the equilibrium condition of the whole scour hole will be reached in the first ninety minutes of the run. Based on these results, a model runtime of two hours is selected.

6.2 Longitudinal Profiles of Scour Holes

The lift coefficient which was stated in Chapter III is found by experimental observations to be, $C_L = 0.0024$. Einstein (55) recommended the value of $C_L = 0.178$. The

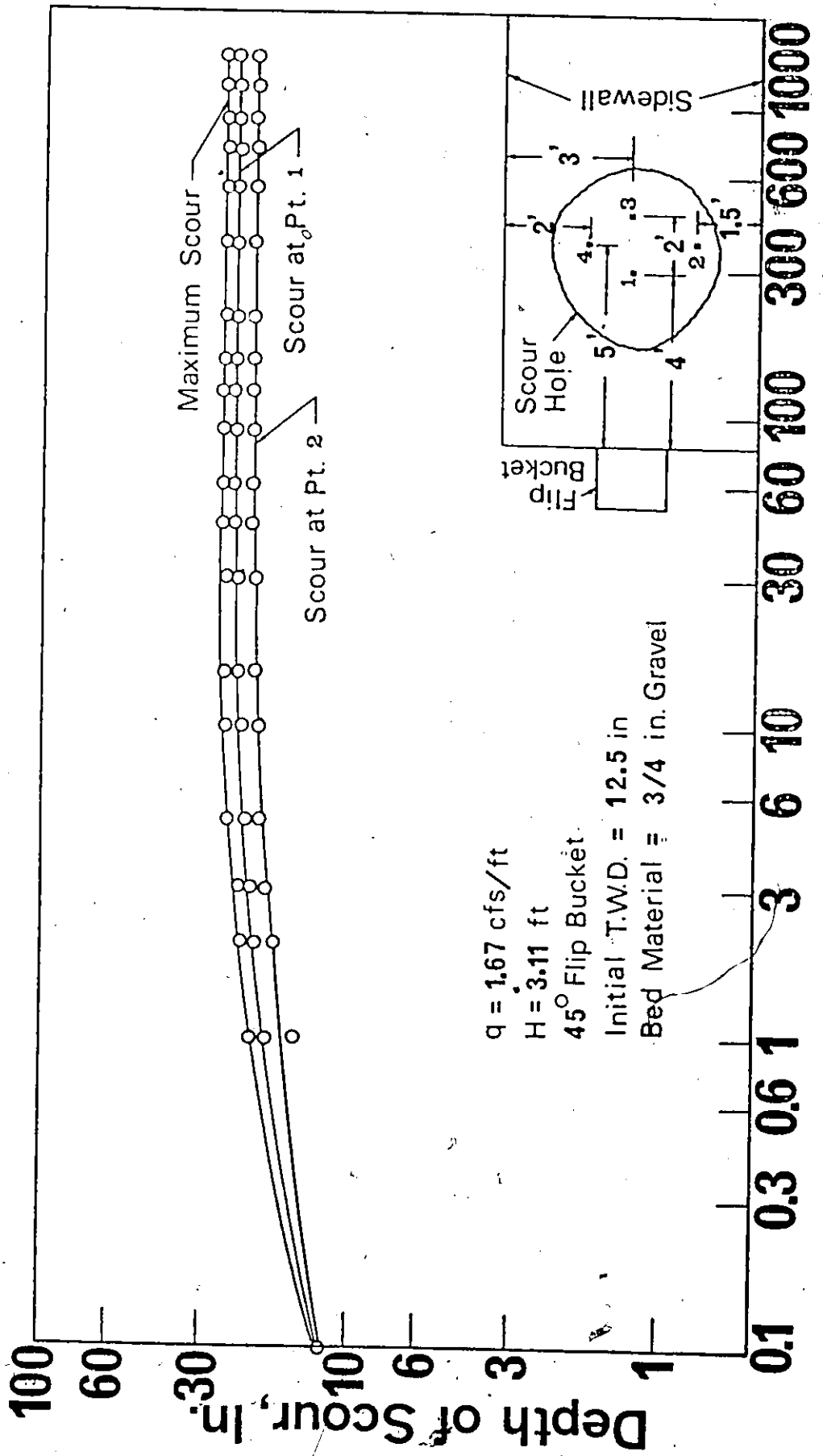

FIG. 6.1 DEVELOPMENT OF SCOUR DEPTH WITH TIME (A)

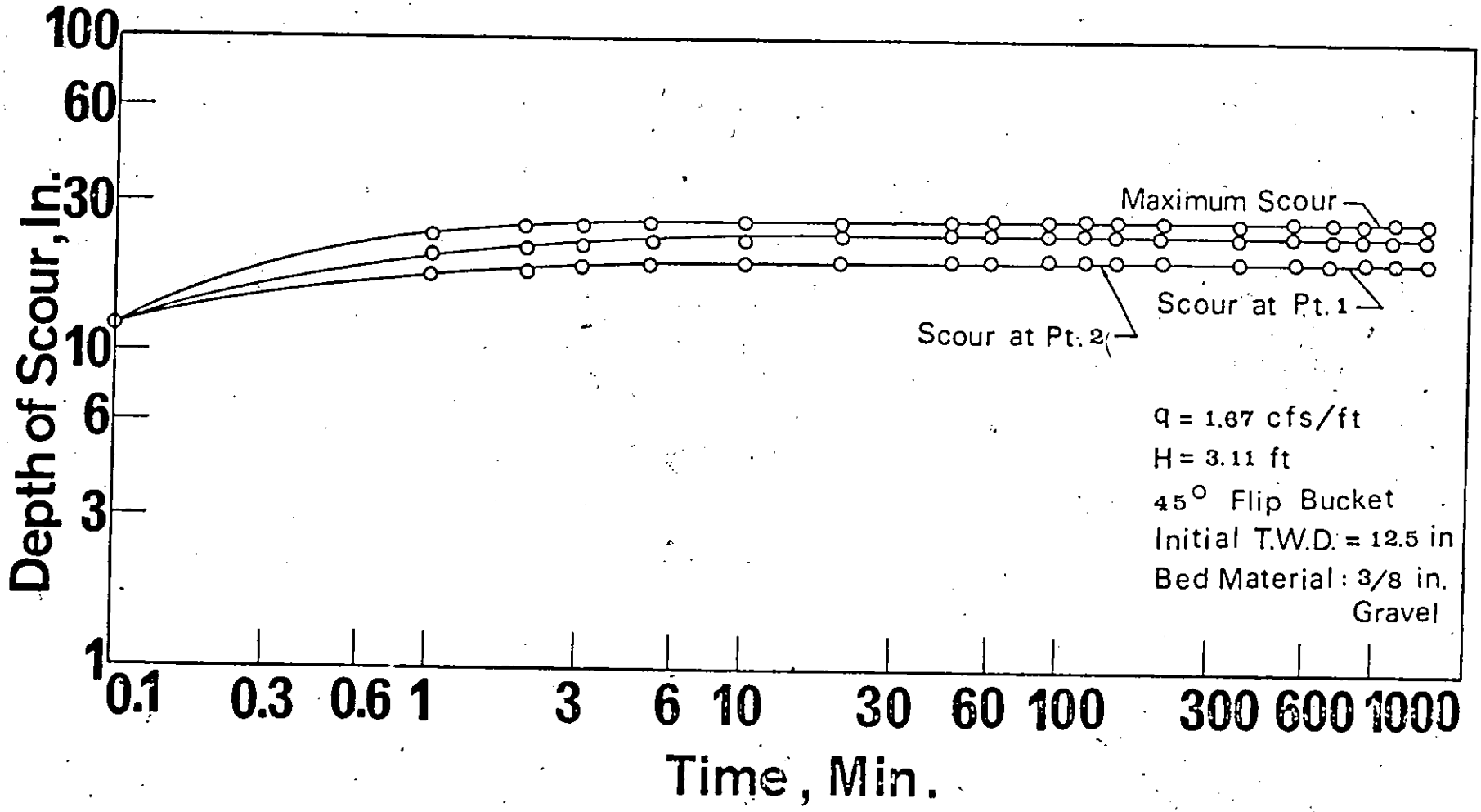

FIG.6.2 DEVELOPMENT OF SCOUR DEPTH WITH TIME (B)

difference between the values of C_L is due to the different velocities used in the analysis. The lift stress suggested by Einstein (55) is

$$L = C_L (\rho / 2) u_{35}^2 \qquad (6.1)$$

where u_{35} = velocity measured at a distance equal to $0.35\, d_{35}$, and

d_{35} = grain size of which 35% by weight of bed material is finer.

However, the velocity used in the present analysis is the maximum velocity at the cross-section.

The coefficient C_2 mentioned in Chapter III is also obtained from the experimental results which is shown in the following table.

Table 6.1

Values of Coefficient C_2

		d/s part of scour hole from the maximum point of scour		u/s part of scour hole from maximum scour point	
d, in.		0.25	0.75	0.25	0.75
C_2	center line	0.0560	0.0968	0.0742	0.1164
	at distance 1/3 R_{90} from C.L.	0.0101	0.0176	0.0149	0.0267
	at distance 2/3 R_{90} from C.L.	0.0039	0.0100	0.0058	0.0157

The fact that the values of C_2 are higher for bigger bed material, may be explained by fact that the roughness is greater with the larger sizes material. The difference in the values of the coefficient between the downstream part and the upstream one is caused by the fact that the flow is always in the same direction to the wall jet in the downstream part, but in the opposite direction to the wall jet in the upstream part. The unit discharge is decreased as

the distance measured from the center line of the scour hole is increased. That is the reason why the coefficient C_2 is decreased as the distance measured from the center line is increased. The variation of the coefficient C_2 is also shown in Fig. 6.3.

Fig. 6.4. shows the comparision between the experimental profiles and the theoretical ones calculated by Eq.(3.29) at the center line of the scour holes with good agreement. The corresponding profiles of scour hole at the distance 1/3 R_{90} and 2/3 R_{90} measured from the center line of the scour hole are shown in Fig. 6.5. Fig. 6.5 also shows the experimental profiles of the scour hole match the calculated ones very well. The results of calculated profiles are given in Tables B.2 , B.3, and B.4.

6.3 Cross-sectional Porfiles of Scour Holes

The cross-sectional profiles of scour holes can be studied under two cases.

Case 1. The spillway width is not very wide. In this case, the profile of scour hole, curve ACB as shown in Fig.6.6.a, can be plotted by Eq.3.47.

$$\frac{y+h}{y_o+h} = \text{Sin}\left(-\frac{\text{Tan}\,\theta}{y_o+h} + \text{Sin}^{-1}\frac{h}{y_o+h} + \frac{\text{Tan}\theta\ R_{90}}{y_o + h}\right) \tag{3.47}$$

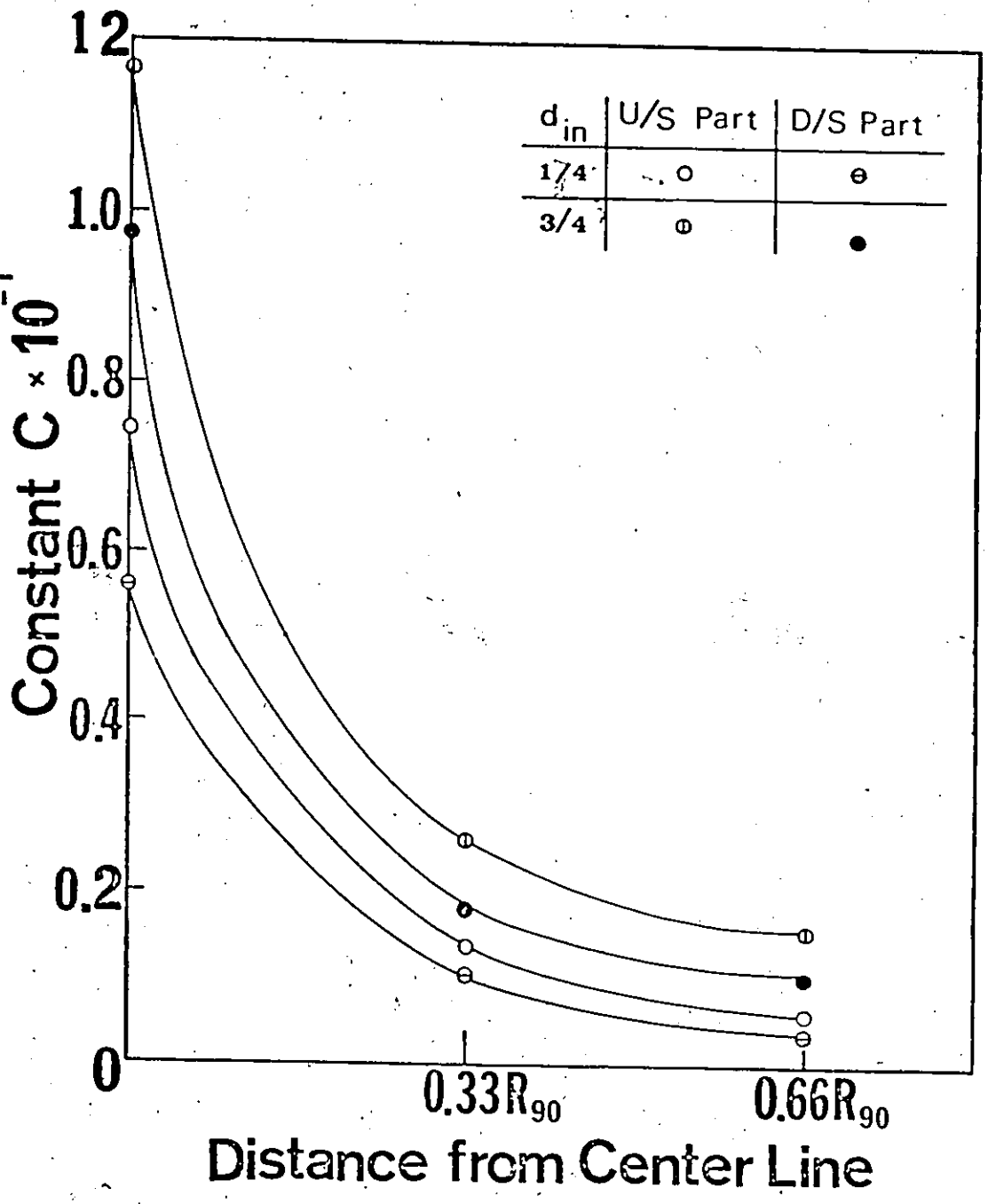

FIG.6.3 VARIATION OF C_2

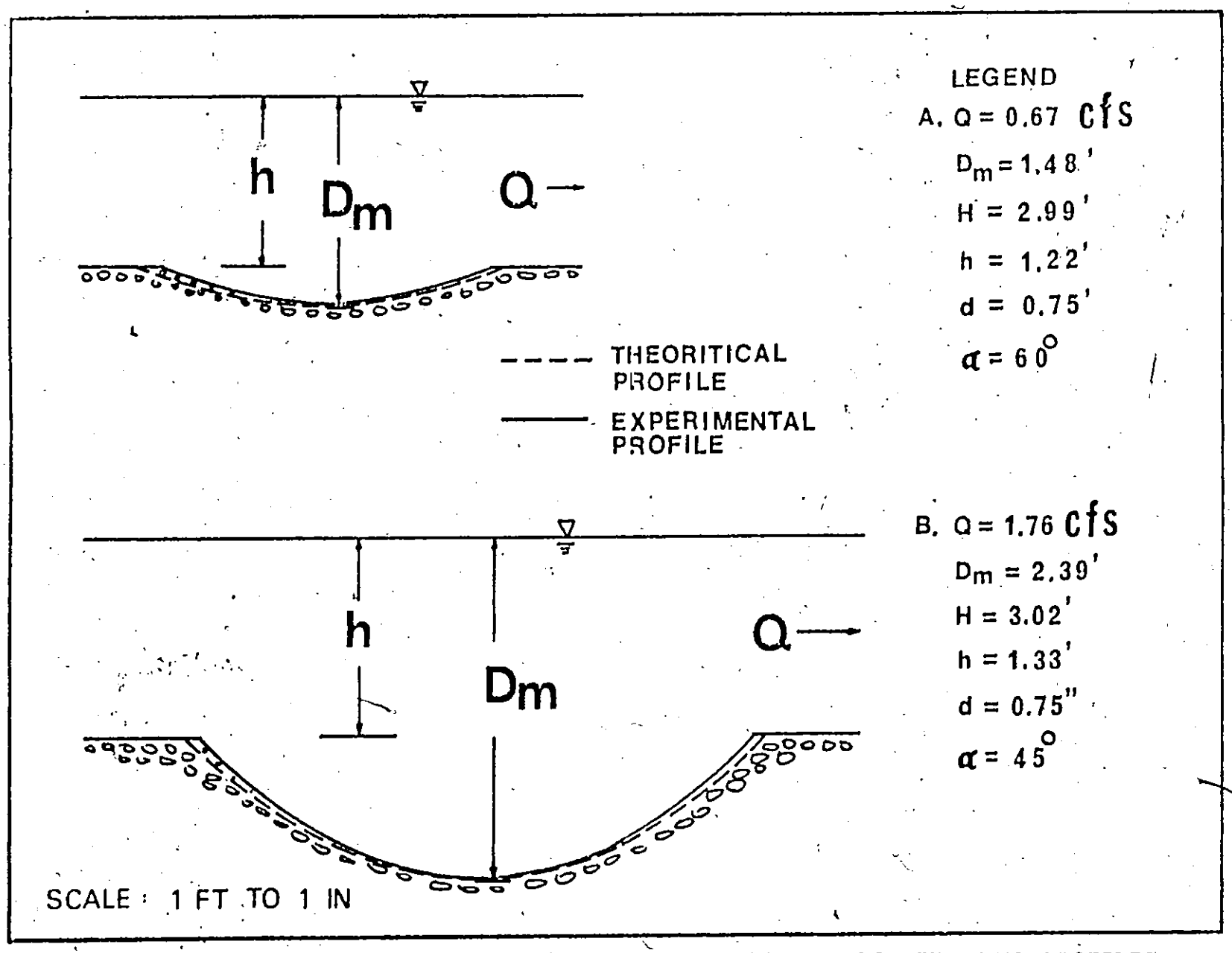

FIG.6.4 COMPARISION BETWEEN THEORETICAL AND EXPERIMENTAL LONGITUDINAL PROFILES OF SCOUR HOLES(A)

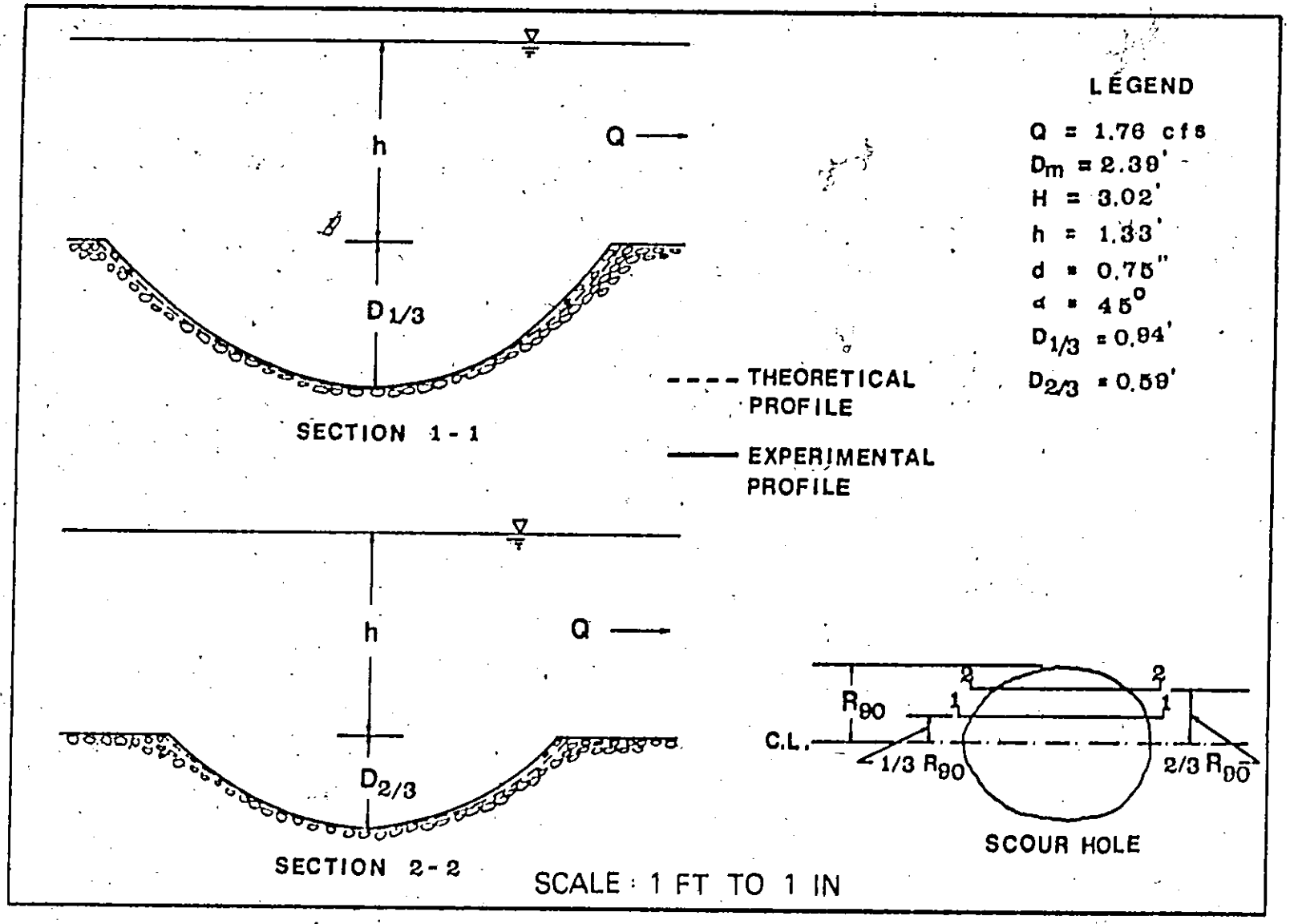

FIG.6.5 COMPARISION BETWEEN THEORETICAL AND EXPERIMENTAL LONGITUDINAL PROFILES OF SCOUR HOLES (B)

The comparision between the experimental profiles and the corresponding ones calculated by Eq.(3.47) are shown in Fig. 6.7. The results of calculated profiles are also shown in Table B.5. The discrepancy between the theoretical and experimental profiles is due to the severe flow curvature on both sides from the section with the maximum scour point.

Although the mechanics of the scour phenomenon is one of the jet action, the measured velocity profiles in the hole and at the sides where no scour occurred are similar as shown in Fig. 6.8. This would explain why the tractive force method of obtaining the cross-sectional shape of scour hole agrees well with the observed profiles.

Case 2. For the wider spillway.

If $1/2\ W'$ is greater than $0.85\ R_{90}$, (6.2)

the cross-sectional profile of scour hole, as shown as the envelope curve A'EDB' in the definition sketch Fig. 6.6.b, can be determined by deviding the entire curve into three parts, i.e. curves A'E, ED, and DB'. The symbol W' denotes the width of wider spillway. Curves A'E and DB can be plotted by Eq.(3.47). The bottom part, line ED, is determined by

$$y' = y_o \tag{6.3}$$

The width R_{90}' of the profiles of scour hole is obtained by

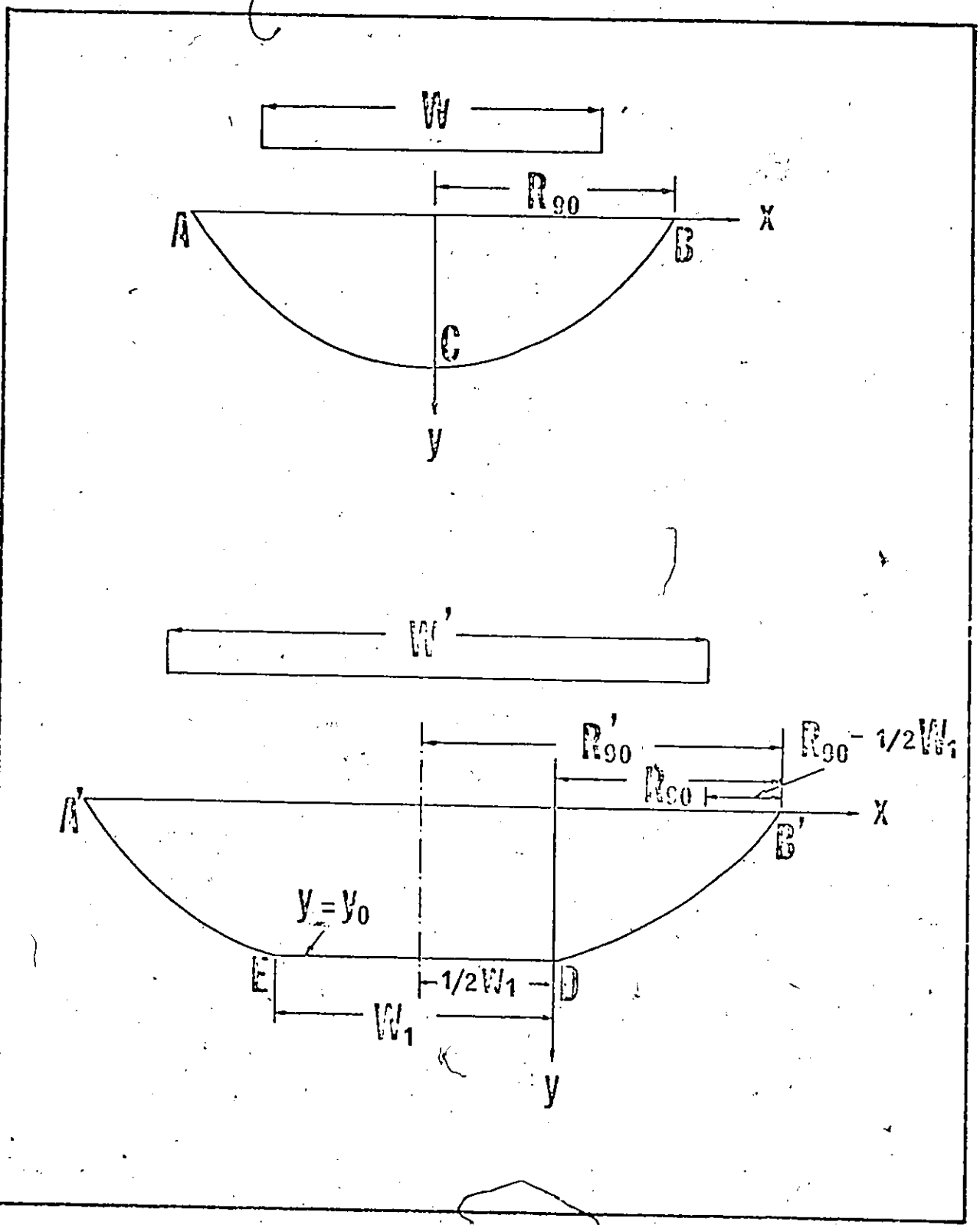

FIG.6.6 DEFINITION SKETCH OF CROSS-SECTIONAL PROFILES OF SCOUR HOLE

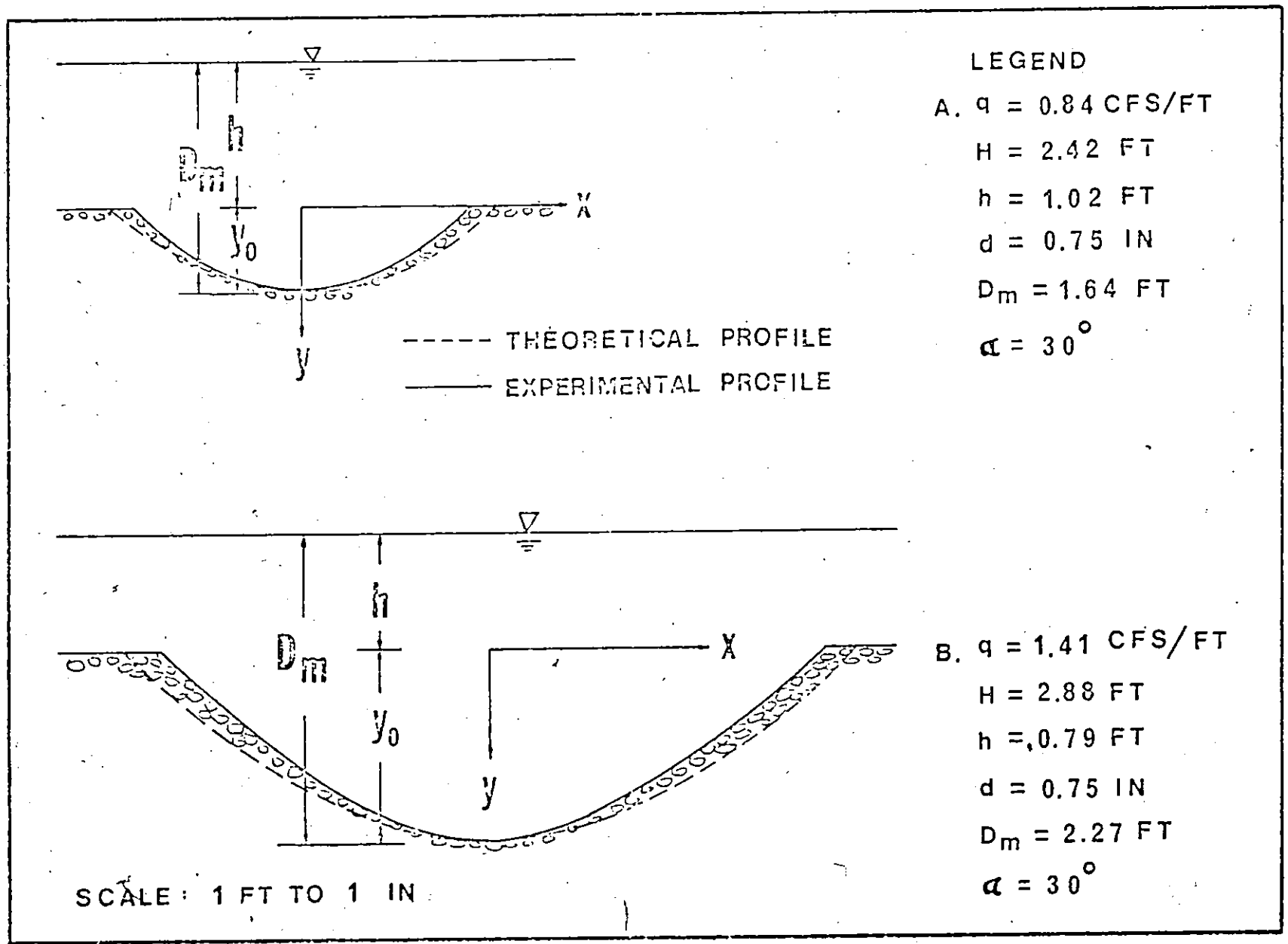

FIG.6.7 COMPARISION BETWEEN THEORETICAL AND EXPERIMENTAL CROSS-SECTIONAL PROFILES OF SCOUR HOLE.

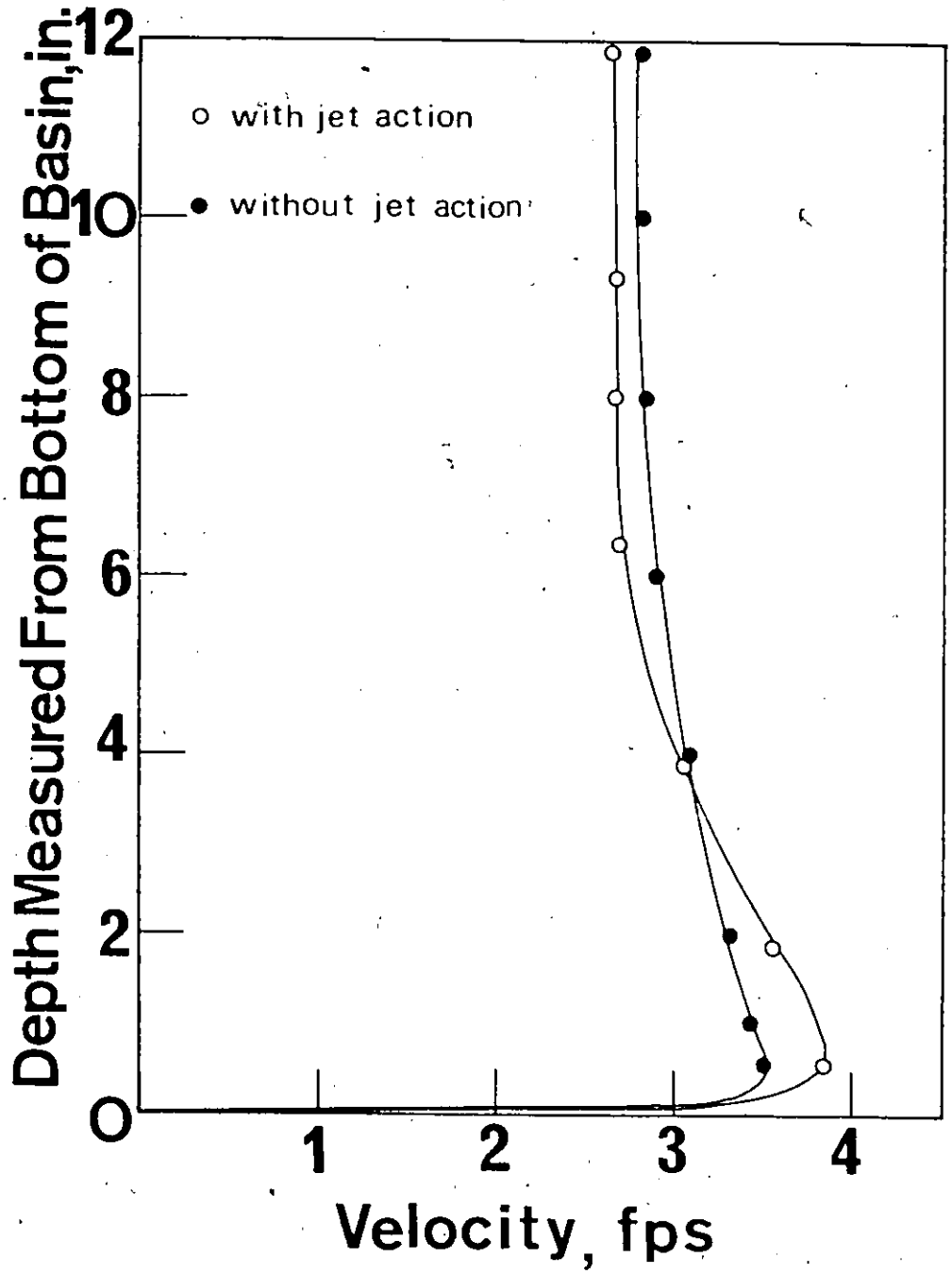

FIG. 6.8 VELOCITY PROFILES AT THE CASES WITH AND WITHOUT THE JET ACTION

the following equation

$$R_{90}' = 1/2\ W' + (R_{90} - 1/2\ W_1) \qquad (6.4)$$

where $$W_1 = 0.85\ R_{90} \qquad (6.5)$$

and $$R_{90} = \frac{\left[\pi/2 - \mathrm{Sin}^{-1}\left(\frac{h}{y_o+h} \right)\right]}{\mathrm{Tan}\ \theta} \left(y_o + h \right) \qquad (6.6)$$

The symbols R_{90}, y_o, h, and O are the same as previously defined. The Eq.(6.6) is obtained after subtituting the value $y = y_o$ with x = 0 into Eq.(3.47). The comparision between the calculated and observed values of R_{90} is shown in Fig. 6.9 with good agreement.

6.4 Maximum Depth of Scour

6.4.a No Scour Hole Formation

The empirical constants C_3, K_3, K_4, K_5, and K_6 mentioned in Eq.(4.8) were determined using the experimental data with the aid of statistical methods. The numerical values of these constants are found to be,

$$C_3 = 0.73 \quad , K_3 = 1.5 \quad , \quad K_4 = 0.35$$

$$K_5 = 0.83 \quad , K_6 = 0.87$$

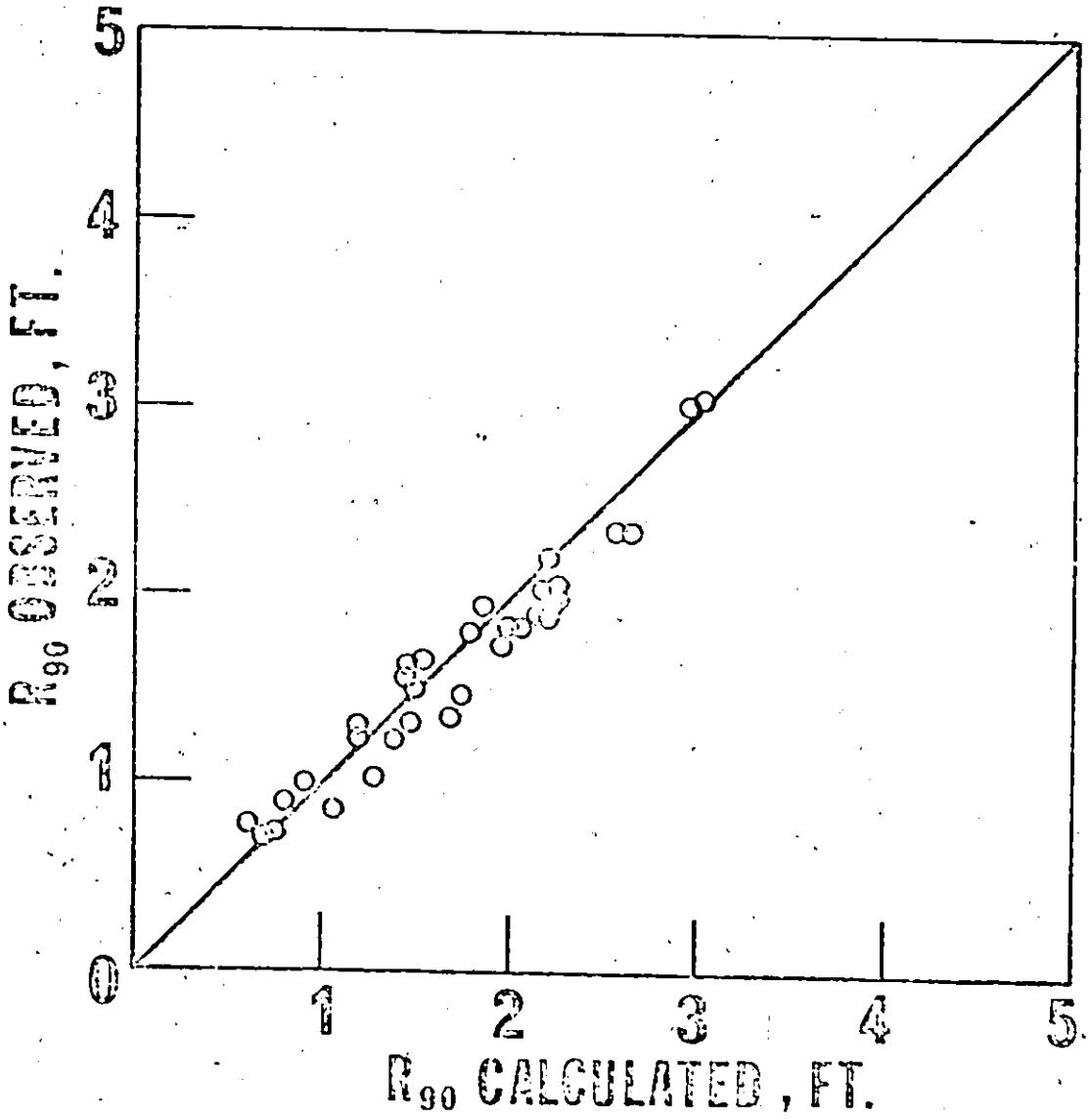

FIG.6.9 COMPARISION OF CALCULATED AND OBSERVED VALUES OF R_{90}

Therefore, the general equation for maximum scour depth becomes,

$$\frac{D_m}{d} = 0.73 \left(\frac{V_m^2}{gd} \right)^{1.5} \left(\frac{1}{S_s - 1} \right)^{0.35} \left(\frac{1}{1 + z/d} \right)^{0.83} \beta^{0.87} \qquad (6.7)$$

Eq.(6.7) is also presented with the 90% confidence limits in Fig. 6.10. It is seen that the value of D_m will increase when the values of V_m and β increase or the values of S_s, d, and z decrease. The increased depth D_m for increasing values of β is a result of the steeper angle of entry of the jet into the tailwater thereby increasing the vertical component of the scour action and causing the jet to plunge deeper into the river bed. It is also seen from Eq.(6.7) that the value of maximum scour depth depends greatly on the velocity of the submerged jet and to a lesser degree on the specific gravity and the ratio of z/d.

The relationship relating the velocity V_m, unit discharge q, head H, and depth D_m can be obtained from Eqs. (4.2),(4.3), and (4.5), as

$$V_m \propto q^{1/2} H^{1/4} D_m^{-1/2} \qquad (6.8)$$

Substituting Eq.(6.8) into Eq.(6.7), the following rela-

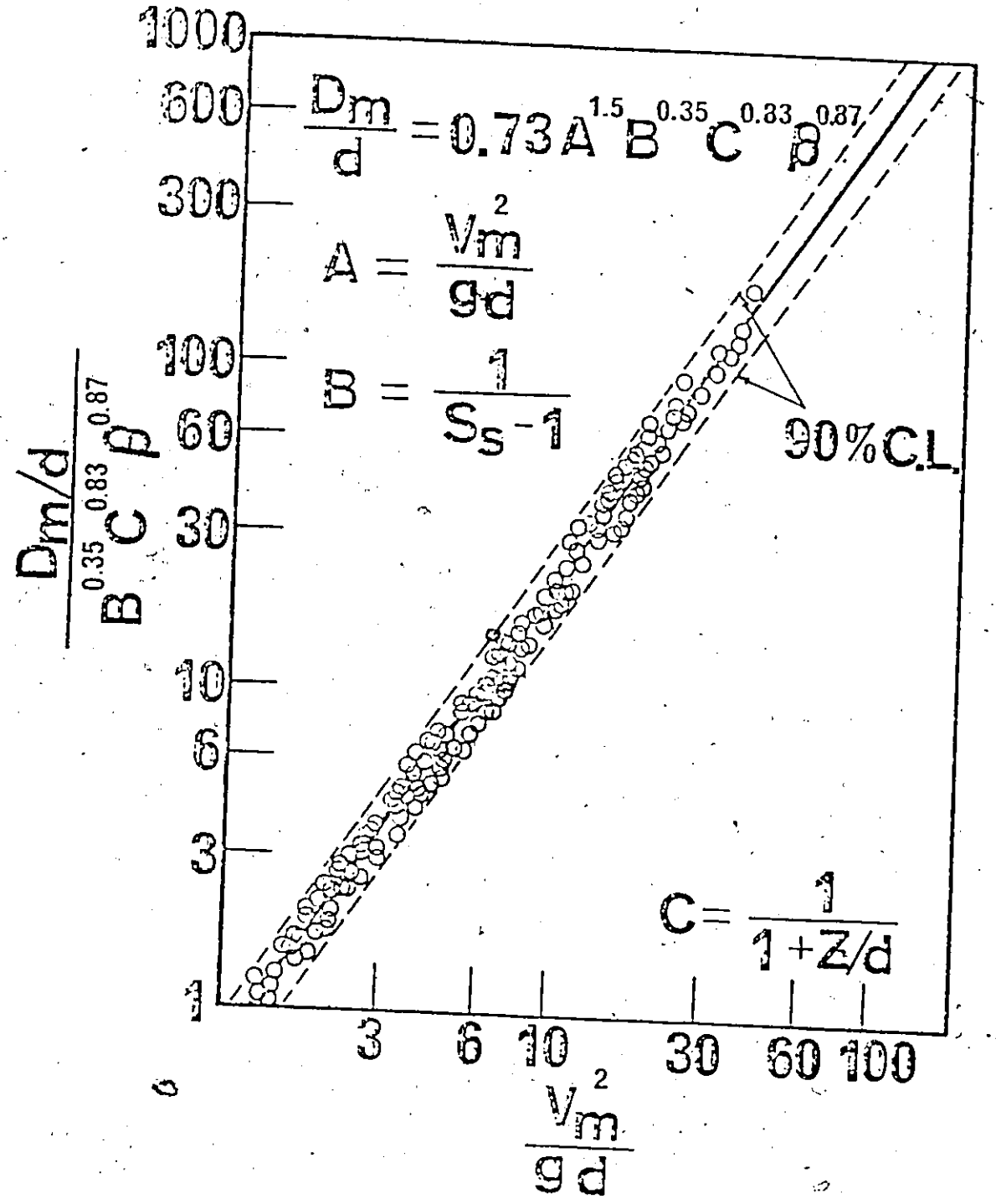

FIG. 6.10 PLOT OF EQ.(6.7)

tionship can be obtained,

$$D_m \propto q^{0.6} H^{0.3} / d^{0.2} \qquad (6.9)$$

Therefore, it is noted that the maximum scour depth is largely affected by the unit discharge and to a lesser extend by the difference in elevation between the reservoir and tail-water levels. It is also indicated that it is not very sensitive to the bed material size. These findings are confirmed by the empirical equations on limiting scour depth suggested by Khosla(34), Schoklitsch (54), Veronese (68), and Chee and Kung (13) mentioned in Chapter II.

6.4.b With Scour Hole Formation

The interlocking action of the bed of gravels is influenced by the angle of repose of the bed material. The greater the angle of repose of the bed material, the larger the resistance to movement and this is reflected in having higher values of the z/d ratio. To relate the relative roughness ratio z/d to stone beds in nature, the z/d ratios of a wide range of gravel beds are determined experimentally and their values are given in Fig. 6.11 and Table 6.2.

Table 6.2

Relative Roughness Ratio z/d

d_{in}	S_s	angularity	0^o	z/d
0.63	2.62	moderately angular	35.1	0.360
1.50	2.59	very angular	39.9	0.479
0.25	2.58	moderately angular	30.2	0.270
0.38	2.56	moderately rounded	25.9	0.170
2.00	2.08	very angular	40.4	0.509
0.63	2.63	moderately rounded	29.8	0.270
0.25	2.55	moderately angular	30.5	0.300
0.75	2.25	moderately angular	36.0	0.400

In this analysis, Eq.(6.7) is used to solve for the ratio z/d while the other quantities are measured in the experiments. The data of this portion of experiments are presented in Table B.6.a.

6.5 Scour Hole Configuration

The dimensions of the scour hole are defined by horizontal and vertical coordinates using the point on the original bed level directly above the deepest scour position as

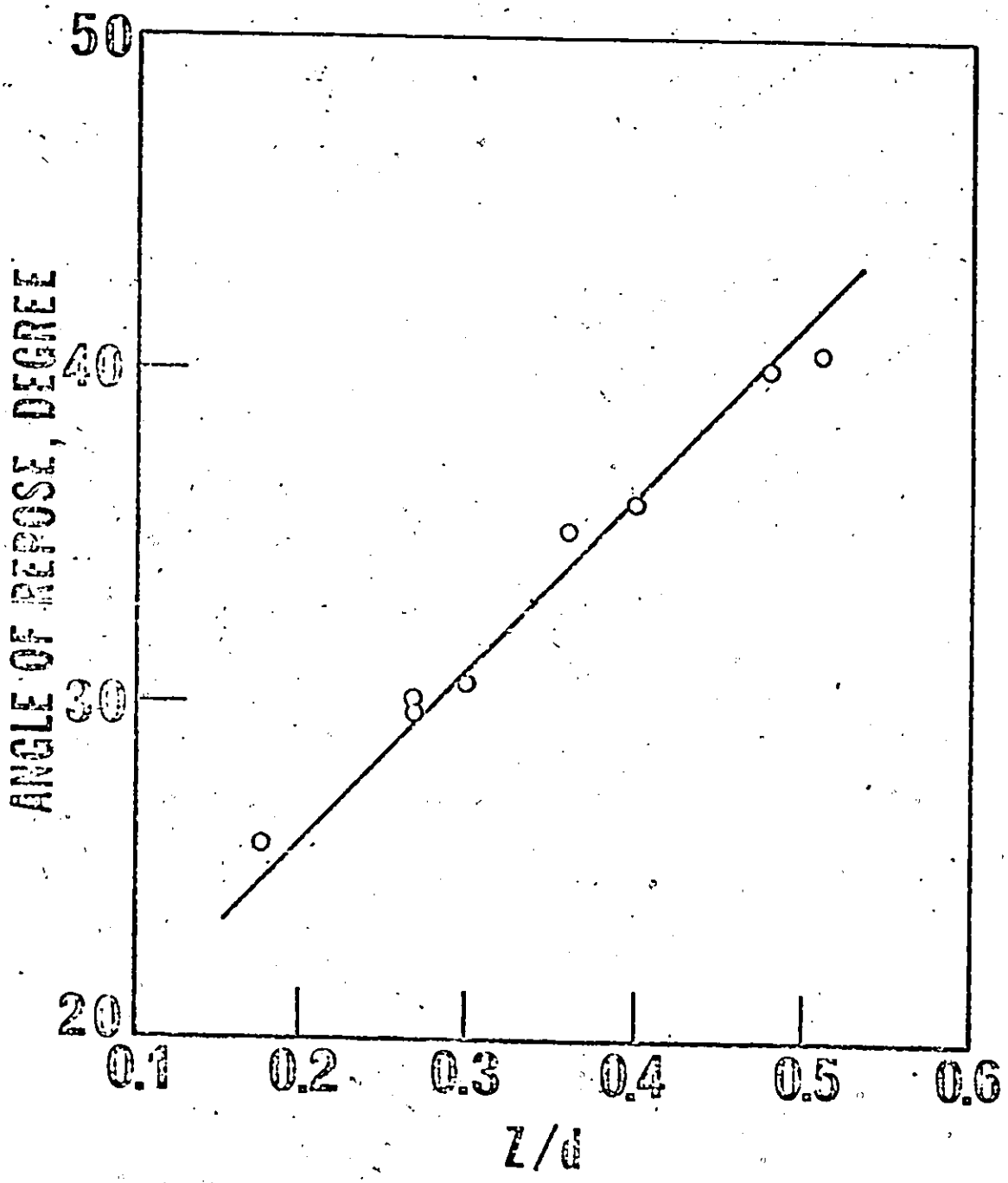

FIG.6.11 VARIATION OF VALUE OF z/d WITH ANGLE OF REPOSE

the origin with radius vectors radiating from it.

6.5.a Radius Vector Length at the Bed Level

The emperical equation for the reference radius vector R_o as found from the experimental data as,

$$R_o = 1.55 \left(D_m - h \right)^{0.24} \qquad (6.10)$$

It is noted that the value of R_o increases as the maximum depth of scour D_m increases. A plot of calculated values of R_o from Eq.(6.10) versus observed ones is presented in Fig.6.12.

The constants C_4 and K_7 mentioned in Eq.(4.11) for solving the radius vector R_O are obtained experimentally as follows,

$$C_4 = 0.094 \qquad (6.11)$$

and

$$K_7 = 0.81 \qquad (6.12)$$

Then, the equation for determining the radius vectors becomes,

$$R_O = R_o \left(1 + 0.095\, \theta_b^{0.81} \right) \qquad (6.13)$$

Fig. 6.13 shows the comparision between the observed

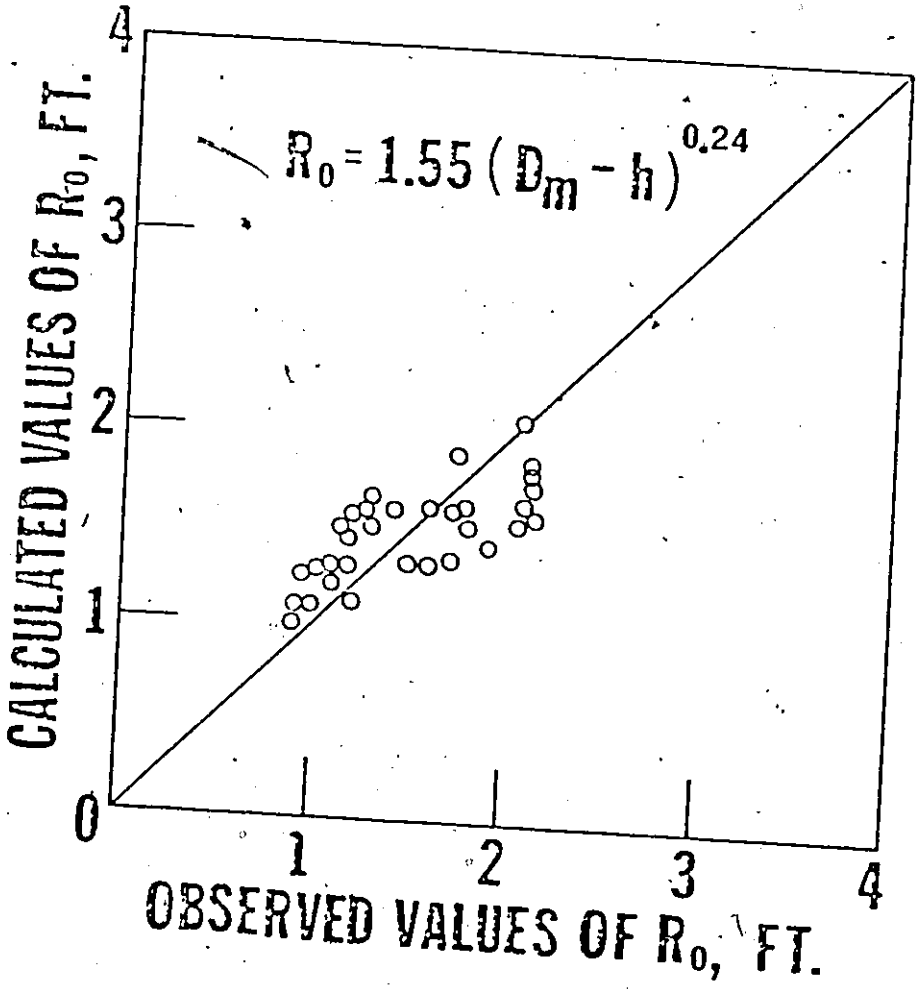

FIG.6.12 PLOT OF OBSERVED VERSUS CALCULATED R_o

values of R_0 and the corresponding ones calculated by Eq.(6.13).

6.5.b Intermediate Depths of Scour

The intermediate scour depths calculated by Eq.(4.13) are verified by experiments which are shown in Fig. 6.13.

$$D = (D_m - h) (1 - r^2/R_\theta^2)$$

The agreement between the experimental depths and calculated ones are good.

6.6 Incipient Motion of Bed Materials below Sharp-edged Weirs

Using experimental data, the empirical equation has the form given by that of Eq.(4.8) using the flip bucket, that is,

$$\frac{D_m}{d} = 3.11 \left(\frac{V_m^2}{gd} \right)^{1.5} \left(\frac{1}{1 + z/d} \right)^{0.83} \beta^{0.87} \qquad (6.14)$$

This equation can determine the maximum depth of scour for given material size and hydraulic conditions. Alternatively, the size of blocks can be obtained by Eq.(6.14) for protecting river beds from erosion at the impact zone of water nappe from overflowing weirs.

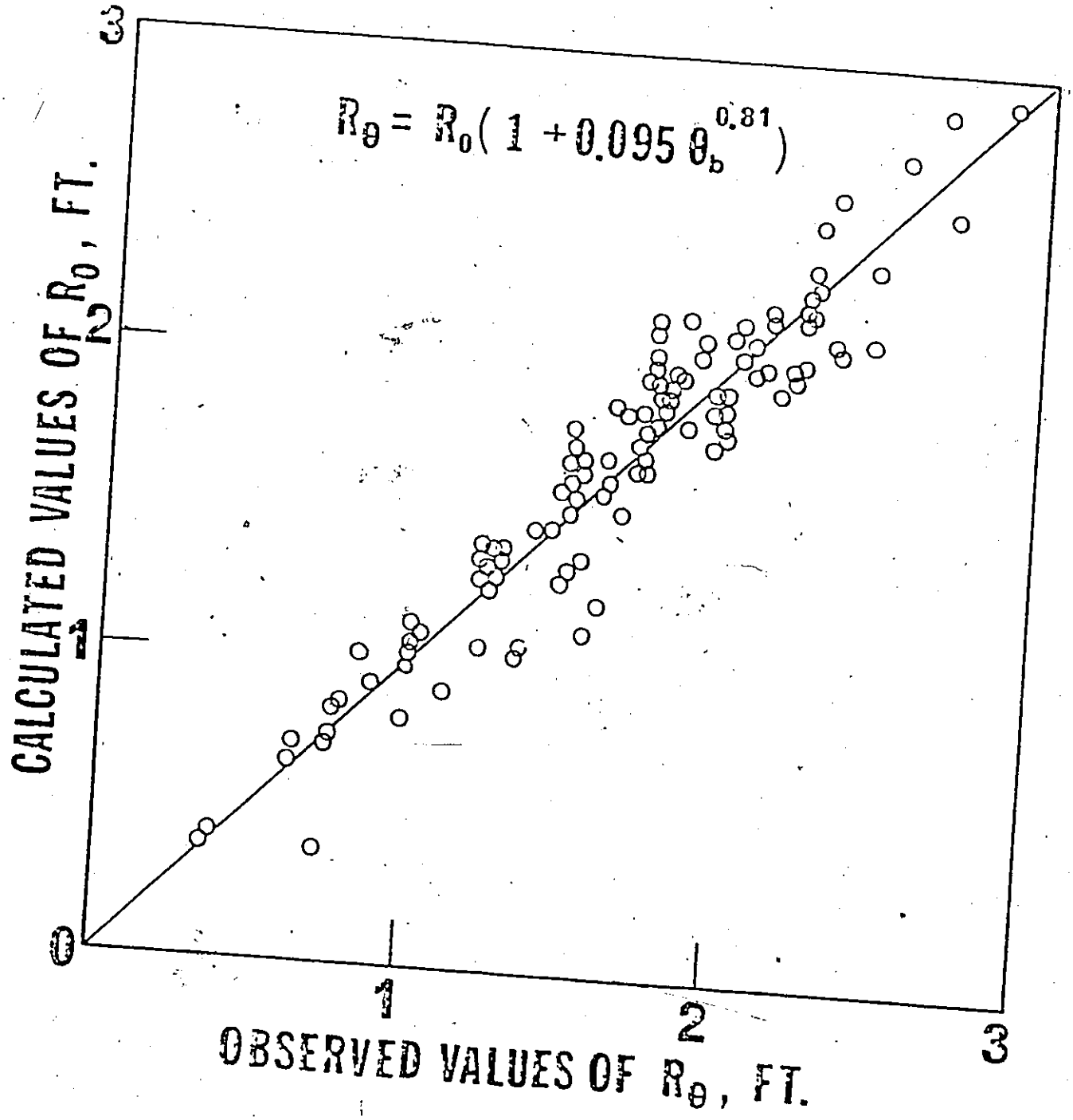

FIG. 6.13 PLOT OF CALCULATED AND OBSERVED R_0

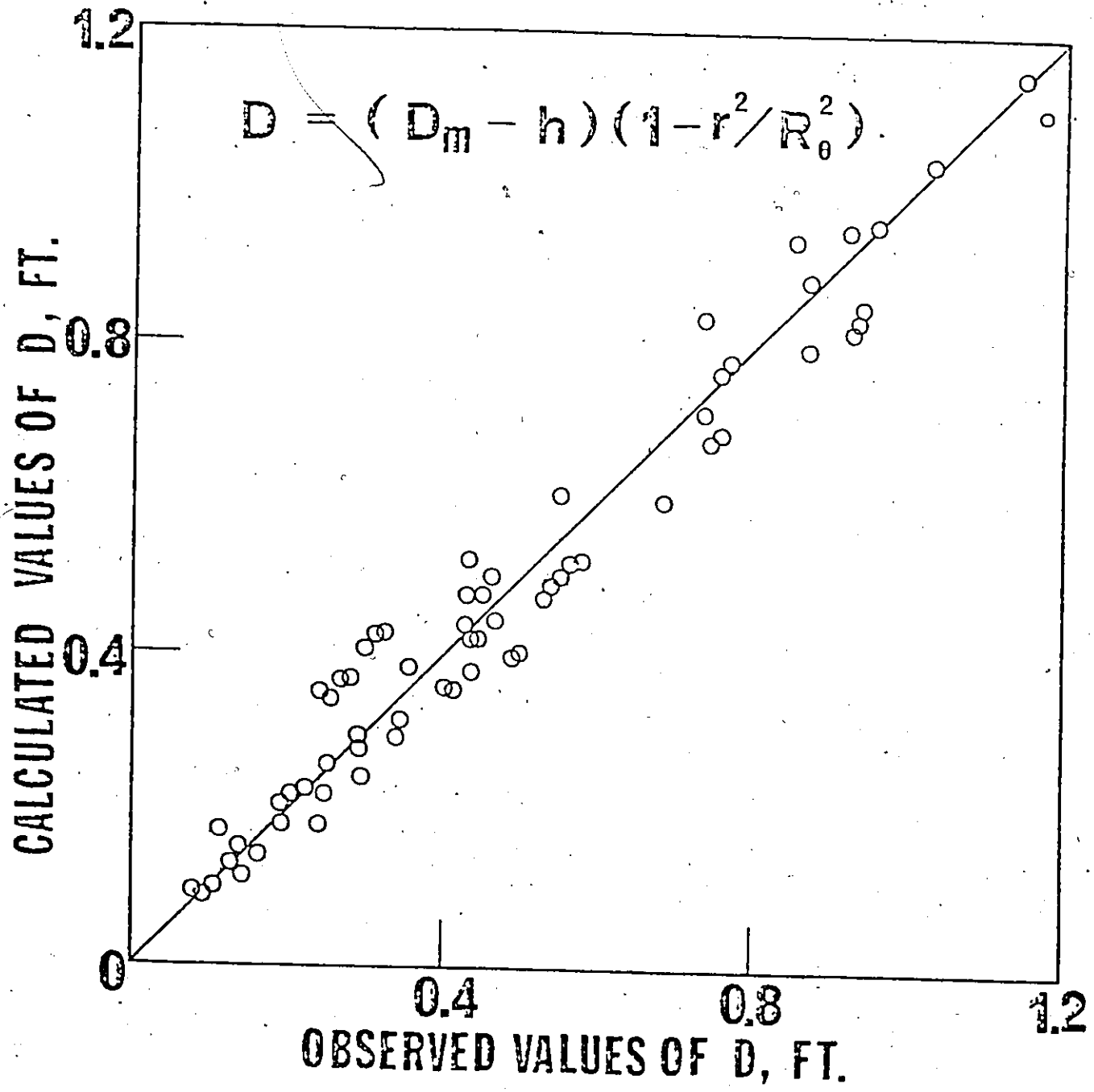

FIG. 6.14 PLOT OF OBSERVED AND CALCULATED DEPTH OF SCOUR

Eq.(6.14) is plotted and shown in Fig. 6.15 with 90% confidence limits.

6.7 Jet trajectory Length

The experimental observations indicate that the observed jet trajectory lengths are about 96% of the values of the calculated ones. This can be expressed as

$$L_{obs.} = 0.96 \left(L_a + L_w \right) \qquad (6.15)$$

where L_a and L_w are determined using Eqs.(4.19),(4.21), and (4.24). This is mainly due to neglecting the effect of air resistance as a retarding factor in the jet trajectory length and the energy losses on the spillway bucket. Therefore, an allowance for air resistance and wind drift should be made in determining throw of the jet in the protype. It has been suggested that protype trajectory lengths are approximately 5% less than the model jet trajectory lengths (20).

6.8 Recommended Shape of Plunge Basin

If the riverbed is made up of homogenous granular material, a dish-shaped hole as formed by a falling water jet. The holes thus formed may progress upstream and undermine the hydraulic structures. One solution to the problem is that a plunge basin

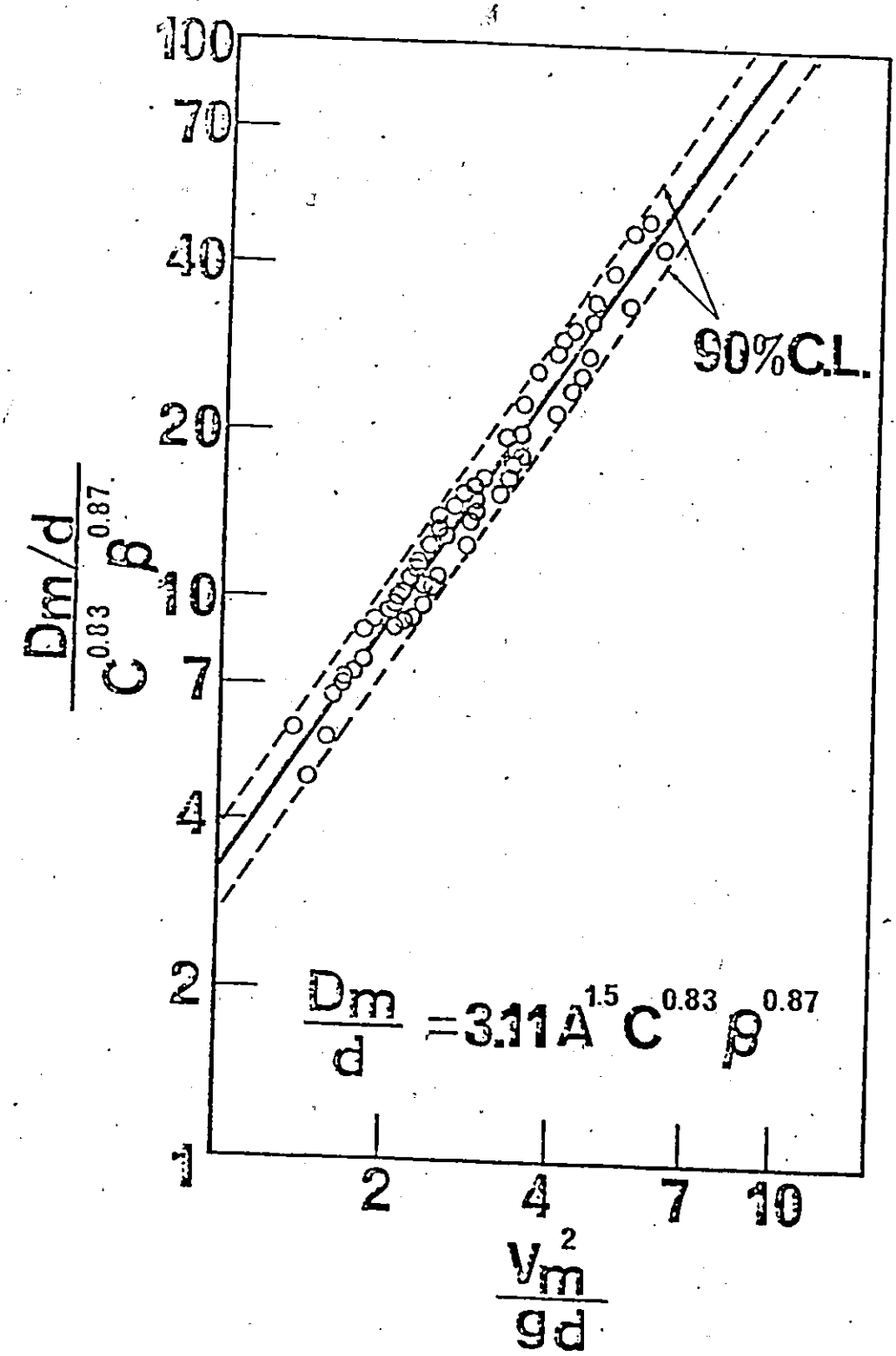

FIG. 6.15 PLOT OF EQ.(6.14)

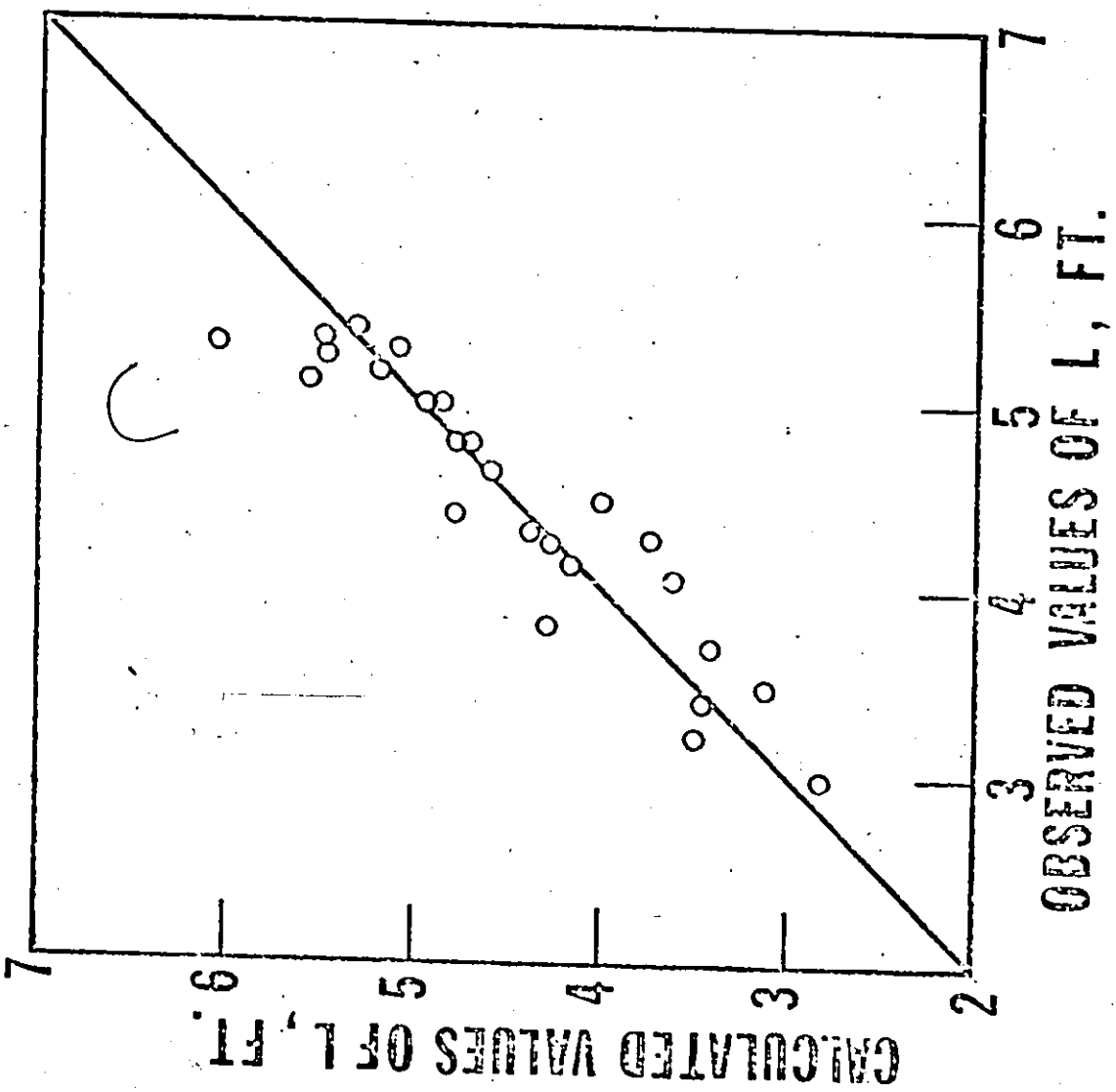

FIG. 6.16 PLOT OF OBSERVED VERSUS CALCULATED L

of the scour hole whose configuration is that observed in the model be excavated in the downstream riverbed.

The recommended shape of plunge basin is discussed as follows.

6.8.a Basin Depth

The maximum water depth of the basin can be computed by Eq.(6.7). In using Eq.(6.7), geological data such as angle of bedding plane and size of bed material lining the river or outlet channel are necessary to the solution of the depth.

6.8.b Trajectory Length

The throw distance of the water jet can be determined from Eqs.(4.21),(4.24) and (4.25). Eq.(4.21) is derived on the assumption that the air resistance is neglected. Allowances for air resistance and wind drift should be made when calculations are applied to the trajectory length of the prototype.

6.8.c Central Basin Cross-section

Fig. 6.17 indicates a plan of the plunge basin. Cross-sections at the deepest part are shown in Fig. 6.17, 6.19, and 6.20. Actual scour hole profiles of two observed cases are included in Figs. 6.19 and 6.20 as well.

The width of the central basin is made equal to the width of the jet which is the width of the spillway bucket if an expansion is not included in the structure. Otherwise,

the width of the jet when it srikes the basin has to be calculated to determine the dimension of the floor width.

For practical and economical considerations, the basin is designed to have a trapezoidal shape with side slopes made equal to the angle of repose of the material which is the maximum angle for stability. This design has been further tested for efficiency and stability in the model over the full range of discharge to ensure that there are no undesirable vortices or erosion.

6.8.d Longitudinal Profiles

The observed longitudinal section is a curved profile and a trapezoidal shape (Figs. 6.17 and 6.18) with different upstream and downstream slopes are fitted around it as shown in Figs. 6.19 and 6.20.

Various horizontal bottom lengths are tried in conjunction with different combinations of upstream and downstream slopes. The best selection is by setting the horizontal floor length not less than the exit width of the bucket.

The downstream part of the basin serves not only to remain stable with turbulence generated by the water jet, but also as a transition for the outlet channel. A slope of 4:1 or flatter performed well in the tests.

As the head falls below the design value, the jet trajectory distance decreases and the water depth of the upstream

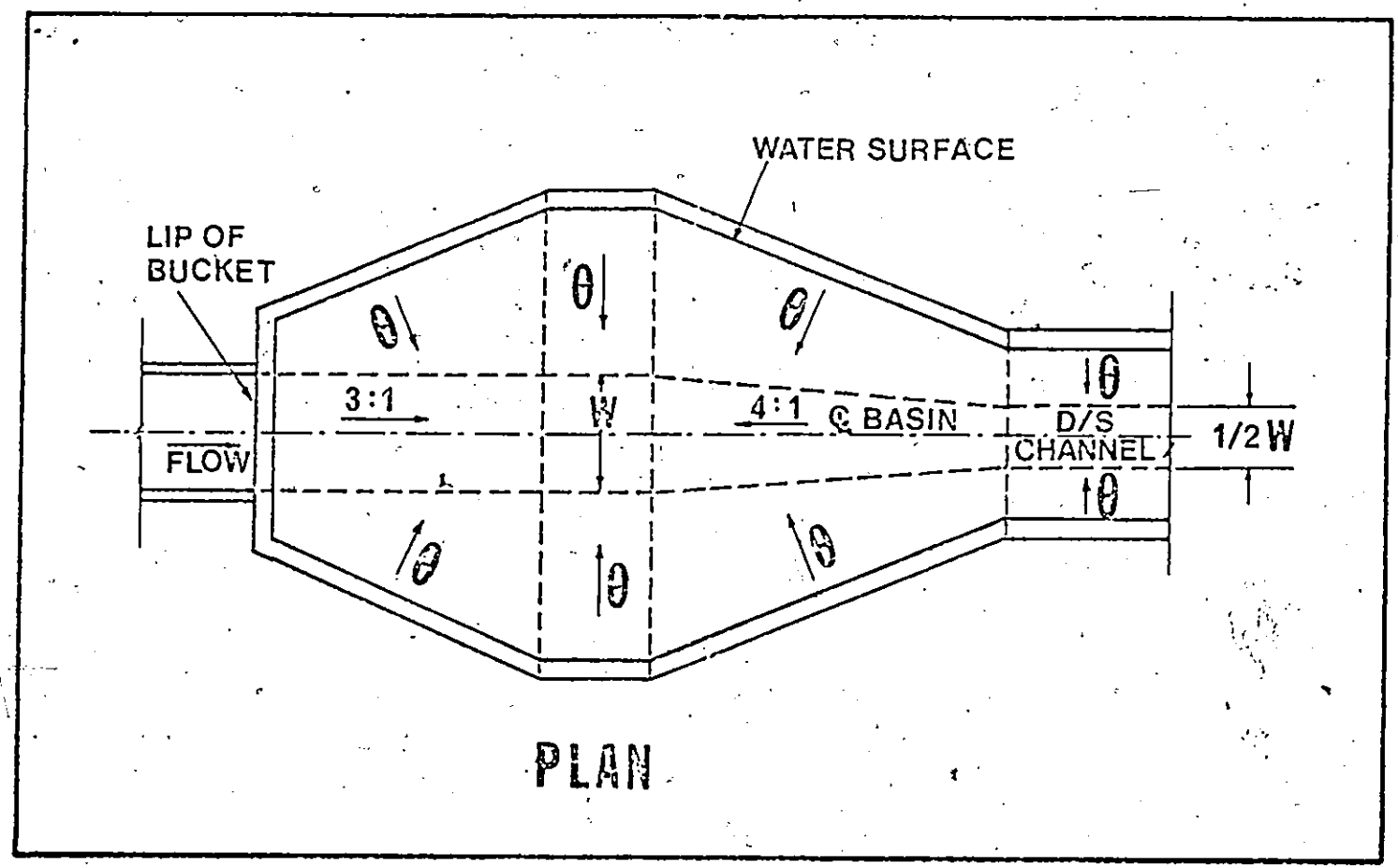

FIG.6.17 PLAN OF RECOMMENDED PLUNGE BASIN

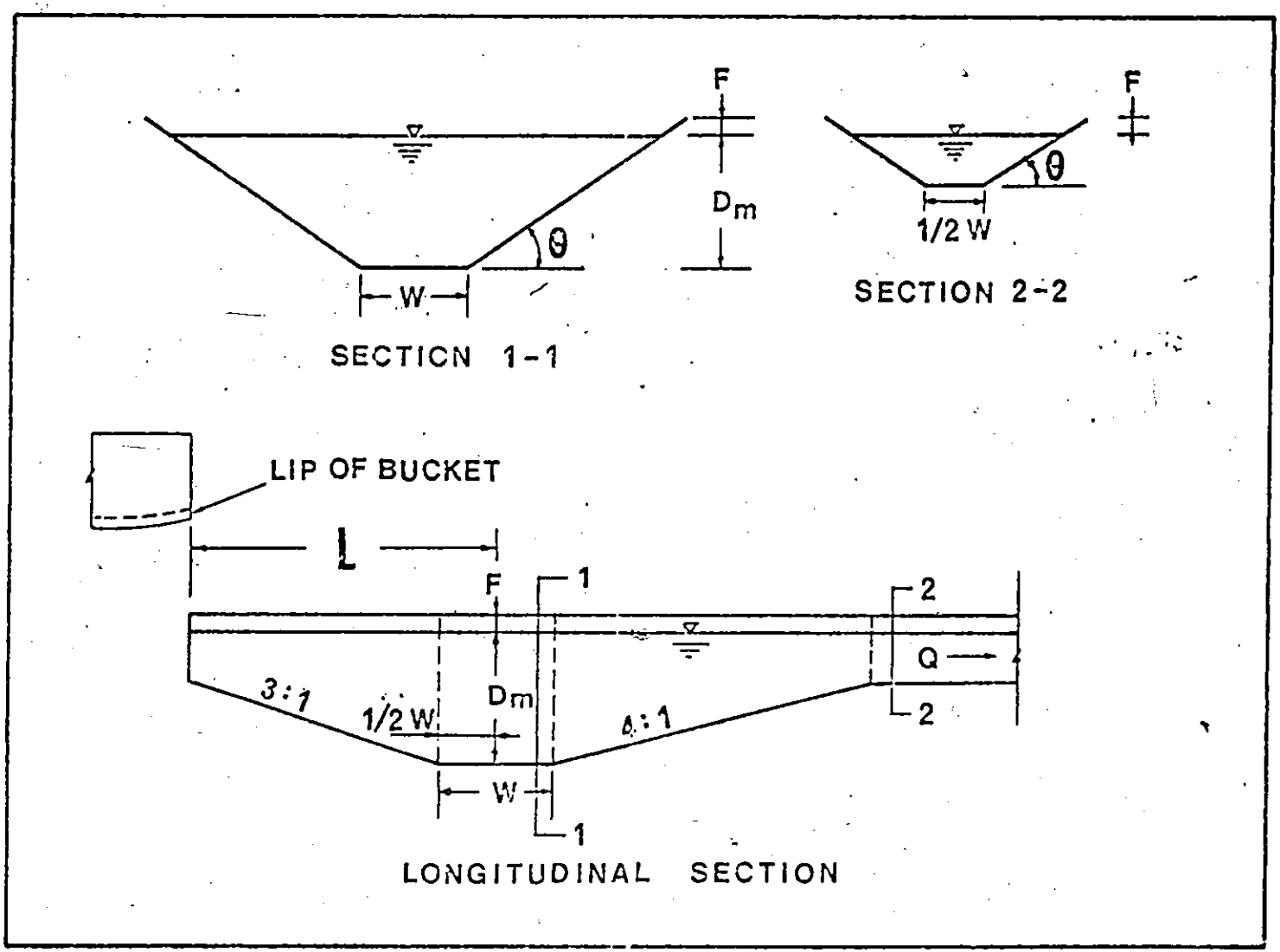

FIG. 6.18 LONGITUDINAL SECTION OF PLUNGE BASIN

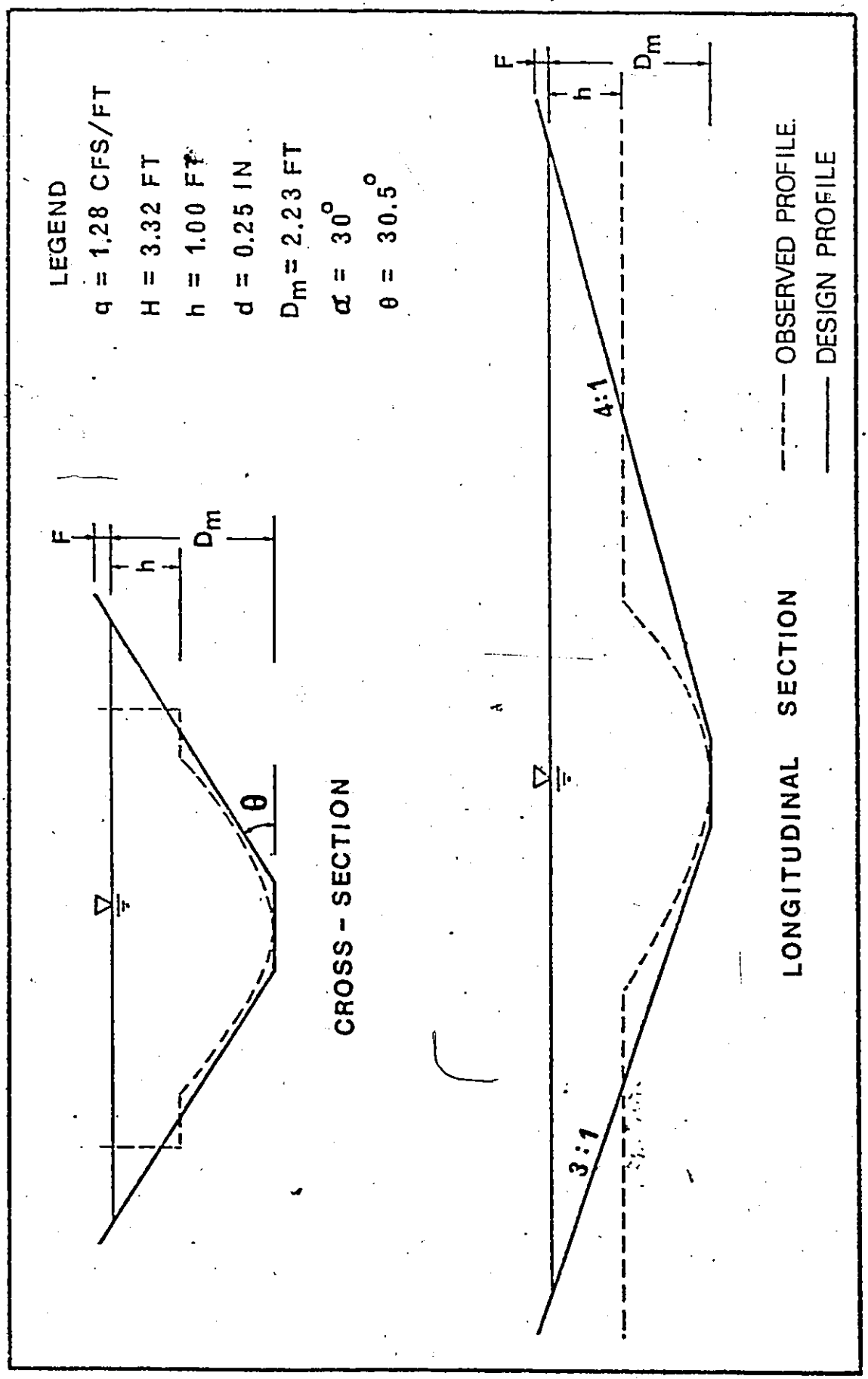

FIG. 6.19 DESIGN AND OBSERVED BASIN PROFILES (A)

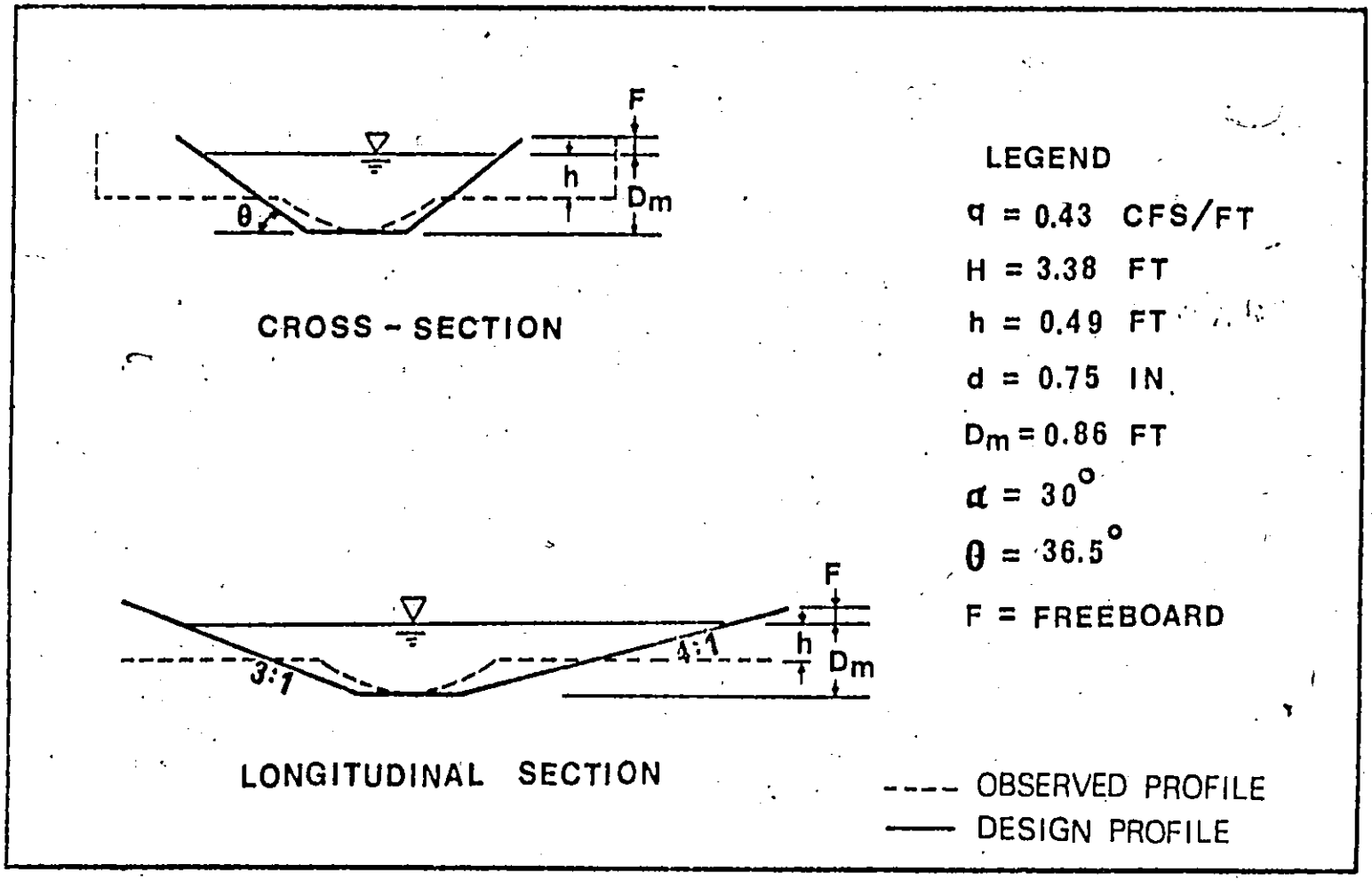

FIG. 6.20 DESIGN AND OBSERVED BASIN PROFILES (B)

face has to be not less than the depth computed using Eq.(6.7). A 3:1 slope or steeper is found to perform successfully.

6.8.e Corner Side Slopes

The four side slopes have been tested using the angle of repose of the bed material to obtain minimum basin size. It is verified that the actual scour profiles are encompassed by these surfaces.

CHAPTER VII

CONCLUSIONS

The scour of bed materials below deflector buckets have been broadly investigated. The conclusions reached are as follows.

a) The longitudinal profiles of scour holes can be predicted by the theories of the wall jet and the submerged diffusion jet. The solution is given by Eq.(3.29).

b) The cross-sectional profiles of scour holes can be obtained using the principles of tractive force as given by Eq.(3.47).

c) For given flow conditions, characteristics of bed materials, and angle of bucket, the maximum depth of scour below the bucket can be determined by Eq.(6.7). The corresponding case for weirs can be solved by Eq.(6.14).

d) The location of the maximum scour point can be determined applying the theory of the simple projectile with good accuracy under laboratory conditions.

e) Based on the calculations using Eqs.(3.29),(3.47), (6.14),(4.21) and (4.25), the scour basin can be plotted. As the entire surface in curved, it is not an economical shape for construction. A trapezoidal shape as shown in Figs.6.17 and 6.18 is suggested as the most feasible one for construction.

APPENDIX A

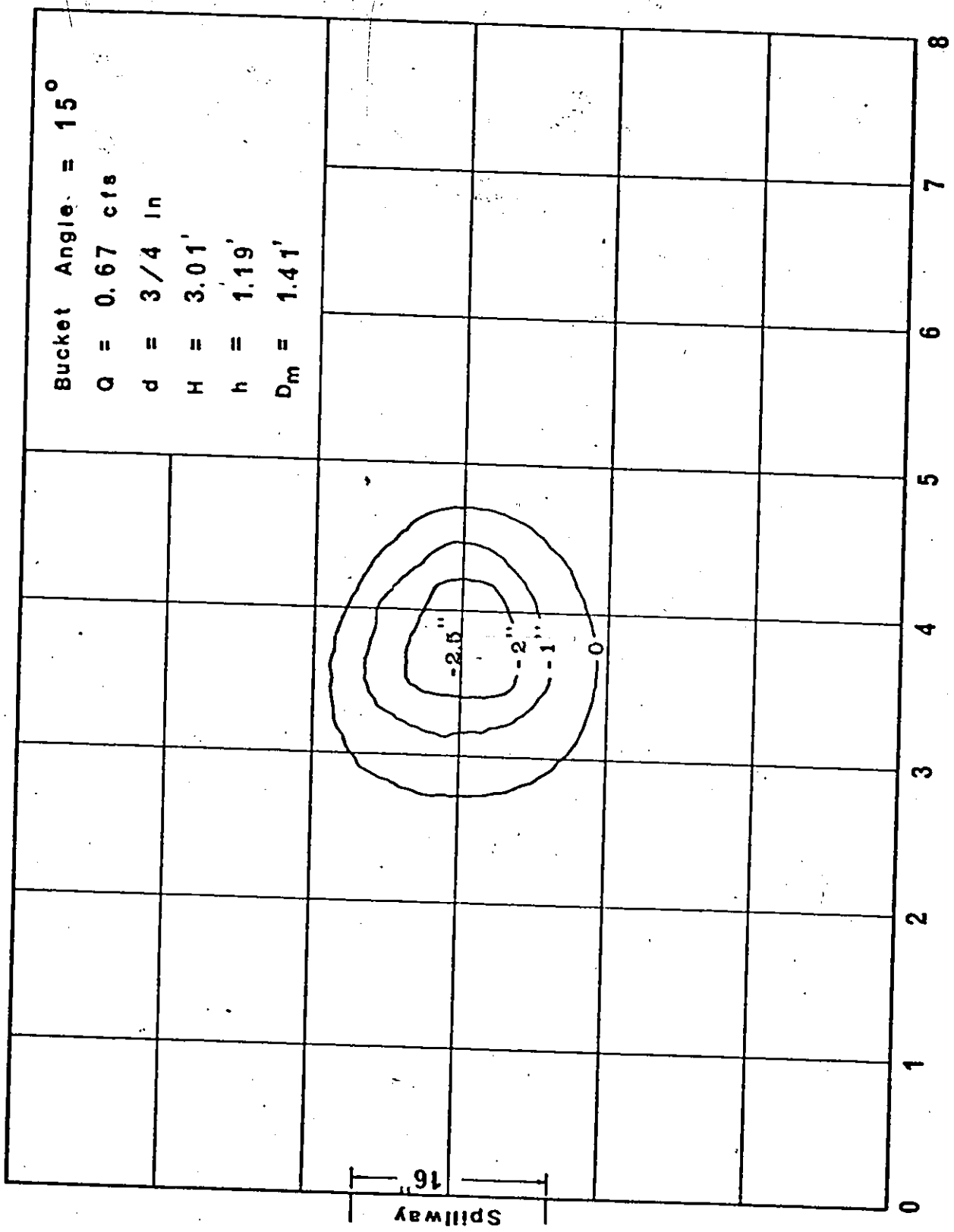
Bucket Angle = 15°
Q = 0.67 cfs
d = 3/4 in
H = 3.01'
h = 1.19'
D_m = 1.41'
-2.5"
-2"
-1"
0
16"
Spillway
0
1
2
3
4
5
6
7
8

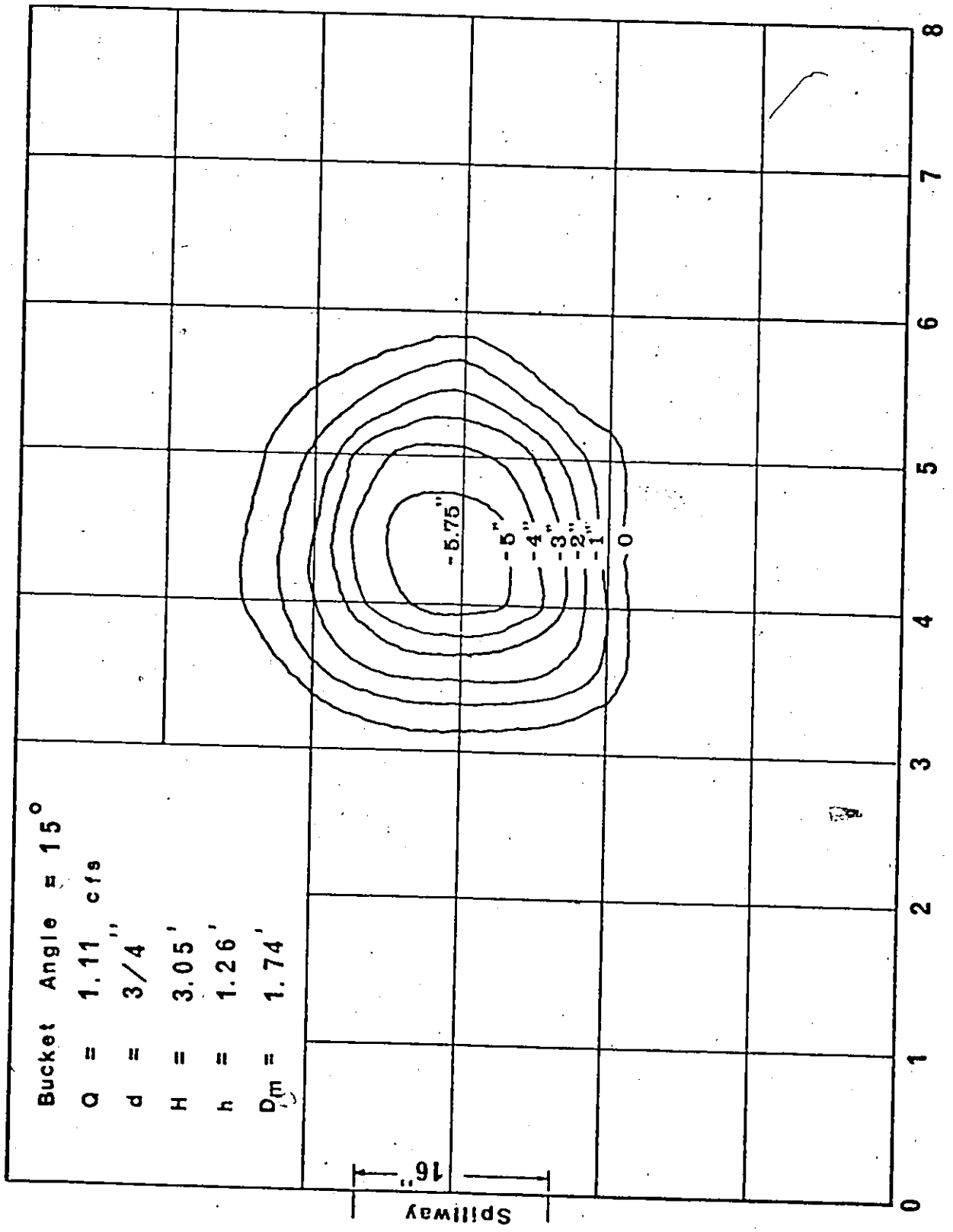
Bucket Angle = 15°
Q = 1.11 cfs
d = 3/4"
H = 3.05'
h = 1.26'
Dm = 1.74'
-5.75"
-5"
-4"
-3"
-2"
-1"
0
16"
Spillway
0
1
2
3
4
5
6
7
8

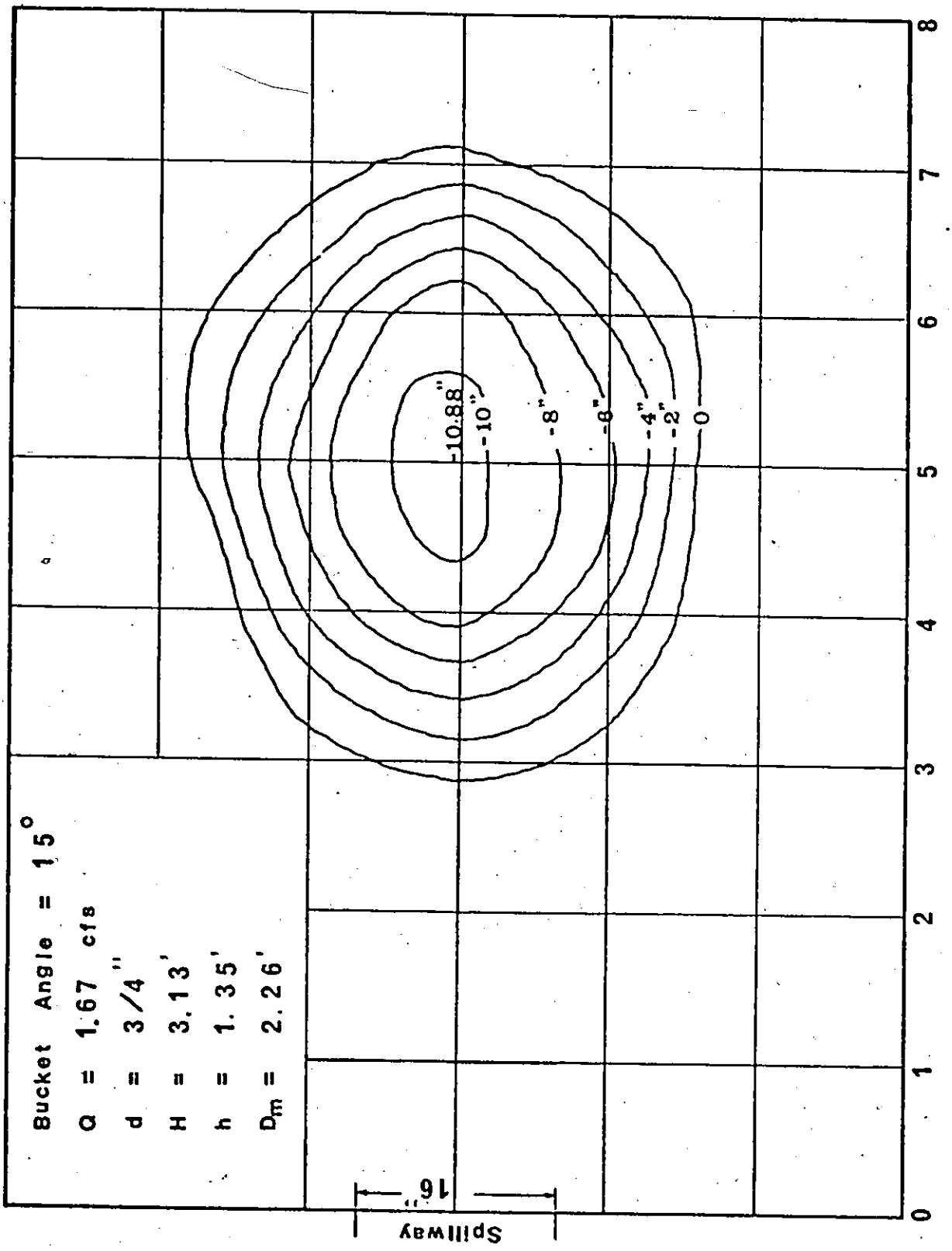
Bucket Angle = 15°
Q = 1.67 cfs
d = 3/4"
H = 3.13'
h = 1.35'
D_m = 2.26'
-10.88"
-10"
-8"
-8"
-4"
-2"
0
16"
Spillway
0
1
2
3
4
5
6
7
8

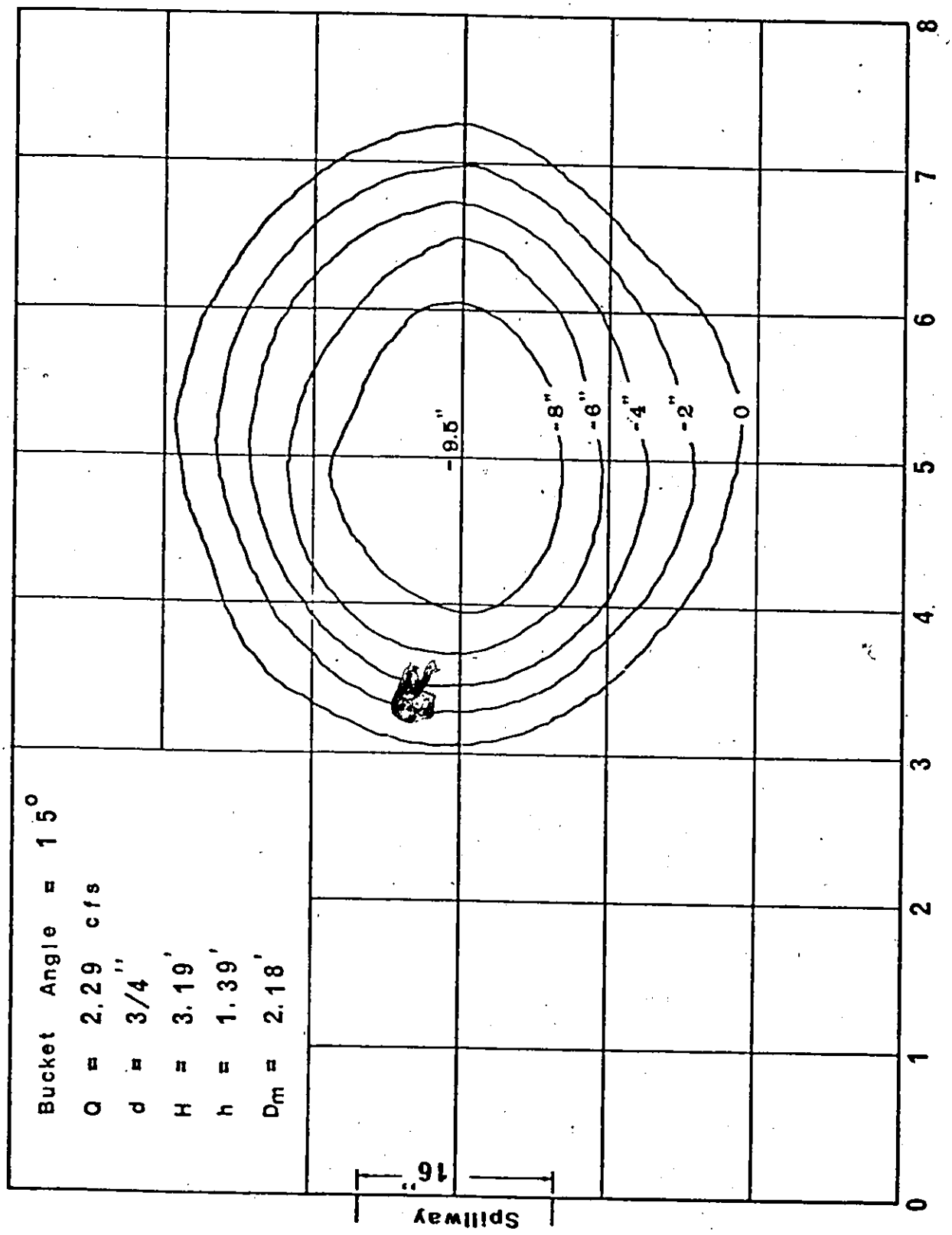
Bucket Angle = 15°
Q = 2.29 cfs
d = 3/4"
H = 3.19'
h = 1.39'
Dm = 2.18'
-9.5"
-8"
-6"
-4"
-2"
0
16"
Spillway
0
1
2
3
4
5
6
7
8

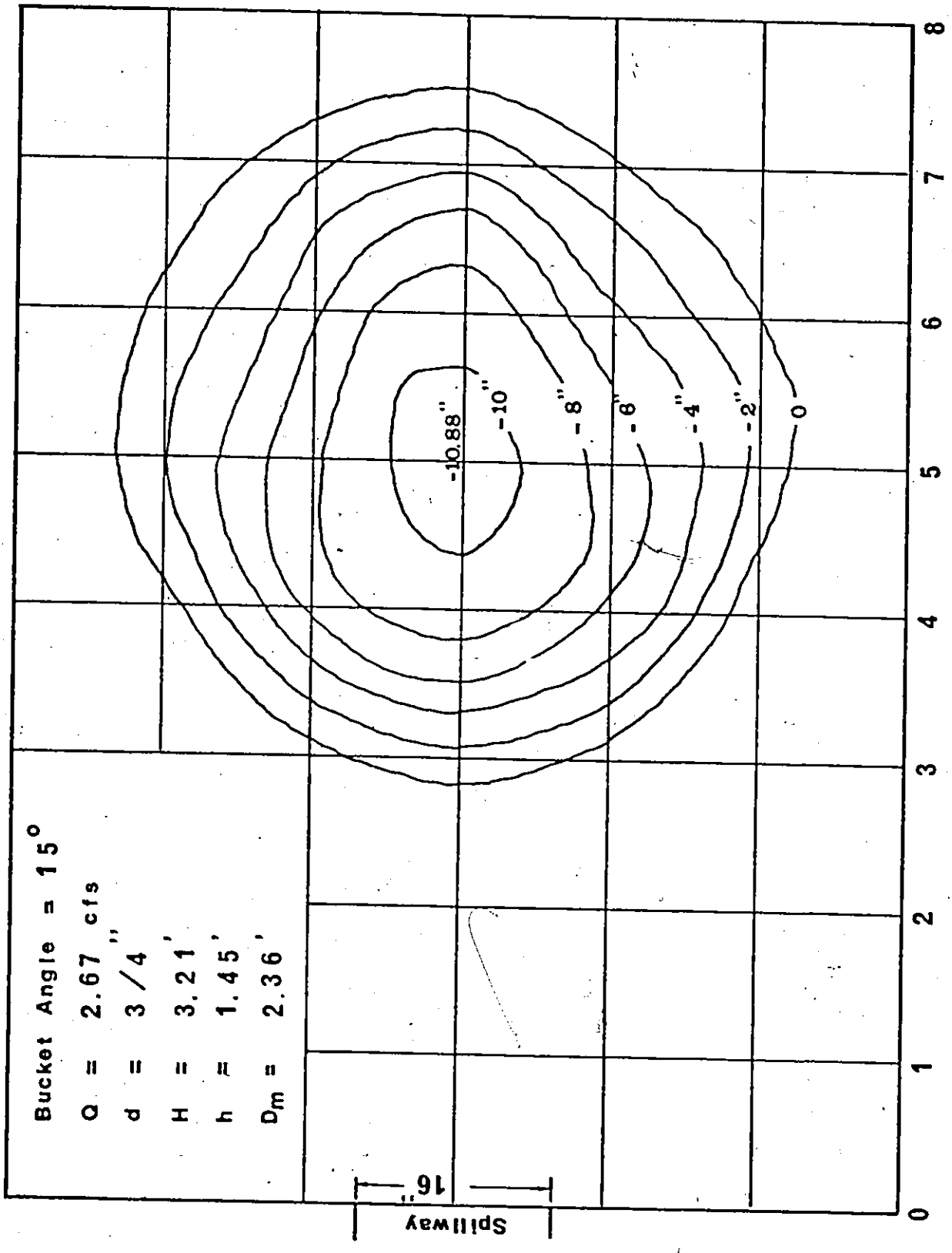
Bucket Angle = 15°
Q = 2.67 cfs
d = 3/4"
H = 3.21'
h = 1.45'
D_m = 2.36'
-10.88"
-10"
-8"
-6"
-4"
-2"
0
16"
Spillway
0
1
2
3
4
5
6
7
8

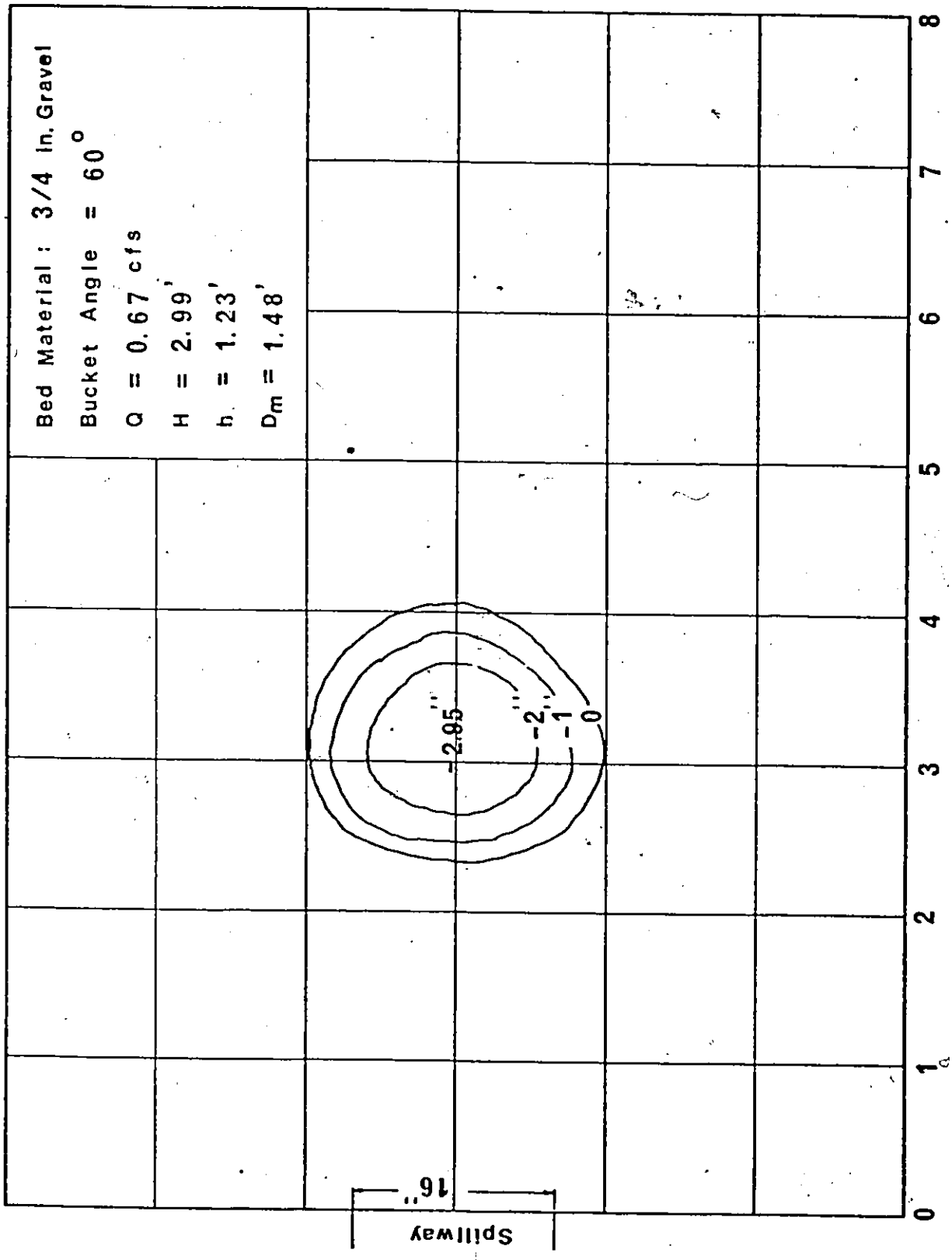
Bed Material : 3/4 in. Gravel
Bucket Angle = 60°
Q = 0.67 cfs
H = 2.99'
h = 1.23'
D_m = 1.48'
-2.95''
-2''
-1
0
16''
Spillway
0
1
2
3
4
5
6
7
8

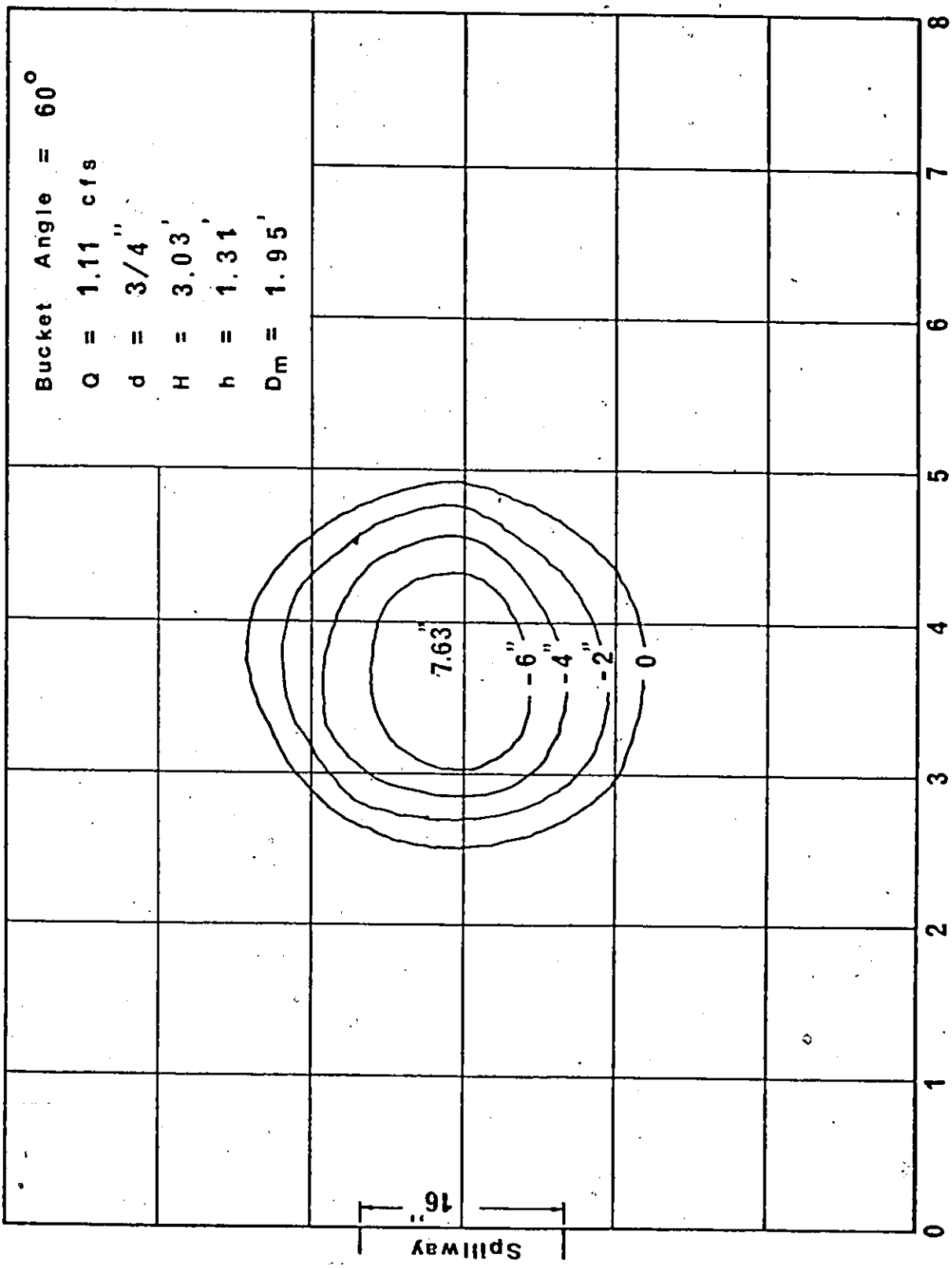
Bucket Angle = 60°
Q = 1.11 cfs
d = 3/4"
H = 3.03'
h = 1.31'
Dm = 1.95'
7.63'
-6"
-4"
-2"
0
16'
Spillway
0
1
2
3
4
5
6
7
8

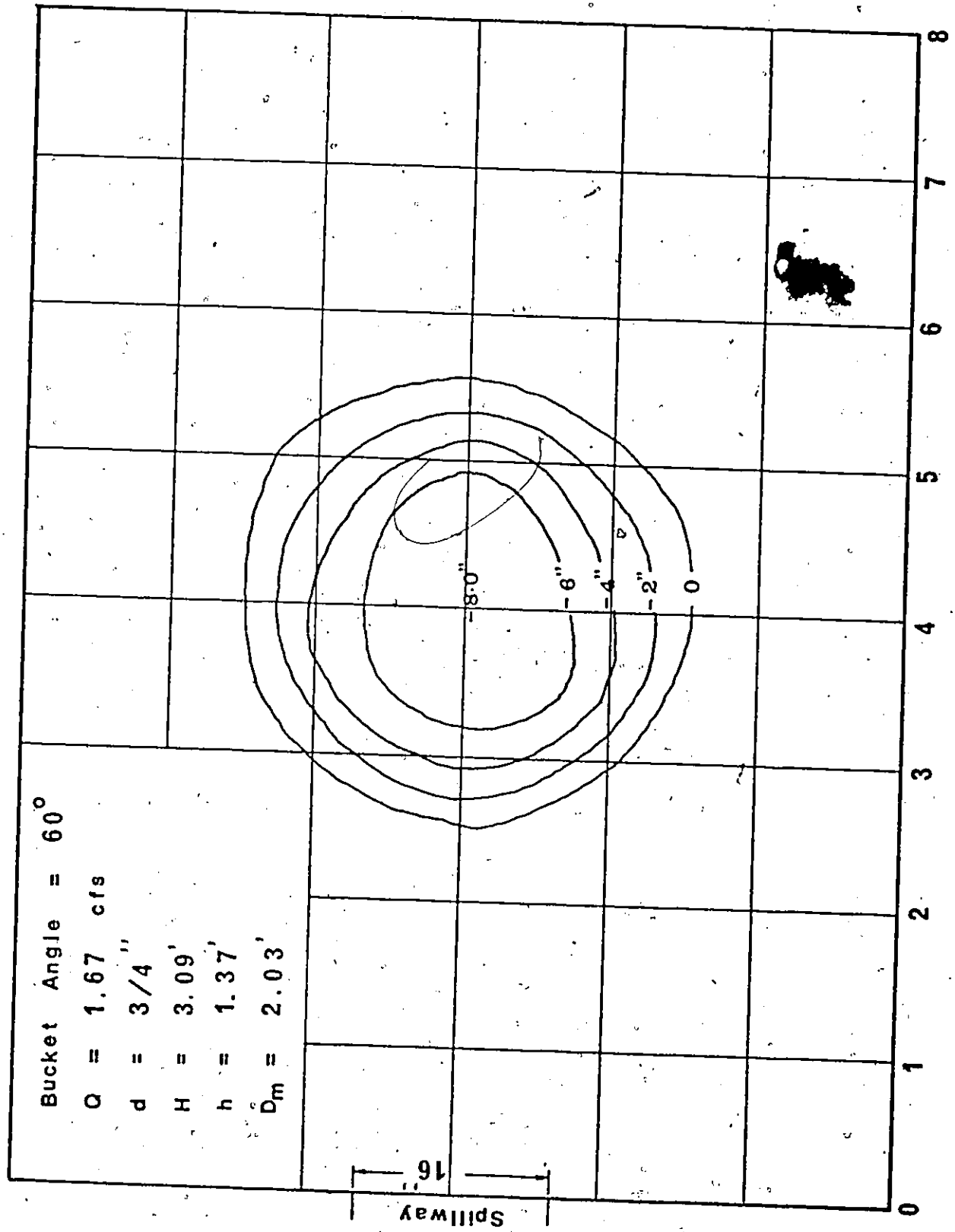
Bucket Angle = 60°
Q = 1.67 cfs
d = 3/4"
H = 3.09'
h = 1.37'
D_m = 2.03'
-8.0"
-6"
-4"
-2"
0
16"
Spillway
0
1
2
3
4
5
6
7
8

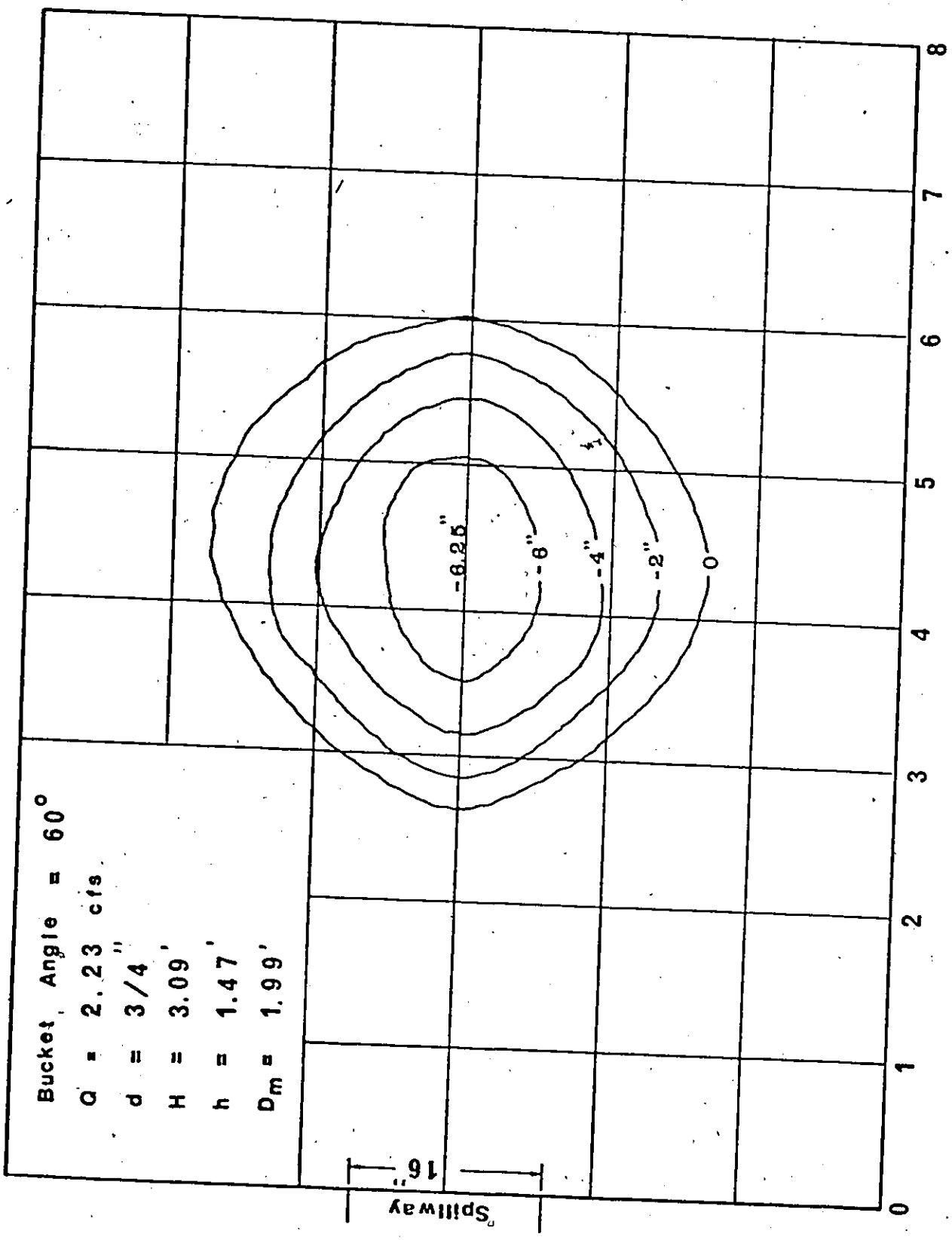
Bucket Angle = 60°
Q = 2.23 cfs
d = 3/4"
H = 3.09'
h = 1.47'
D_m = 1.99'
-8.25"
-8"
-4"
-2"
0
16"
Spillway
0
1
2
3
4
5
6
7
8

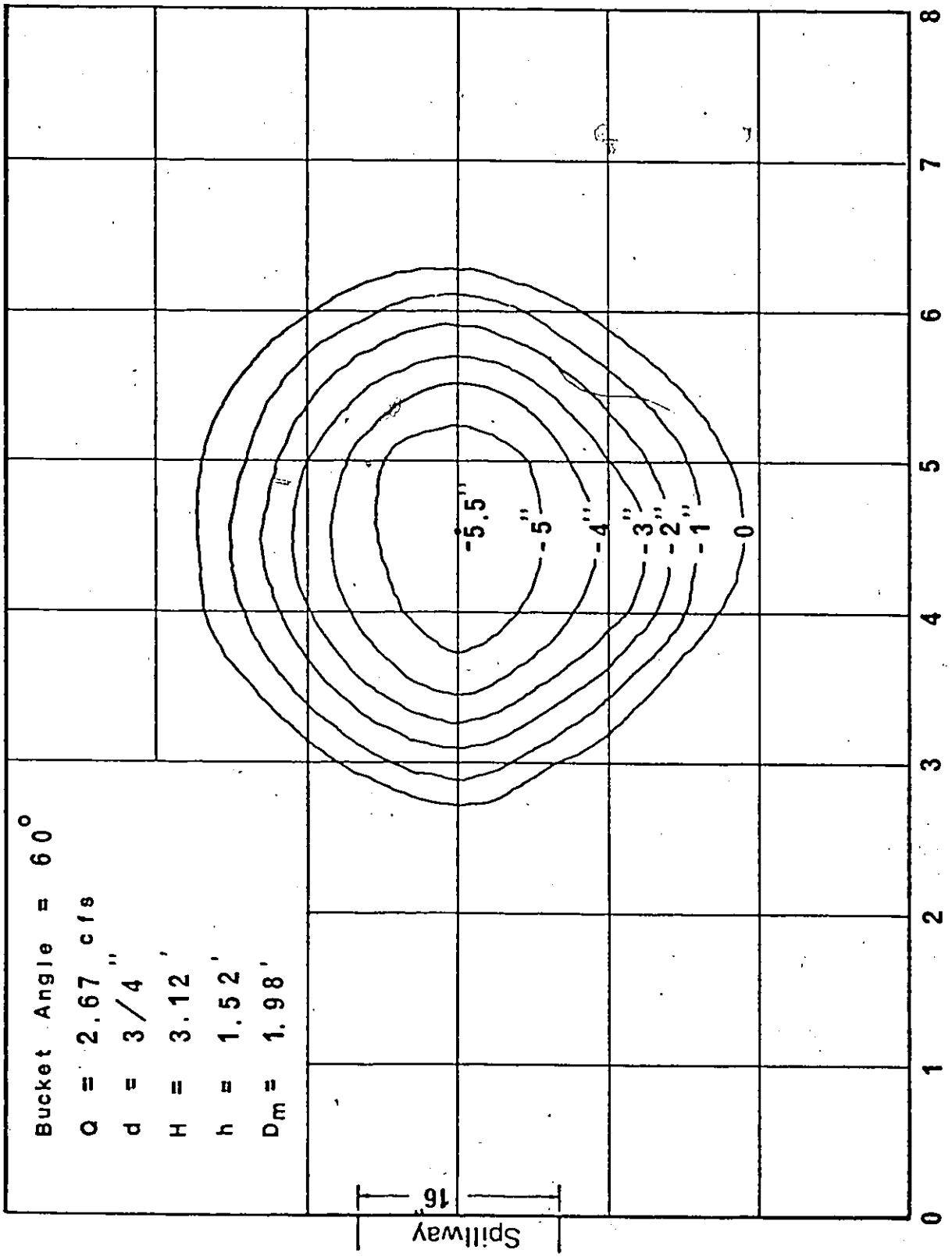
Bucket Angle = 60°
Q = 2.67 cfs
d = 3/4"
H = 3.12'
h = 1.52'
D_m = 1.98'
-5.5"
-5"
-4"
-3"
-2"
-1
0
16"
Spillway
0
1
2
3
4
5
6
7
8

APPENDIX B

Table B.1.a

Time Factor for Development of Scour (a)

Q = 1,000 usgpm

q = 1.67 cfs/ft

45° flip bucket

H = 3.11 ft

Bed Material: 3/4" gravel

Initial T.W.D. = 12.5"

Time in Minute	Maximum Depth of Scour in inches	Depth of Scour in Inches			
		At Pt.1	At Pt.2	At Pt.3	At Pt.4
1	20.05	19.07	15.00	18.78	18.70
2	22.08	20.39	17.30	21.11	20.00
3	22.90	21.08	18.58	21.90	20.60
5	24.20	23.28	19.60	22.13	21.32
10	24.55	23.30	19.65	23.11	21.79
15	24.61	23.35	20.19	23.65	22.85
20	24.70	23.30	20.15	23.75	23.45
30	24.90	23.55	20.30	23.87	23.95
45	25.20	23.50	20.25	24.31	24.31
60	25.20	23.73	20.50	24.30	24.30
90	25.20	23.60	20.45	24.50	24.45
120	25.20	23.75	20.45	24.50	24.30
150	25.25	23.75	20.55	24.50	24.30
180	25.25	23.80	20.60	24.60	24.45
210	25.30	23.80	20.45	24.60	24.45
270	25.25	23.90	20.55	24.60	24.35

Table B.1.a (continued)

Time in Minutes	Maximum Depth of Scour in inches	Depth of Scour in Inches			
		At Pt.1	At Pt.2	At Pt.3	At Pt.4
360	25.25	23.90	20.60	24.50	24.30
450	25.25	23.90	20.55	24.50	24.35
540	25.20	23.80	20.55	24.60	24.35
720	25.25	23.80	20.50	24.60	24.30
900	25.20	23.90	20.55	24.50	24.30
1140	25.20	23.80	20.55	24.50	24.35
1440	25.20	23.80	20.55	24.50	24.30

Table B.1.b

Time Factor for Development of Scour(b)

Q = 1000 usgpm

q = 1.67 cfs/ft

45° flip bucket

H = 3.11 ft

Bed Material : 3/8" gravel

Initail T.W.D. = 12.5"

Time in minutes	Maximum Depth of Scour in Inches	Depth of Scour in Inches			
		At Pt.1	At Pt.2	At Pt.3	At Pt.4
1	23.90	21.50	17.50	22.50	20.90
2	24.70	22.07	17.70	23.30	21.40
3	25.10	22.19	18.39	23.69	22.59
5	25.20	23.05	19.09	24.05	22.79
10	25.65	23.75	19.15	24.71	23.71
15	25.85	24.10	19.19	25.10	23.90
20	26.05	24.05	19.25	25.49	24.05
30	26.30	24.20	19.35	25.75	24.20
45	26.55	24.25	19.80	26.13	24.35
60	26.60	24.63	19.90	26.15	24.40
90	26.60	24.65	20.00	26.05	24.40
120	26.67	24.65	19.90	26.02	24.45
150	26.65	24.68	20.00	26.03	24.40
180	26.70	24.60	20.00	26.05	24.45
210	26.65	24.65	19.90	26.00	24.40
270	26.50	24.65	19.90	26.05	24.40

Table B.1.b (continued)

Time in Minutes	Maximum Depth of Scour in Inches	Depth of Scour in Inches			
		At Pt.1	At Pt.2	At Pt.3	At Pt.4
360	26.65	24.63	20.00	26.05	24.45
450	26.60	24.65	20.00	26.03	24.40
540	26.60	24.60	20.00	26.05	24.40
720	26.60	24.65	19.95	26.00	24.40
900	26.65	24.65	20.00	26.05	24.40
1140	26.65	24.60	20.00	26.05	24.40
1440	26.60	24.65	20.00	26.05	24.40

Table B.2

Longitudinal Profiles of Scour Holes at the Center Line

B.A. : Bucket Angle

Expt. No.	B.A. deg.	W in	d in	Q cfs	H ft	h ft	d/s part y ft	d/s part x ft	u/s part y ft	u/s part x ft
A1	15	16	0.75	0.67	3.01	1.19	0.008	0.212	0.008	-0.264
							0.033	0.425	0.033	-0.528
							0.075	0.638	0.075	-0.792
							0.133	0.851	0.143	-1.056
							0.209	1.064	0.219	-1.320
A2	15	16	0.75	1.11	3.06	1.26	0.019	0.259	0.019	-0.332
							0.076	0.519	0.076	-0.644
							0.172	0.779	0.172	-0.966
							0.306	1.039	0.306	-1.288
							0.479	0.299	0.499	-1.610
A3	15	16	0.75	1.67	3.13	1.35	0.036	0.303	0.066	-0.376
							0.146	0.606	0.146	-0.752
							0.328	0.909	0.328	-1.128
							0.584	1.213	0.584	-1.504
							0.912	1.516	0.922	-1.880
A4	15	16	0.75	2.29	3.20	1.39	0.151	0.293	0.111	-0.363
							0.276	0.586	0.266	-0.727
							0.405	0.879	0.495	-1.090
							0.506	1.172	0.596	-1.454
							0.791	1.465	0.891	-1.817

Table B.2 (continued)

Expt. No.	B.A. deg.	W in	d in	Q cfs	H ft	h ft	d/s part y ft	d/s part x ft	u/s part y ft	u/s part x ft
A5	15	16	0.75	2.67	3.22	1.45	0.246	0.302	0.276	-0.375
							0.445	0.605	0.505	-0.751
							0.596	0.908	0.686	-1.126
							0.730	1.211	0.850	-1.502
							0.907	1.514	0.966	-1.877
A6	16	16	0.75	1.67	3.12	1.35	0.036	0.302	0.066	-0.375
							0.144	0.605	0.144	-0.750
							0.326	0.908	0.326	-1.126
							0.579	1.210	0.579	-1.501
							0.905	1.513	0.915	-1.877
A7	30	24	0.75	0.57	2.75	0.50	0.010	0.226	0.010	-0.280
							0.043	0.452	0.043	-0.561
							0.097	0.679	0.087	-0.842
							0.172	0.905	0.122	-1.123
							0.270	1.132	0.282	-1.403
A8	30	24	0.75	1.14	2.65	0.77	0.019	0.262	0.019	-0.325
							0.079	0.524	0.079	-0.650
							0.179	0.787	0.189	-0.976

Table B.2(continued)

Expt. No.	B.A. deg.	W in	d in	Q cfs	H ft	h ft	d/s part y ft	d/s part x ft	u/s part y_{ft}	u/s part x_{ft}
A8	30	24	0.75	1.14	2.65	0.77	0.319	1.049	0.289	-1.301
							0.499	1.311	0.490	-1.626
A9	30	24	0.75	1.71	2.42	1.02	0.024	0.276	0.024	-0.342
							0.099	0.552	0.099	-0.685
							0.223	0.829	0.204	-1.028
							0.396	1.105	0.376	-1.371
							0.550	1.381	0.491	-1.713
A10	30	24	0.75	2.27	2.29	0.67	0.053	0.332	0.053	-0.412
							0.214	0.665	0.194	-0.825
							0.453	0.998	0.473	-1.237
							0.639	i.330	0.539	-1.650
							0.992	1.663	0.982	-2.060
A11	30	24	0.75	2.84	2.88	0.79	0.059	0.340	0.059	-0.422
							0.236	0.680	0.236	-0.844
							0.532	1.021	0.532	-1.266
							0.945	1.361	0.856	-1.688
							1.477	1.702	1.407	-2.111
A12	30	16	0.75	1.14	3.25	0.77	0.043	0.315	0.043	-0.391

Table B.2 (continued)

Exp. No.	B.A. deg.	W in	d in	Q cfs	H ft	h ft	d/s part y ft	d/s part x ft	u/s part y ft	u/s part x ft
A12	30	16	0.75	1.14	3.25	0.77	0.175	0.480	0.145	-0.595
							0.214	0.720	0.154	-0.893
							0.221	0.961	0.221	-0.191
							0.346	1.201	0.305	-1.489
A13	30	16	0.75	1.14	3.38	0.50	0.043	0.315	0.043	-0.391
							0.173	0.631	0.173	-0.793
							0.389	0.947	0.389	-1.175
							0.693	1.263	0.598	-1.567
							1.082	1.579	0.922	-1.959
A14	30	16	0.75	3.21	0.94	0.94	0.135	0.320	0.165	-0.397
							0.243	0.640	0.297	-0.794
							0.412	0.960	0.412	-1.191
							0.732	1.280	0.732	-1.588
							1.144	1.601	1.184	-1.985
A15	30	16	0.75	2.27	3.08	1.21	0.123	0.315	0.153	-0.391
							0.213	0.631	0.243	-0.783
							0.469	0.947	0.499	-1.175
							0.693	1.263	0.723	-1.567

Table B.2 (continued)

Exp. No.	B.A. deg.	W in.	Q cfs	H ft	h ft	d in	d/s part y ft	d/s part x ft	u/s part y ft	u/s part x ft
A15	30	16	2.27	3.08	1.21	0.75	1.082	1.579	1.082	-1.959
A16	45	16	0.81	2.92	1.21	0.75	0.037	0.208	0.039	-0.258
							0.060	0.416	0.068	-0.516
							0.068	0.624	0.068	-0.774
							0.121	0.832	0.129	-1.032
							0.190	1.040	0.198	-1.290
A17	45	16	1.15	2.82	1.47	0.75	0.022	0.270	0.022	-0.335
							0.091	0.541	0.091	-0.671
							0.205	0.812	0.205	-0.997
							0.364	1.083	0.344	-1.343
							0.570	1.354	0.540	-1.679
A18	45	16	1.50	2.83	1.32	0.75	0.068	0.306	0.068	-0.380
							0.153	0.613	0.153	-0.761
							0.345	0.920	0.345	-0.992
							0.614	1.227	0.614	-1.522
							0.959	1.534	0.949	-1.903
A19	45	16	1.73	3.02	1.33	0.75	0.102	0.314	0.102	-0.389
							0.169	0.628	0.189	-0.779

Table B.2(con inued)

Exp. No.	B.A. deg.	W in.	Q cfs	H ft	d in	h ft	d/s part y ft	d/s part x ft	u/s part y ft	u/s part x ft
A19	45	16	1.73	3.02	0.75	1.33	0.381	0.943	0.389	-1.169
							0.678	1.257	0.698	-1.559
							1.059	1.571	1.059	-1.949
A20	45	16	2.09	3.06	0.75	1.37	0.164	0.317	0.194	-0.394
							0.297	0.635	0.357	-0.788
							0.399	0.953	0.489	-1.182
							0.710	1.271	0.719	-1.576
							1.110	1.589	1.189	-1.970
A21	45	16	2.45	3.05	0.75	1.43	0.084	0.317	0.144	-0.394
							0.207	0.635	0.297	-0.788
							0.499	0.953	0.589	-1.182
							0.760	1.271	0.850	-1.576
							1.110	1.580	1.109	-1.975
A22	60	16	0.67	2.99	1.23	1.23	0.009	0.221	0.009	-0.274
							0.039	0.442	0.039	-0.594
							0.088	0.664	0.088	-0.823
							0.157	0.885	0.147	-1.098
							0.246	1.107	0.196	-1.372
A23	60	16	1.11	3.03	0.75	1.31	0.055	0.277	0.055	-0.344

Table B.2 (continued)

Exp. No.	B.A. deg	W in	d in	Q cfs	H ft	h ft	d/s part y ft	d/s part x ft	u/s part y ft	u/s part x ft
A23	60	16	0.75	1.11	3.03	1.31	0.101	0.555	0.109	-0.689
							0.228	0.833	0.220	-1.034
							0.406	1.111	0.406	-1.378
							0.634	1.389	0.594	-1.723
A24	60	16	0.75	1.67	3.09	1.37	0.076	0.281	0.136	-0.348
							0.216	0.562	0.206	-0.697
							0.349	0.843	0.439	-1.046
							0.446	1.124	0.536	-1.394
							0.665	1.405	0.695	-1.743
A25	60	16	0.75	2.67	3.02	1.52	0.019	0.262	0.015	-0.305
							0.079	0.524	0.061	-0.610
							0.179	0.787	0.137	-0.910
							0.242	0.905	0.372	-1.309
							0.460	1.132	0.511	-1.636
A26	60	16	0.75	2.67	3.10	1.48	0.017	0.260	0.117	-0.308
							0.087	0.531	0.066	-0.640
							0.176	0.786	0.143	-0.960
							0.309	1.049	0.245	-1.221

Table B.2 (continued)

Exp. No.	B.A. deg	W in	d in	Q cfs	H ft	h ft	d/s part y ft	d/s part x ft	u/s part y ft	u/s part x ft
A26	60	16	0.75	2.67	3.02	1.52	0.399	1.311	0.383	-1.526
A27	30	24	0.25	0.57	2.95	0.38	0.020	0.262	0.019	-0.325
							0.080	0.524	0.080	-0.651
							0.180	0.787	0.160	-0.976
							0.299	1.049	0.289	-1.302
							0.459	1.312	0.379	-1.627
A28	30	24	0.25	0.82	2.96	0.38	0.045	0.279	0.055	-0.346
							0.103	0.558	0.103	-0.692
							0.232	0.837	0.232	-1.038
							0.413	1.116	0.453	-1.384
							0.625	1.395	0.615	-1.730
A29	30	24	0.25	1.02	2.98	0.45	0.031	0.293	0.061	-0.363
							0.126	0.586	0.126	-0.727
							0.285	0.879	0.285	-1.090
							0.506	1.172	0.446	-1.454
							0.791	1.465	0.751	-1.817
A30	30	24	0.25	1.48	2.97	0.53	0.060	0.310	0.100	-0.385
							0.161	0.621	0.161	-0.770

Table B.2 (continued)

Exp. No.	B.A. deg	W in	d in	Q cfs	H ft	h ft	d/s part y ft	d/s part x ft	u/s part y ft	u/s part x ft
A30	30	24	0.25	1.48	2.97	0.53	0.363	0.932	0.365	-1.156
							0.646	1.242	0.606	-1.541
							1.009	1.553	0.989	-1.926
A31	30	24	0.25	2.38	2.81	0.79	0.075	0.335	0.115	-0.416
							0.223	0.671	0.225	-0.832
							0.502	1.007	0.504	-1.249
							0.892	1.343	0.894	-1.556
							1.390	1.680	1.394	-2.082
A32	30	16	0.25	0.79	3.46	0.65	0.059	0.309	0.099	-0.384
							0.159	0.619	0.159	-0.786
							0.359	0.929	0.359	-1.153
							0.639	1.239	0.619	-1.537
							0.998	1.549	0.879	-1.921
A33	30	16	0.25	1.14	3.39	0.78	0.088	0.325	0.138	-0.403
							0.195	0.650	0.255	-0.806
							0.438	0.975	0.438	-1.209
							0.780	1.300	0.780	-1.612
							1.219	1.625	1.248	-2.015
A34	30	16	0.25	1.71	3.23	1.00	0.129	0.325	0.109	-0.403

Table B.2 (continued)

Exp. No.	B.A. deg	W in	d in	Q cfs	H ft	h ft	d/s part y ft	d/s part x ft	u/s part y ft	u/s part x ft
A34	30	16	0.25	1.71	3.23	1.00	0.216	0.651	0.276	-0.807
							0.462	0.977	0.492	-1.211
							0.786	1.302	0.856	-1.615
							1.228	1.628	0.998	-2.019
A35	30	16	0.25	2.27	3.22	1.18	0.049	0.326	0.049	-0.405
							0.198	0.652	0.198	-0.809
							0.446	0.979	0.448	-1.214
							0.792	1.305	0.799	-1.618
							1.238	1.631	1.258	-2.023

Table B.3

Longitudinal Porfiles of Scour Holes at the Distance $1/3\ R_{90}$ from the C.L.

Expt. No.	Q usgpm	q cfs/ft	downstream part y ft	downstream part x ft	upstream part y ft	upstream part x ft
A1	300	0.50	0.013	0.161	0.019	-0.201
			0.032	0.322	0.038	-0.402
			0.070	0.483	0.075	-0.603
			0.113	0.644	0.129	-0.804
			0.190	0.805	0.198	-1.005
A2	500	0.83	0.021	0.253	0.023	-0.262
			0.072	0.505	0.077	-0.524
			0.150	0.757	0.155	-0.786
			0.271	1.009	0.279	-1.048
			0.422	1.259	0.438	-1.309
A3	750	1.26	0.032	0.352	0.035	-0.441
			0.130	0.704	0.136	-0.882
			0.291	1.055	0.297	-0.993
			0.521	1.406	0.528	-1.765
			0.911	1.758	0.819	-2.206
A4	1000	1.72	0.031	0.411	0.034	-0.420

Table B.3 (continued)

Expt. No.	Q usgpm	q cfs/ft	downstream part		upstream part	
			y ft	x ft	y ft	x ft
A4	1000	1.72	0.110	0.821	0.114	-0.840
			0.250	1.233	0.257	-1.261
			0.451	1.644	0.459	-1.682
			0.709	2.054	0.780	-2.102
A5	1200	2.01	0.031	0.440	0.034	-0.461
			0.136	0.881	0.135	-0.922
			0.291	1.320	0.299	-1.382
			0.521	1.761	0.535	-1.843
			0.812	1.901	0.841	-1.964
A6	750	1.26	0.032	0.351	0.035	-0.441
			0.132	0.702	0.137	-0.882
			0.291	1.052	0.298	-1.322
			0.521	1.303	0.532	-1.663
			0.819	1.654	0.846	-1.904
A7	250	0.28	0.012	0.121	0.017	-0.182
			0.042	0.241	0.048	-0.364
			0.091	0.362	0.098	-0.546
			0.153	0.483	0.159	-0.724
			0.240	0.604	0.249	-0.904

Table B.3 (continued)

Expt. No.	Q usgpm	q cfs/ft	downstream part		upstream part	
			y ft	x ft	y ft	x ft
A8	500	0.41	0.020	0.242	0.029	-0.280
			0.071	0.484	0.078	-0.560
			0.160	0.726	0.169	-0.841
			0.281	0.968	0.289	-1.121
			0.440	1.169	0.449	-1.301
A9	750	0.85	0.021	0.280	0.025	-0.380
			0.091	0.560	0.098	-0.761
			0.203	0.840	0.211	-1.040
			0.351	1.100	0.359	-1.301
			0.550	1.311	0.559	-1.702
A10	1000	1.13	0.050	0.401	0.054	-0.480
			0.191	0.800	0.198	-0.860
			0.430	1.001	0.439	-1.241
			0.761	1.502	0.768	-1.621
			1.191	1.803	1.199	-1.920
A11	1250	1.41	0.051	0.502	0.056	-0.561
			0.211	0.804	0.217	-0.832
			0.479	1.206	0.490	-1.483

Table B.3 (continued)

Expt. No.	Q usgpm	q cfs/ft	downstream part		upstream part	
			y ft	x ft	y ft	x ft
A11	1250	1.41	0.841	1.578	0.819	-1.694
			1.141	1.830	1.129	-1.934
A12	250	0.42	0.011	0.151	0.016	-0.180
			0.051	0.302	0.059	-0.361
			0.114	0.453	0.123	-0.512
			0.209	0.604	0.221	-0.722
			0.310	0.704	0.331	-0.804
A13	500	0.84	0.041	0.281	0.047	-0.302
			0.150	0.462	0.158	-0.508
			0.331	0.743	0.359	-0.806
			0.614	1.024	0.605	-1.108
			0.910	1.305	0.949	-1.402
A14	750	1.27	0.041	0.312	0.043	-0.311
			0.155	0.604	0.161	-0.602
			0.376	0.936	0.393	-0.993
			0.651	1.248	0.659	-1.324
			1.027	1.559	1.032	-1.555
A15	1000	1.71	0.041	0.320	0.047	-0.403

Table B.3 (continued)

Expt. No.	Q usgpm	q cfs/ft	downstream part		upstream part	
			y ft	x ft	y ft	x ft
A15	1000	1.71	0.151	0.631	0.159	-0.802
			0.350	0.902	0.359	-1.109
			0.623	1.182	0.638	-1.402
			0.960	1.403	0.969	-1.804
A16	365	0.61	0.010	0.121	0.100	-0.112
			0.032	0.242	0.038	-0.224
			0.061	0.363	0.067	-0.336
			0.119	0.484	0.140	-0.448
			0.173	0.605	0.195	-0.559
A17	515	0.86	0.023	0.233	0.028	-0.292
			0.081	0.466	0.088	-0.584
			0.181	0.699	0.189	-0.876
			0.329	0.922	0.332	-0.968
			0.519	1.155	0.541	-1.450
A18	675	1.13	0.032	0.251	0.038	-0.303
			0.141	0.502	0.148	-0.606
			0.319	0.753	0.341	-0.909
			0.551	1.004	0.550	-1.202
			0.851	1.255	0.859	-1.505

Table B.3 (continued)

Expt. No.	Q usgpm	q cfs/ft	downstream part		upstream part	
			y ft	x ft	y ft	x ft
A19	780	1.30	0.042	0.301	0.045	-0.351
			0.151	0.602	0.158	-0.702
			0.349	0.903	0.380	-1.053
			0.609	1.204	0.661	-1.404
			0.940	1.505	0.949	-1.755
A20	940	1.57	0.041	0.322	0.042	-0.381
			0.163	0.642	0.168	-0.762
			0.361	0.904	0.369	-1.104
			0.635	1.186	0.655	-1.424
			0.990	1.509	0.998	-1.805
A21	1100	1.84	0.031	0.311	0.045	-0.351
			0.142	0.622	0.161	-0.700
			0.321	0.933	0.360	-1.050
			0.615	1.244	0.517	-1.400
			0.911	1.555	0.959	-1.750
A22	300	0.50	0.011	0.162	0.014	-0.173
			0.032	0.324	0.038	-0.346
			0.081	0.486	0.089	-0.519
			0.149	0.646	0.180	-0.682

Table B.3 (continued)

Expt. No.	Q usgpm	q cfs/ft	downstream part		upstream part	
			y ft	x ft	y ft	x ft
A22	300	0.50	0.221	0.808	0.242	-0.858
A23	500	0.83	0.021	0.202	0.024	-0.220
			0.091	0.404	0.099	-0.440
			0.209	0.606	0.221	-0.661
			0.368	0.808	0.379	-0.881
			0.563	1.009	0.561	-1.101
A24	750	1.26	0.021	0.280	0.022	-0.031
			0.093	0.560	0.097	-0.602
			0.212	0.840	0.218	-0.903
			0.381	1.121	0.389	-1.204
			0.591	1.401	0.598	-1.505
A25	1000	1.72	0.020	0.250	0.021	-0.280
			0.072	0.501	0.071	-0.561
			0.165	0.751	0.162	-0.780
			0.251	0.998	1.290	-1.120
			0.469	1.251	0.467	-1.401
A26	1200	2.01	0.018	0.301	0.011	-0.310
			0.054	0.602	0.051	-0.621

Table B.3 (continued)

Expt. No.	Q usgpm	q cfs/ft	downstream part		upatream part	
			Y ft	x ft	y ft	x ft
A26	1200	2.01	0.229	1.201	0.222	-1.240
			0.128	0.903	0.122	-0.931
			0.348	1.505	0.341	-1.550
A27	250	0.28	0.023	0.220	0.024	-0.301
			0.071	0.440	0.079	-0.602
			0.160	0.661	0.169	-0.903
			0.281	0.881	0.789	-1.204
			0.449	1.101	0.485	-1.505
A28	360	0.41	0.021	0.261	0.028	-0.310
			0.092	0.522	0.098	-0.620
			0.219	0.843	0.241	-0.931
			0.379	0.989	0.391	-1.241
			0.579	1.044	0.595	-1.550
A29	450	0.51	0.031	0.301	0.034	-0.351
			0.112	0.602	0.119	-0.702
			0.252	0.903	0.259	-1.053
			0.450	1.204	0.459	-1.404
			0.709	1.505	0.723	-1.755
A30	650	0.73	0.041	0.312	0.044	-0.371

Table B.3 (continued)

Expt. No.	Q usgpm	q cfs/ft	downstream part		upstream part	
			y ft	x ft	y ft	x ft
A30	650	0.73	0.142	0.624	0.148	-0.742
			0.321	0.936	0.329	-1.113
			0.576	1.248	0.592	-1.484
		———	0.908	1.561	0.919	-1.855
A31	1050	1.19	0.051	0.361	0.054	-0.372
			0.202	0.722	0.208	-0.744
			0.451	1.083	0.459	-1.116
			0.791	1.444	0.719	-1.451
			1.040	1.805	1.181	-1.860
A32	350	0.59	0.041	0.281	0.043	-0.380
			0.142	0.562	0.147	-0.760
			0.329	0.843	0.341	-1.140
			0.578	1.124	0.592	-1.521
			0.891	1.405	0.899	-1.901
A33	500	0.85	0.043	0.320	0.044	-0.362
			0.171	0.640	0.175	-0.724
			0.339	0.960	0.397	-1.086
			0.698	1.280	0.691	-1.449
			1.009	1.601	1.080	-1.809

Table B.3 (continued)

Expt. No.	Q usgpm	q cfs/ft	downstream part		upstream part	
			y ft	x ft	y ft	x ft
A34	750	1.27	0.041	0.322	0.042	-0.341
			0.158	0.644	0.171	-0.682
			0.371	0.966	0.391	-1.023
			0.701	1.288	0.701	-1.164
			1.011	1.610	1.029	-1.705
A35	1000	1.70	0.042	0.340	0.043	-0.361
			0.181	0.680	0.185	-0.722
			0.401	1.020	0.401	-1.083
			0.701	1.360	0.702	-1.444
			1.001	1.701	1.005	-1.806

Table B.4

Longitudinal Profiles of Scour Holes at the Distance $2/3\ R_{90}$ from the Center Line

Expt. No.	D_m ft	H_a ft	downstream part		upstream part	
			y ft	x ft	y ft	x ft
A1	1.41	1.17	0.011	0.110	0.009	-0.161
			0.021	0.220	0.022	-0.322
			0.043	0.330	0.046	-0.483
			0.072	0.441	0.077	-0.644
			0.121	0.551	0.128	-0.805
A2	1.74	1.27	0.012	0.212	0.011	-0.222
			0.042	0.424	0.041	-0.444
			0.103	0.636	0.102	-0.666
			0.175	0.848	0.175	-0.888
			0.273	1.059	0.272	-1.100
A3	2.26	1.41	0.027	0.282	0.025	-0.320
			0.081	0.564	0.083	-0.640
			0.182	0.846	0.181	-0.960
			0.321	1.117	0.327	-1.280
			0.516	1.409	0.540	-1.600
A4	2.18	1.54	0.022	0.301	0.021	-0.343

Table B.4 (continued)

Expt. No.	D_m ft	H_a ft	downstream part		upstream part	
			y ft	x ft	y ft	x ft
A4	2.18	1.54	0.072	0.602	0.072	-0.686
			0.161	0.903	0.163	-0.989
			0.281	1.204	0.286	-1.362
			0.443	1.505	0.445	-1.705
A5	2.36	1.64	0.021	0.310	0.020	-0.321
			0.081	0.620	0.080	-0.642
			0.181	0.930	0.184	-0.963
			0.321	1.240	0.327	-0.284
			0.501	1.550	0.506	-1.605
A6	2.26	1.42	0.021	0.281	0.023	-0.360
			0.081	0.562	0.084	-0.720
			0.181	0.843	0.188	-1.081
			0.320	1.124	0.329	-1.441
			0.509	1.405	0.520	-1.801
A7	0.77	1.45	0.011	0.083	0.014	-0.170
			0.021	0.166	0.028	-0.321
			0.051	0.249	0.059	-0.510
			0.101	0.323	0.110	-0.681

Table B.4 (continued)

Expt. No.	D_m ft	H_a ft	downstream part		upstream part	
			y ft	x ft	y ft	x ft
A7	0.77	1.45	0.151	0.406	0.164	-0.851
A8	1.27	1.62	0.011	0.162	0.016	-0.260
			0.040	0.324	0.048	-0.520
			0.101	0.488	0.110	-0.780
			0.181	0.648	0.198	-1.041
			0.281	0.809	0.298	-1.300
A9	1.64	1.64	0.011	0.222	0.016	-0.341
			0.061	0.444	0.068	-0.682
			0.122	0.666	0.132	-1.023
			0.221	0.888	0.241	-1.364
			0.349	1.109	0.381	-1.705
A10	2.01	1.79	0.031	0.330	0.037	-0.361
			0.122	0.762	0.127	-0.722
			0.279	0.990	0.291	-1.183
			0.482	1.320	0.498	-1.805
			0.751	1.560	0.759	-1.810
A11	2.27	1.87	0.034	0.350	0.035	-0.380
			0.135	0.700	0.133	-0.760

Table B.4 (continued)

Expt. No.	D_m ft	H_a ft	downstream part		upstream part	
			y ft	x ft	y ft	x ft
A11	2.27	1.87	0.305	1.050	0.303	-1.140
			0.534	1.400	0.537	-1.520
			0.821	1.750	0.828	-1.901
A12	0.85	0.77	0.013	0.130	0.012	-0.172
			0.032	0.260	0.034	-0.344
			0.073	0.390	0.078	-0.516
			0.122	0.520	0.128	-0.688
			0.191	0.651	0.199	-0.859
A13	1.85	0.92	0.028	0.240	0.023	-0.243
			0.107	0.480	0.106	-0.486
			0.227	0.721	0.222	-0.729
			0.398	0.961	0.391	-0.963
			0.608	1.201	0.601	-1.205
A14	2.08	1.05	0.034	0.231	0.031	-0.232
			0.106	0.462	0.102	-0.464
			0.239	0.693	0.233	-0.696
			0.419	0.924	0.411	-0.928
			0.649	1.152	0.641	-1.151

Table B.4 (continued)

Expt. No.	D_m ft	H_a ft	downstream part		upstream part	
			y ft	x ft	y ft	x ft
A15	2.29	1.19	0.024	0.244	0.026	-0.322
			0.102	0.486	0.107	-0.643
			0.225	0.728	0.233	-0.964
			0.391	0.969	0.399	-1.285
			0.609	1.209	0.618	-1.505
A16	1.40	0.95	0.012	0.080	0.009	-0.098
			0.025	0.160	0.023	-0.224
			0.047	0.241	0.048	-0.336
			0.078	0.321	0.079	-0.448
			0.129	0.401	0.128	-0.559
A17	2.04	1.09	0.013	0.171	0.011	-0.203
			0.055	0.342	0.054	-0.406
			0.118	0.513	0.119	-0.609
			0.203	0.684	0.208	-0.802
			0.320	0.855	0.329	-1.005
A18	2.28	0.96	0.021	0.201	0.023	-0.232
			0.091	0.402	0.094	-0.464
			0.191	0.603	0.194	-0.696

Table B.4 (continued)

Expt. No.	D_m ft	H_a ft	downstream part		upstream part	
			y ft	x ft	y ft	x ft
A18	2.28	0.96	0.342	0.804	0.345	-0.928
			0.533	1.004	0.539	-1.159
A19	2.39	1.18	0.024	0.240	0.025	-0.262
			0.091	0.480	0.094	-0.524
			0.212	0.721	0.216	-0.785
			0.381	0.961	0.388	-1.047
			0.590	1.201	0.599	-1.309
A20	2.48	1.24	0.024	0.281	0.023	-0.321
			0.103	0.562	0.105	-0.642
			0.225	0.842	0.229	-0.963
			0.391	1.123	0.398	-1.284
			0.623	1.404	0.631	-1.606
A21	2.54	1.29	0.024	0.281	0.022	-0.293
			0.106	0.562	0.105	-0.586
			0.223	0.843	0.224	-0.879
			0.396	1.123	0.399	-1.169
			0.623	1.404	0.621	-1.458
A22	1.48	0.93	0.013	0.131	0.012	-0.142

Table B.4 (continued)

Expt. No.	D_m ft	H_a ft	downstream part		upstream part	
			y ft	x ft	y ft	x ft
A22	1.48	0.93	0.022	0.261	0.023	-0.284
			0.053	0.392	0.055	-0.426
			0.091	0.522	0.094	-0.568
			0.144	0.653	0.146	-0.709
A23	1.95	1.05	0.012	0.171	0.013	-0.193
			0.063	0.342	0.065	-0.385
			0.132	0.512	0.134	-0.577
			0.233	0.685	0.235	-0.768
			0.355	0.854	0.359	-0.959
A24	2.03	1.67	0.012	0.232	0.013	-0.243
			0.064	0.464	0.067	-0.485
			0.133	0.696	0.137	-0.726
			0.241	0.927	0.245	-0.968
			0.371	1.158	0.377	-1.209
A25	1.99	1.27	0.012	0.220	0.011	-0.222
			0.055	0.440	0.053	-0.443
			0.105	0.660	0.102	-0.666
			0.187	0.881	0.184	-0.888

Table B.4 (continued)

Expt. No.	D_m ft	H_a ft	downstream part		upstream part	
			y ft	x ft	y ft	x ft
A25	1.99	1.27	0.288	1.101	0.285	-1.109
A26	1.90	1.35	0.015	0.241	0.013	-0.253
			0.032	0.482	0.030	-0.505
			0.084	0.722	0.085	-0.757
			0.141	0.963	0.144	-1.008
			0.213	1.204	0.218	-1.258
A27	0.88	1.51	0.011	0.142	0.013	-0.241
			0.042	0.284	0.045	-0.482
			0.101	0.426	0.107	-0.723
			0.181	0.567	0.189	-0.964
			0.281	0.708	0.299	-1.205
A28	1.02	1.54	0.011	0.221	0.013	-0.282
			0.062	0.442	0.065	-0.564
			0.131	0.663	0.135	-0.846
			0.232	0.884	0.238	-0.998
			0.360	1.105	0.373	-1.409
A29	1.24	1.63	0.021	0.231	0.024	-0.282
			0.070	0.461	0.076	-0.564

Table B.4 (continued)

Expt. No.	D_m ft	H_a ft	downstream part		upstream part	
			y ft	x ft	y ft	x ft
A29	1.24	1.63	0.021	0.692	0.168	-0.846
			0.280	0.923	0.289	-1.128
			0.445	1.154	0.458	-1.409
A30	1.54	1.70	0.021	0.322	0.025	-0.360
			0.091	0.644	0.098	-0.720
			0.209	0.966	0.221	-1.080
			0.360	1.288	0.384	-1.440
			0.360	1.288	0.384	-1.801
A31	2.19	1.81	0.035	0.350	0.031	-0.370
			0.127	0.701	0.121	-0.740
			0.289	1.050	0.280	-1.110
			0.515	1.400	0.509	-1.480
			0.789	1.750	0.780	-1.850
A32	1.65	1.01	0.025	0.210	0.021	-0.213
			0.096	0.420	0.092	-0.425
			0.209	0.631	0.202	-0.636
			0.368	0.840	0.362	-0.847
			0.569	1.050	0.560	-1.059

Table B.4 (continued)

Expt. No.	D_m ft	H_a ft	downstream part		upstream part	
			y ft	x ft	y ft	x ft
A33	2.42	1.30	0.031	0.281	0.033	-0.292
			0.112	0.562	0.115	-0.584
			0.241	0.842	0.245	-0.876
			0.431	1.123	0.436	-1.168
			0.690	1.404	0.689	-1.459
A34	2.23	1.22	0.031	0.301	0.033	-0.342
			0.112	0.602	0.118	-0.684
			0.251	0.904	0.259	-1.026
			0.440	1.204	0.449	-1.367
			0.681	1.505	0.695	-1.708
A35	2.42	1.30	0.035	0.360	0.033	-0.363
			0.118	0.720	0.112	-0.726
			0.257	1.081	0.256	-0.998
			0.447	1.441	0.442	-1.444
			0.699	1.801	0.692	-1.808

Table B.5

Cross-sectional Profiles of Scour Holes

Expt. No.	Bucket Angle deg.	Dm ft	h ft	$R_{90,obs.}$ ft	y ft	x ft
A1	15	1.41	1.20	0.96	0.21	0
					0.18	0.26
					0.11	0.51
					0	0.87
A2	15	1.74	1.26	1.30	0.48	0
					0.42	0.43
					0.26	0.85
					0	1.28
A3	15	2.26	1.35	1.77	0.91	0
					0.80	0.67
					0.49	1.35
					0	1.92
A4	15	2.18	1.39	1.80	0.79	0
					0.70	0.62
					0.43	1.24
					0	1.85
A5	15	2.36	1.45	2.32	0.91	0

Table B.5 (continued)

Expt. No.	Bucket Angle deg.	D_m ft	h ft	$R_{90,obs.}$ ft	y_{ft}	x_{ft}
A5	15	2.36	1.45	2.32	0.80	0.69
					0.49	1.38
					0	2.17
A6	15	2.26	1.35	1.84	0.93	0
					0.79	0.65
					0.50	1.37
					0	1.95
A7	30	0.77	0.50	0.75	0.27	0
					0.25	0.16
					0.11	0.48
					0	0.68
A8	30	1.27	0.77	0.95	0.50	0
					0.47	0.28
					0.21	0.84
					0	1.03
A9	30	1.64	1.02	1.13	0.62	0
					0.58	0.36

Table B.5 (continued)

Expt. No.	Bucket Angle deg.	D_m ft	h ft	$R_{90,obs.}$ ft	y ft	x ft
A9	30	1.64	1.02	1.13	0.26	1.07
					0	1.32
A10	30	2.01	0.67	2.10	1.34	0
					1.25	0.60
					0.54	1.79
					0	2.29
A11	30	2.27	0.79	2.35	1.48	0
					1.37	0.67
					0.60	2.00
					0	2.56
A12	30	0.85	0.49	0.63	0.36	0
					0.33	0.19
					0.15	0.59
					0	0.73
A13	30	1.85	0.77	1.55	1.08	0
					1.01	0.51
					0.44	1.53
					0	1.84

Table B.5 (continued)

Expt. No.	Bucket Angle deg.	D_m ft	h ft	$R_{90,obs.}$ ft	y ft	x ft
A14	30	2.08	0.94	1.83	1.15	0
					1.07	0.55
					0.47	1.66
					0	2.02
A15	30	2.29	1.21	2.03	1.08	0
					1.01	0.56
					0.45	1.68
					0	2.21
A16	45	1.40	1.21	0.67	0.19	0
					0.17	0.25
					0.10	0.49
					0	0.74
A17	45	2.04	1.47	0.98	0.57	0
					0.50	0.50
					0.31	1.01
					0	1.24
A18	45	2.28	1.32	1.46	0.96	0
					0.85	0.70

Table B.5 (continued)

Expt. No.	Bucket Angle deg.	D_m ft	h ft	$R_{90,obs.}$ ft	y ft	x ft
A18	45	2.28	1.32	1.46	0.96	0
					0.84	0.70
					0.51	1.40
					0	1.85
A19	45	2.39	1.33	1.83	1.06	0
					0.93	0.75
					0.57	1.51
					0	2.06
A20	45	2.48	1.37	1.91	1.11	0
					0.98	0.79
					0.59	1.57
					0	2.10
A21	45	2.54	1.43	1.98	1.11	0
					0.99	0.80
					0.60	1.59
					0	2.13
A22	60	1.48		0.99	0.25	0
					0.22	0.28

Table B.5 (continued)

Expt. No.	Bucket Angle deg.	D_m ft	h ft	$R_{90,obs.}$ ft	y_{ft}	x_{ft}
A22	60	1.48	1.23	0.99	0.13	0.57
					0	0.88
A23	60	1.95	1.31	1.27	0.63	0
					0.58	0.52
					0.34	1.04
					0	1.39
A24	60	2.03	1.37	1.52	0.67	0
					0.59	0.55
					0.36	1.09
					0	1.64
A25	60	1.99	1.47	1.64	0.52	0
					0.46	0.48
					0.28	0.95
					0	1.53
A26	60	1.98	1.50	1.70	0.56	0
					0.41	0.45
					0.25	0.89
					0	1.55

Table B.5 (continued)

Expt. No.	Bucket Angle deg.	D_m ft	h ft	$R_{90,obs.}$ ft	y ft	x ft
A27	30	0.88	0.38	1.38	0.50	0
					0.47	0.28
					0.21	0.85
					0	1.21
A28	30	1.02	0.38	1.65	0.65	0
					0.60	0.35
					0.26	1.05
					0	1.48
A29	30	1.24	0.45	2.00	0.79	0
					0.74	0.43
					0.32	1.28
					0	1.81
A30	30	1.54	0.53	2.25	1.01	0
					0.94	0.54
					0.41	1.62
					0	2.16
A31	30	2.19	0.79	3.01	1.40	0
					1.30	0.75

Table B.5 (continued)

Expt. No.	Bucket Angle deg.	D_m ft	h ft	$R_{90,obs.}$ ft	y ft	x ft
A31	30	2.19	0.79	3.01	1.40	0
					0.57	2.26
					0	3.02
A32	30	1.65	0.65	1.59	1.00	0
					0.93	0.55
					0.40	1.65
					0	1.91
A33	30	2.00	0.78	1.97	1.20	0
					1.13	0.67
					0.50	2.02
					0	2.30
A34	30	2.23	1.00	2.25	1.23	0
					1.14	0.71
					0.51	2.12
					0	2.51
A35	30	2.42	1.18	3.00	1.24	0
					1.15	0.74
					0.51	2.21
					0	2.95

Table B.6.a

Maximum Depth of Scour with Scour Hole Formation

$$A = \frac{V_m^2}{g\,d} \qquad C = \frac{1}{1 + z/d}$$

$$B = \frac{1}{S_s - 1} \qquad I = \frac{D_m/d}{B^{0.35}\, C^{0.83}\, \beta^{0.87}}$$

Expt. No.	d in	z/d	D_m in	S_s	β rad.	A	I
A1	0.75	0.40	16.87	2.25	0.93	10.24	34.47
A2	0.75	0.40	20.90	2.25	0.90	13.59	43.90
A3	0.75	0.40	27.16	2.25	0.87	15.45	58.96
A4	0.75	0.40	26.14	2.25	0.84	21.08	58.56
A5	0.75	0.40	28.33	2.25	0.81	22.95	64.98
A6	0.75	0.40	27.07	2.25	0.86	15.44	60.98
A7	0.75	0.40	9.24	2.25	0.89	9.57	19.39
A8	0.75	0.40	15.24	2.25	0.83	10.80	34.20
A9	0.75	0.40	19.69	2.25	0.78	11.41	46.74
A10	0.75	0.40	27.24	2.25	0.80	15.31	63.08
A11	0.75	0.40	27.24	2.25	0.83	14.33	54.14
A12	0.75	0.40	10.37	2.25	1.15	16.61	57.34

Table B.6.a (continued)

Expt. no.	d in	z/d	D_m ft	S_s	β rad.	A	I
A13	0.75	0.40	22.25	2.25	1.09	14.82	48.88
A14	0.75	0.40	25.00	2.25	1.05	19.26	55.10
A15	0.75	0.50	27.49	2.25	1.00	22.19	51.85
A16	0.75	0.40	16.80	2.25	1.16	14.12	38.11
A17	0.75	0.40	24.48	2.25	1.12	13.18	42.28
A18	0.75	0.40	27.36	2.25	1.15	15.72	46.12
A19	0.75	0.40	28.68	2.25	1.11	17.62	49.64
A20	0.75	0.40	29.76	2.25	1.10	20.51	51.90
A21	0.75	0.40	30.48	2.25	1.09	23.26	53.63
A22	0.75	0.40	17.70	2.25	1.29	11.70	26.86
A23	0.75	0.40	23.38	2.25	1.27	14.78	35.88
A24	0.75	0.40	24.40	2.25	1.26	21.38	47.80
A25	0.75	0.40	23.86	2.25	1.25	29.06	47.32
A26	0.75	0.40	22.80	2.25	1.23	35.81	56.07
A27	0.25	0.30	10.50	2.55	0.90	26.45	66.14
A28	0.25	0.30	12.25	2.55	0.90	32.59	77.68
A30	0.25	0.30	18.49	2.55	0.86	37.73	122.32
A31	0.25	0.30	26.24	2.55	0.80	39.84	183.66
A32	0.25	0.30	19.74	2.55	1.09	36.15	145.47
A33	0.25	0.30	24.00	2.55	1.06	41.43	130.89

Table B.6.a (continued)

Expt. No.	d in	z/d	D_m in	S_s	β rad.	A	I
A34	0.25	0.30	26.75	2.55	1.02	53.79	151.44
A35	0.25	0.30	28.99	1.55	0.99	63.96	168.41

Table B.6.b

Maximum Depth of Scour without Scour Hole Formation
Using Granular Bed Materials

Bucket Angle : 45°

Exp. No.	q cfs/ft	H in	d in	z/d	D_m in	S_s	β rad.	A	I
B1	0.68	35.16	0.75	0.40	14.88	2.25	1.15	17.49	34.86
B2	0.70	32.76	0.75	0.40	17.04	2.25	1.14	15.23	28.73
B3	0.82	29.40	0.75	0.40	20.76	2.25	1.10	13.60	35.97
B4	0.94	26.40	0.75	0.40	24.48	0.25	1.06	12.19	34.01
B5	1.35	23.52	0.75	0.40	28.44	2.25	1.00	13.82	40.85
B6	0.49	38.40	0.75	0.40	14.60	2.25	1.17	13.70	30.04
B7	0.32	38.64	0.25	0.30	14.40	2.55	1.19	27.13	70.94

Table B.6.c

Maximum Depth of Scour without Scour Hole Formation

Using Concrete Blocks as Bed Materials

$$A = \frac{V_m^2}{g\,d} \qquad C = \frac{1}{1 + z/d}$$

$$B = \frac{1}{S_s - 1} \qquad I = \frac{D_m/d}{B^{0.35}\,C^{0.83}\,\beta^{0.87}}$$

Exp no.	Bucket Angle deg.	q cfs/ft	H in	d in	z/d	D_m in	S_s	β rad	A	I
C1	15	1.17	35.13	2.00	0	10.88	1.16	0.93	13.79	23.09
C2	15	1.52	36.00	3.16	0	10.30	1.11	0.91	11.96	20.07
C3	15	1.73	37.75	1.00	0	10.50	3.75	0.91	22.94	46.29
C4	15	1.82	43.38	2.00	0.0	5.00	3.75	0.95	23.37	43.74
C5	15	2.10	39.00	6.00	0.0	8.3	2.95	0.89	11.05	21.94
C6	15	1.82	38.13	6.00	0.25	8.25	1.13	0.90	9.56	12.41
C7	15	2.20	38.95	3.16	0.24	10.85	1.10	0.86	16.31	22.10
C8	15	1.84	39.94	5.00	0.25	6.81	2.06	0.92	14.02	21.81
C9	15	2.13	42.14	3.66	0.27	7.28	3.81	0.89	14.63	23.86
C10	15	2.36	42.94	3.12	0.24	7.75	4.14	0.88	14.90	24.98
C11	15	1.82	32.64	3.94	0.51	9.64	1.06	0.90	10.36	20.42

Table B.6.c (continued)

Exp No.	Bucket Angle deg.	q cfs/ft	H in	d in	z/d	D_m in	S_s	β rad.	A	I
C12	15	2.15	40.50	2.98	0.50	8.51	1.95	0.89	22.66	44.35
C13	15	2.20	42.88	3.21	0.47	6.90	4.14	0.90	10.71	24.86
C14	15	2.33	41.00	1.00	0.50	10.50	3.75	0.86	18.28	23.87
C15	15	2.20	38.88	3.16	0.71	10.92	1.10	0.86	11.18	22.77
C16	15	1.59	36.00	1.00	0.75	11.50	2.66	0.91	15.32	23.77
C17	15	1.72	39.85	1.00	0.75	8.40	2.66	0.93	15.82	21.04
C18	15	2.30	43.25	5.00	0.75	5.50	2.90	0.90	10.30	12.40
C19	15	0.59	26.18	4.27	0.0	11.11	2.11	0.73	2.30	3.58
C20	30	0.53	26.05	5.00	0.0	10.63	2.06	0.73	1.83	2.86
C21	30	0.58	26.05	6.00	0.0	10.38	2.17	0.73	1.70	2.43
C22	30	0.81	26.80	6.00	0.0	13.38	2.17	0.72	1.87	3.16
C23	30	0.48	26.48	3.21	0.0	10.65	2.95	0.75	2.68	5.42
C24	30	0.57	26.60	5.07	0.0	9.97	2.90	0.74	2.13	3.22
C25	30	0.66	26.60	6.00	0.0	9.88	2.95	0.73	2.06	2.75
C26	30	0.29	28.48	2.00	0.0	8.25	3.54	0.81	3.70	6.87
C27	30	1.07	30.93	3.86	0.0	11.07	3.81	5.28	5.28	5.15
C28	30	0.58	29.10	6.00	0.0	7.00	2.95	0.79	2.84	2.82
C29	30	0.56	31.30	5.00	0.25	15.40	1.12	0.81	1.60	2.13
C30	30	1.59	4.85	6.00	0.25	12.60	1.13	0.64	1.49	1.85

Table B.6.c (continued)

Expt. No.	Bucket Angle deg.	q cfs/ft	H in	d in	z/d	D_m in	S_s	β rad	A	I
C31	30	1.04	33.85	2.00	0.25	15.60	2.08	0.82	7.63	11.53
C32	30	1.76	30.29	4.27	0.23	18.40	2.11	0.91	5.22	5.82
C33	30	0.92	34.51	2.00	0.25	14.56	3.54	0.84	7.42	14.25
C34	30	0.92	33.07	1.00	0.25	16.50	3.75	0.82	12.60	33.91
C35	30	0.99	31.14	2.00	0.50	16.19	0.98	0.98	7.62	9.41
C36	30	0.99	31.19	3.94	0.51	13.97	1.06	0.98	4.21	5.03
C37	30	1.45	32.01	5.00	0.50	15.56	1.12	0.95	4.60	5.18
C38	30	1.16	31.01	2.00	0.50	16.81	1.16	0.97	8.54	9.46
C39	30	1.72	32.88	1.00	0.75	17.32	2.66	0.94	20.77	38.80
C40	30	1.33	37.57	2.98	0.76	10.39	1.95	1.01	12.06	25.19
C41	30	1.51	33.01	1.00	0.75	16.69	2.66	0.95	22.80	35.11
C42	30	1.33	38.95	2.00	0.75	13.50	5.54	0.94	13.40	25.11
C43	45	0.23	34.95	3.16	0.0	11.92	1.10	1.17	1.82	1.47
C44	45	0.33	32.95	5.00	0.0	12.00	1.12	1.18	1.59	0.99
C45	45	0.50	32.64	2.00	0.0	13.06	2.08	1.19	5.37	5.73
C46	45	0.40	34.70	2.98	0.0	10.51	1.95	1.20	4.73	4.97
C47	45	0.44	36.14	1.00	0.0	12.31	3.75	1.17	10.51	15.29
C48	45	0.66	35.64	2.00	0.0	11.81	4.54	1.17	8.29	9.10
C49	45	0.54	31.67	2.00	0.25	15.56	1.16	1.42	5.16	5.64
C50	45	0.54	31.87	5.00	0.25	14.11	1.12	1.13	2.09	1.44

Table B.6.c (continued)

B.A. = Bucket Angle

Exp. No.	B.A. deg.	q cfs/ft	H in	d in	z/d	D_m in	S_s	β rad	A	I
C51	45	0.92	33.08	6.00	0.25	15.00	1.13	1.09	2.80	2.36
C52	45	1.01	32.80	2.00	0.25	16.19	2.08	1.11	8.58	9.90
C53	45	1.01	32.90	2.98	0.25	15.70	1.95	1.11	5.95	3.97
C54	45	1.17	33.17	4.27	0.23	15.30	2.11	1.10	4.97	4.95
C55	45	1.16	33.17	1.00	0.25	16.94	5.75	1.10	19.03	29.59
C56	45	1.18	33.17	2.00	0.25	16.44	3.54	1.10	9.92	12.55
C57	45	1.51	33.97	3.21	0.23	16.28	4.14	1.09	8.01	8.99
C58	45	1.84	34.30	3.86	0.26	16.51	3.81	1.07	8.02	9.97
C59	45	1.34	30.89	3.21	0.23	14.21	4.14	1.17	8.05	9.85
C60	45	0.75	31.30	2.00	0.50	15.81	1.16	1.14	6.51	6.25
C61	45	0.75	32.42	3.94	0.76	14.84	1.06	1.12	3.56	3.03
C62	45	0.75	32.43	6.00	0.50	13.81	1.13	1.12	2.51	2.42
C63	45	0.43	35.14	2.00	0.50	13.06	1.16	1.14	4.82	4.32
C64	45	1.34	28.27	5.00	0.50	22.31	1.12	1.01	2.90	2.95
C65	45	0.34	33.39	6.00	0.50	12.94	1.13	1.13	1.24	1.33
C66	45	0.99	32.18	2.00	0.50	16.19	2.08	1.12	8.38	10.54
C67	45	1.49	33.68	2.98	0.50	16.45	1.95	1.09	8.41	9.06
C68	45	1.16	35.38	5.00	0.50	16.61	2.08	1.08	3.95	4.48
C69	45	1.16	35.38	5.00	0.50	16.61	2.08	1.08	11.40	21.15
C70	45	1.34	32.28	2.00	0.50	17.19	3.54	1.10	10.70	15.29

Table B.6.c (continued)

B.A. = Bucket Angle

Exp. No.	B.A. deg.	q cfs/ft	H in	d in	z/d	D_m in	S_s	β rad	A	I
C71	45	2.00	34.48	3.21	0.47	16.83	4.14	1.07	10.29	11.14
C72	45	1.34	32.89	2.00	0.50	18.56	3.54	1.06	9.71	17.02
C73	45	1.81	36.52	3.21	0.47	15.83	4.14	1.07	10.16	10.54
C74	45	1.83	32.48	2.00	0.50	20.10	3.54	1.03	11.99	18.95
C75	45	1.83	32.48	2.00	0.50	20.10	3.54	1.03	11.99	15.95
C66	45	0.77	32.30	3.94	0.76	14.97	1.06	1.12	3.60	2.98
C77	45	0.45	34.78	2.00	0.75	13.42	1.16	1.14	4.84	5.06
C78	45	1.92	29.14	5.00	0.75	23.06	1.12	0.99	4.04	4.54
C79	45	0.94	35.99	2.00	0.75	12.88	2.08	1.13	10.66	11.40
C80	45	1.46	33.55	2.98	0.76	16.57	1.95	1.09	8.14	8.99
C81	45	0.77	31.98	1.00	0.75	14.47	2.66	1.17	12.94	23.97
C82	45	1.50	31.82	2.00	0.75	20.42	2.06	1.04	9.63	15.99
C83	45	1.88	33.86	2.98	0.76	18.60	1.95	1.05	9.20	11.38
C84	45	1.59	33.67	1.00	0.75	17.31	3.75	1.09	25.42	39.37
C85	45	1.33	33.37	2.00	0.75	16.61	3.54	1.10	11.09	16.88
C86	45	1.52	35.50	2.00	0.75	16.20	3.74	1.08	13.28	19.10
C87	45	0.33	30.38	3.16	0.0	15.30	1.10	1.28	1.97	1.83
C88	60	0.33	30.38	3.94	0.0	14.90	1.06	1.28	1.62	1.13
C89	60	0.41	32.71	5.00	0.0	12.42	1.12	1.29	1.95	1.94

Table B.6.c (continued)

B.A. = Bucket Angle

Exp. No.	B.A. deg.	q cfs/ft	H in	d in	z/d	D_m in	S_s	β rad	A	I
C90	60	0.41	30.13	6.00	0.0	14.88	1.13	1.27	1.31	0.98
C91	60	0.42	30.31	3.16	0.0	16.11	1.10	1.27	2.32	1.84
C92	60	0.42	30.31	5.00	0.0	15.19	1.12	1.27	1.56	1.27
C93	60	0.55	33.38	2.00	0.0	13.88	2.08	1.28	5.91	5.81
C94	60	0.58	30.63	2.98	0.0	16.38	1.95	1.26	3.37	4.18
C95	60	0.62	30.75	5.00	0.0	15.38	2.06	1.26	2.29	2.25
C96	60	0.69	31.13	6.00	0.0	14.88	2.17	1.26	2.20	2.13
C97	60	0.62	30.94	2.00	0.0	16.69	3.03	1.26	5.29	6.83
C98	60	0.66	30.31	3.00	0.0	16.19	1.95	1.27	3.85	4.28
C99	60	0.40	32.13	2.00	0.0	13.88	3.54	1.29	4.28	4.64
C100	60	0.99	32.63	3.21	0.0	15.27	4.14	1.29	5.34	5.65
C101	60	0.93	34.14	3.86	0.0	13.94	3.81	1.26	5.18	5.21
C102	60	0.90	29.88	5.00	0.0	17.38	2.90	1.24	2.89	3.18
C103	60	0.41	29.31	2.00	0.25	17.31	1.16	1.27	3.30	3.48
C104	60	0.62	26.65	3.16	0.24	20.40	1.10	1.24	2.52	2.84
C105	60	0.55	29.64	5.00	0.25	16.11	1.12	1.26	1.91	1.50
C106	60	1.01	28.92	6.00	0.25	18.33	1.13	1.23	2.49	1.90
C107	60	0.75	28.31	5.00	0.25	18.69	1.12	1.24	2.18	1.77
C108	60	1.17	26.57	5.00	0.30	21.68	1.13	1.21	2.81	2.23

Table B.6.c (continued)

B.A. : Bucket Angle

Exp. No.	B.A. deg.	q cfs/ft	H in	d in	z/d	D_m in	S_s	β rad	A	I
C109	60	1.01	29.69	2.00	0.25	19.44	2.08	1.24	7.16	9.93
C110	60	1.01	29.43	2.98	0.25	19.20	1.95	1.23	4.84	5.31
C111	60	0.94	30.21	4.27	0.23	17.40	2.11	1.24	3.54	4.04
C112	60	2.51	27.56	5.00	0.25	21.94	2.06	1.20	6.02	6.59
C113	50	0.94	28.76	2.98	0.25	19.50	1.95	1.23	4.40	5.40
C114	60	1.17	28.77	2.00	0.25	21.10	3.54	1.22	7.54	12.71
C115	60	1.16	31.59	3.21	0.23	17.55	4.14	1.24	5.91	8.02
C116	60	1.76	27.06	3.86	0.26	23.63	3.84	1.18	5.00	7.17
C117	60	1.17	29.31	2.00	0.25	20.44	5.54	1.22	7.87	12.20
C118	60	0.51	28.69	2.00	0.50	18.81	1.16	1.25	3.72	4.72
C119	60	0.67	28.19	3.94	0.50	18.84	1.06	1.24	2.44	2.07
C120	60	0.69	32.19	6.00	0.50	13.81	1.13	1.26	2.41	2.28
C121	60	0.50	31.94	2.00	0.50	15.06	1.16	1.28	4.83	4.90
C122	60	0.51	26.36	3.94	0.51	20.17	1.06	1.24	1.68	1.22
C123	60	1.34	27.56	5.00	0.50	21.31	1.12	1.20	3.32	2.40
C124	60	0.67	29.75	6.00	0.50	16.25	1.13	1.25	1.92	1.52
C125	60	0.99	31.31	2.00	0.50	17.81	2.06	1.24	7.92	11.45
C126	60	1.34	26.56	2.98	0.50	23.32	1.95	1.20	4.98	6.17
C127	60	1.49	27.06	4.27	0.47	22.68	2.11	1.19	4.01	5.46
C128	60	0.99	27.31	2.00	0.50	21.81	2.08	1.22	5.99	10.11

Table B.6.c (continued)

B.A.: Bucket Angle

Exp. No.	B.A. deg.	q cfs/ft	H in	d in	z/d	D_m in	S_s	β rad	A	I
C129	60	1.48	28.06	2.98	0.50	22.32	1.95	1.20	5.92	8.26
C130	60	1.17	30.51	4.27	0.47	21.61	2.11	1.20	3.53	4.12
C131	60	1.82	26.30	1.00	0.50	21.69	3.75	1.21	21.72	39.35
C132	60	2.10	30.64	3.21	0.47	22.01	4.14	1.19	8.22	12.04
C133	60	0.99	30.88	1.00	0.50	18.75	3.75	1.24	14.92	30.78
C134	60	0.54	31.76	2.00	0.75	15.61	1.16	1.27	4.98	5.33
C135	60	0.94	25.45	0.71	0.71	22.60	1.10	1.21	3.34	3.19
C136	60	0.67	25.39	2.93	0.76	21.65	1.06	1.22	2.01	2.25
C137	60	1.34	27.76	5.00	0.75	21.11	1.12	1.21	3.37	2.70
C138	60	1.49	27.26	6.00	0.75	21.61	1.13	1.20	3.01	2.39
C139	60	0.54	29.46	2.00	0.75	17.91	1.16	1.26	4.16	5.17
C140	60	0.75	24.62	3.94	0.76	22.91	1.06	1.21	2.09	2.13
C141	60	1.51	22.80	5.00	0.75	26.70	1.12	1.16	2.66	3.15
C142	60	1.84	23.27	6.00	0.75	26.60	1.13	1.15	2.74	3.05
C143	60	1.33	29.76	2.98	0.76	20.00	1.95	1.22	6.17	8.79
C144	60	1.00	30.30	2.00	0.75	18.95	2.08	1.24	7.35	11.79
C145	60	1.33	32.19	2.98	0.76	17.57	1.95	1.23	7.34	8.64
C146	60	1.45	24.77	1.00	0.75	26.60	3.75	1.18	13.49	32.14
C147	60	1.33	30.25	2.00	0.75	20.00	3.54	1.22	9.28	18.31

Table B.7

Maximum Depth of Scour below Sharp-edged Weirs

$$A = \frac{V_m^2}{g\,d} \qquad J = \frac{D_m / d}{C^{0.83}\,\beta^{0.87}}$$

$$C = \frac{1}{1 + z/d} \qquad S_s = 2.22$$

Expt. No.	q cfs/ft	H in	d in	z/d	D_m in	β rad.	A	J
D1	0.96	4.25	2.00	0.33	11.75	0.50	2.16	10.30
D2	0.32	4.50	1.75	0.33	8.75	1.00	2.01	8.75
D3	0.64	3.75	1.75	0.33	11.00	0.56	2.00	10.22
D4	0.96	4.25	1.75	0.33	11.88	0.50	2.44	12.90
D5	0.32	3.63	1.50	0.33	9.75	0.93	1.79	7.84
D6	0.96	4.25	1.50	0.33	12.00	0.50	2.82	14.92
D7	0.32	4.13	1.25	0.33	9.38	0.98	2.47	9.78
D8	0.64	3.63	1.25	0.33	11.38	0.53	2.33	15.35
D9	0.96	4.25	1.25	0.33	12.13	0.50	3.35	19.91
D10	0.32	3.13	1.00	0.33	10.50	0.87	2.21	13.20
D11	0.96	4.25	1.00	0.33	12.25	0.50	4.14	29.48
D12	0.96	4.25	2.00	0.66	11.75	0.50	2.16	11.51

Table B.7 (continued)

Expt. No.	q cfs/ft	H in	d in	z/d	D_m in	β rad.	A	I
D13	0.64	4.25	1.75	0.66	10.50	0.67	2.40	9.98
D14	0.96	4.25	1.75	0.66	11.88	0.50	2.44	13.30
D15	0.96	4.25	1.50	0.66	12.00	0.50	2.82	15.67
D16	0.32	3.75	1.25	0.66	9.75	0.94	2.21	10.93
D17	0.64	3.50	1.25	0.66	11.50	0.49	2.10	14.19
D18	0.96	4.25	1.26	0.66	12.13	0.50	3.32	19.86
D19	0.64	3.75	1.00	0.66	11.38	0.56	3.13	20.66
D20	0.96	4.25	1.00	0.66	12.25	0.50	4.14	28.99
D21	0.64	3.63	0.75	0.66	11.63	0.53	3.80	29.21
D22	0.96	4.25	0.75	0.66	12.38	0.50	5.57	38.33
D23	0.64	3.38	0.50	0.66	12.00	0.45	4.54	45.24
D24	0.32	4.13	2.00	0.00	9.00	0.98	1.61	7.37
D25	0.64	3.88	2.00	0.00	10.75	0.60	1.77	7.33
D26	0.96	4.25	2.00	0.00	11.75	0.50	2.16	9.93
D27	0.32	3.75	1.75	0.00	9.50	0.94	1.62	6.63
D28	0.64	3.63	1.75	0.00	11.12	0.53	1.70	8.29
D29	0.96	4.25	1.75	0.00	11.88	0.50	2.44	11.32
D30	0.32	3.38	1.50	0.00	10.00	0.90	1.65	7.11
D31	0.64	3.88	1.50	0.00	11.00	0.60	2.31	10.99

Table B.7 (continued)

Expt. No.	q cfs/ft	H in	d in	z/d	D_m in	β rad.	A	I
D32	0.96	4.25	1.50	0.00	12.00	0.50	2.82	14.16
D33	0.64	3.63	1.25	0.00	11.38	0.53	2.23	13.31
D34	0.96	4.25	1.25	0.00	12.13	0.50	3.35	19.75
D35	0.64	3.63	1.00	0.00	11.50	0.53	2.88	16.81
D36	0.64	5.25	2.00	0.33	13.50	0.79	2.07	9.97
D37	0.96	4.88	2.00	0.33	15.00	0.47	1.72	10.62
D38	0.64	5.25	1.75	0.33	13.63	0.79	2.35	11.33
D39	0.96	4.88	1.75	0.33	15.13	0.47	1.95	11.70
D40	0.64	4.75	1.50	0.33	14.25	0.73	2.33	13.28
D41	0.96	4.88	1.50	0.33	15.25	0.47	2.25	14.46
D42	0.64	4.75	1.24	0.33	14.38	0.73	2.77	16.08
D43	0.96	4.88	1.25	0.33	15.38	0.47	2.68	20.34
D44	0.64	4.25	1.00	0.33	14.50	0.73	3.43	22.27
D45	0.96	4.88	1.00	0.33	15.50	0.47	3.33	25.14
D46	0.64	4.75	0.75	0.33	14.63	0.73	4.53	29.27
D47	0.96	4.88	0.75	0.33	15.63	0.47	4.40	37.83
D48	0.64	4.50	0.50	0.33	15.00	0.69	6.17	49.32
D49	0.96	4.88	1.75	0.66	15.13	0.47	1.95	12.53
D50	0.32	5.25	1.50	0.66	12.38	1.01	1.80	10.15

Table B.7 (continued)

Expt. No.	q cfs/ft	H ft	d in	z/d	D_m in	β rad	A	I
D51	0.95	4.88	1.50	0.66	15.25	0.47	2.24	17.62
D52	0.96	4.88	1.25	0.66	15.38	0.47	2.68	20.95
D53	0.96	4.88	1.00	0.66	15.50	0.47	3.33	30.44
D54	0.64	4.25	0.75	0.66	15.13	0.64	3.74	32.89
D55	0.96	4.88	0.75	0.66	15.63	0.47	4.40	42.27
D56	0.64	4.25	0.50	0.66	15.25	0.64	5.57	51.23
D57	0.32	4.87	2.00	0.0	12.50	0.99	1.27	4.29
D58	0.64	4.25	2.00	0.0	14.50	0.64	1.46	6.45
D59	0.96	4.87	2.00	0.0	15.00	0.47	1.71	8.85
D60	0.32	5.38	1.75	0.0	12.13	1.02	1.60	6.84
D61	0.64	4.25	1.75	0.0	14.63	0.64	1.56	7.90
D62	0.96	4.88	1.75	0.0	15.13	1.95	1.95	12.61
D63	0.64	4.25	1.50	0.0	14.50	0.64	1.9	12.60
D64	0.96	4.88	1.50	0.0	15.25	0.47	2.25	14.00
D65	0.64	4.75	1.25	0.0	14.38	0.73	2.77	15.94
D66	0.96	4.88	1.31	0.0	15.38	0.47	2.56	17.48
D67	0.64	4.75	1.00	0.0	14.50	0.73	3.43	19.57
D68	0.96	4.87	0.75	0.0	15.50	0.47	4.41	32.65

Table B.8

Comparision between the Observed and Calculated Values of R_o

$$R_o = 1.55 \left(D_m - h \right)^{0.24}$$

Expt. No.	D_m ft	h ft	$R_{o,obs.}$ ft	$R_{o,cal.}$ ft
A1	1.41	1.20	1.18	1.07
A2	1.74	1.26	1.50	1.36
A3	2.26	1.35	1.83	1.62
A4	2.18	1.39	2.08	1.57
A5	2.36	1.45	2.07	1.62
A6	2.25	1.35	1.81	1.60
A7	0.77	0.50	0.97	1.12
A8	1.27	0.77	0.99	1.21
A9	1.64	1.02	0.96	1.28
A10	2.01	0.67	2.03	1.76
A11	2.27	0.97	2.06	1.80
A12	0.85	0.49	1.09	1.21
A13	1.85	0.77	1.25	1.43
A14	2.08	0.94	1.35	1.50
A15	2.29	1.21	1.24	1.48
A16	1.40	1.21	0.89	1.01
A17	2.04	1.47	1.18	1.31

Table B.8 (continued)

Expt. No.	D_m ft	h ft	$R_{o,obs.}$ ft	$R_{o,cal}$ ft
A18	2.28	1.32	1.29	1.42
A19	2.39	1.33	1.60	1.57
A20	2.48	1.37	1.69	1.59
A21	2.54	1.43	1.75	1.59
A22	1.48	1.23	0.97	1.11
A23	1.95	1.31	1.18	1.31
A24	2.03	1.37	1.70	1.51
A25	1.99	1.47	1.62	1.43
A26	1.98	1.50	1.64	1.39
A27	0.88	0.38	1.81	1.41
A28	1.02	0.38	1.90	1.51
A29	1.24	0.45	1.93	1.59
A30	1.54	0.53	2.01	1.68
A31	2.19	0.79	1.56	1.71
A32	1.65	0.65	1.29	1.45
A33	2.00	0.78	1.43	1.61
A34	2.26	1.00	1.45	1.62
A35	2.42	1.18	1.47	1.63

Table B.9.a

Data and Calculated Values of Radius Vectors

$$R_\theta = R_o \left(1 + 0.095\, \theta_b^{0.81} \right)$$

$$\theta_b : 30^\circ - 90^\circ$$

Expt. No.	$R_{o,obs.}$ ft	Observed Values, ft.			Calculated Values, ft.		
		R_{30}	R_{60}	R_{90}	R_{30}	R_{60}	R_{90}
A1	1.18	1.21	1.23	1.26	1.25	1.30	1.34
A2	1.50	1.51	1.52	1.50	1.58	1.64	1.70
A3	1.83	1.84	1.85	1.87	1.94	2.01	2.07
A4	2.08	2.14	2.27	2.40	2.22	2.33	2.91
A5	2.07	2.23	2.41	2.53	2.16	2.26	2.38
A6	1.81	1.88	1.90	1.93	1.90	2.00	2.08
A7	0.97	0.80	0.79	1.05	1.00	1.01	1.03
A8	0.99	1.21	1.37	1.32	1.31	1.38	1.44
A9	0.96	1.12	1.15	1.25	1.06	1.13	1.20
A10	2.03	1.95	1.92	2.15	2.11	2.19	2.28
A11	2.06	2.13	2.37	2.50	2.09	2.15	2.22
A12	0.85	0.67	0.80	1.17	0.88	0.96	0.99
A13	1.25	1.35	1.45	1.55	1.33	1.42	1.51
A14	1.35	1.38	1.50	1.62	1.45	1.50	1.56

Table B.9.a (continued)

Expt. No.	R_o ft	Observed Values, ft			Calculated Values, ft.		
		R_{30}	R_{60}	R_{90}	R_{30}	R_{60}	R_{90}
A15	1.24	1.50	1.60	1.81	1.31	1.41	1.52
A16	0.89	0.67	0.61	0.69	0.93	0.97	1.01
A17	1.18	1.25	1.27	1.26	1.26	1.31	1.35
A18	1.29	1.43	1.61	1.73	1.39	1.49	1.60
A19	1.60	1.73	2.00	1.77	1.69	1.79	1.89
A20	1.69	1.77	2.00	1.83	1.77	1.84	1.92
A21	1.75	1.60	1.64	1.74	1.80	1.85	1.90
A22	0.97	0.93	0.97	0.99	0.99	1.02	1.06
A23	1.18	1.12	1.21	1.27	1.21	1.26	1.31
A24	1.70	1.74	1.69	1.72	1.78	1.86	1.93
A25	1.62	1.75	1.78	1.74	1.70	1.78	1.86
A26	1.64	1.79	1.81	1.74	1.73	1.81	1.90
A27	1.81	1.70	1.70	1.65	1.88	1.94	2.01
A28	1.90	1.75	1.70	1.80	1.94	1.98	2.01
A29	1.93	1.87	2.07	2.00	1.97	2.04	2.10
A30	2.01	1.85	1.89	1.92	2.05	2.10	2.15
A31	1.56	1.72	1.86	1.98	1.64	1.73	1.82
A32	1.29	1.45	1.55	1.78	1.36	1.44	1.53
A33	1.43	1.65	1.85	1.96	1.51	1.60	1.69
A34	1.45	1.72	1.92	2.01	1.54	1.63	1.73
A35	1.47	1.75	1.69	1.75	1.56	1.75	1.84

Table B.9.b

Data and Calculated Values of Radius Vectors

$$R_\theta = R_o \left(1 + 0.095\, \theta_b^{0.81} \right)$$

$$\theta_b : 120^\circ - 180^\circ$$

Expt. No.	R_o ft	Observed Values, ft			Calculated Values, ft.		
		R_{120}	R_{150}	R_{180}	R_{120}	R_{150}	R_{180}
A1	1.18	1.29	1.32	1.34	1.38	1.42	1.46
A2	1.50	1.53	1.63	1.58	1.75	1.80	1.75
A3	1.83	1.93	2.11	2.38	2.14	2.20	2.26
A4	2.08	2.41	2.36	2.48	2.53	2.61	2.69
A5	2.07	2.60	2.70	2.73	2.49	2.59	2.70
A6	1.81	1.97	2.12	2.36	2.16	2.21	2.28
A7	0.97	1.10	1.20	1.28	1.13	1.25	1.36
A8	0.99	1.15	1.30	1.30	1.07	1.16	1.24
A9	0.96	1.31	1.42	1.52	1.27	1.39	1.46
A10	2.03	2.37	2.58	2.70	2.37	2.46	2.56
A11	2.06	2.70	2.80	2.90	2.36	2.45	2.61
A12	0.85	1.27	1.45	1.47	1.03	1.06	1.18
A13	1.25	1.62	1.72	1.90	1.60	1.69	1.79

Table B.9.b (continued)

Expt. No.	R_o ft	Observed Values, ft.			Calculated Values, ft.		
		R_{120}	R_{150}	R_{180}	R_{120}	R_{150}	R_{180}
A14	1.35	1.62	1.75	2.00	1.61	1.66	1.73
A15	1.24	1.91	1.70	1.61	1.63	1.72	1.83
A16	0.89	0.89	0.88	0.90	1.05	1.10	1.14
A17	1.18	1.29	1.45	1.70	1.27	1.36	1.45
A18	1.29	1.64	1.83	1.77	1.69	1.79	1.89
A19	1.60	1.71	2.02	2.08	1.98	2.06	2.14
A20	1.69	1.88	1.89	2.03	2.00	2.08	2.16
A21	1.75	1.76	1.83	1.78	1.94	1.98	2.03
A22	0.97	1.01	0.87	0.83	1.08	1.12	1.15
A23	1.18	1.20	1.21	1.27	1.34	1.38	1.42
A24	1.70	1.69	1.72	1.73	1.99	2.04	2.09
A25	1.62	1.67	1.70	1.76	1.94	2.02	2.10
A26	1.64	1.79	1.83	1.92	2.00	2.09	2.10
A27	1.81	1.72	1.77	2.20	2.06	2.11	2.15
A28	1.90	1.70	2.00	2.25	2.05	2.09	2.15
A29	1.93	2.15	2.49	2.25	2.14	2.21	2.29
A30	2.01	1.97	1.99	2.03	2.19	2.23	2.27
A31	1.56	2.15	2.25	2.37	1.92	2.01	2.11
A32	1.29	1.89	1.99	2.05	1.63	1.72	1.81

Table B.9.b (continued)

Expt. No.	R_o ft	Observed Values, ft.			Calculated Values, ft.		
		R_{120}	R_{150}	R_{180}	R_{120}	R_{150}	R_{180}
A33	1.43	2.05	2.15	2.24	1.78	1.87	1.96
A34	1.45	2.10	2.19	2.25	1.83	1.92	2.02
A35	1.47	1.79	2.00	2.12	1.93	2.02	2.10

Table B.10.a

Observed and Calculated Values of D

for $r/R_\theta = 1/3$

$$D = (D_m - h) (1 - r^2/R_\theta^2)$$

Expt. No.	Observed Values of D in ft. 0°	30°	60°	90°	120°	150°	180°	Ave.	$D_{cal.}$
A1	0.09	0.09	0.11	0.16	0.17	0.17	0.17	0.14	0.17
A2	0.42	0.42	0.42	0.42	0.42	0.42	0.40	0.42	0.43
A3	0.84	0.80	0.79	0.74	0.74	0.76	0.76	0.77	0.80
A4	0.71	0.69	0.69	0.70	0.70	0.72	0.70	0.70	0.70
A5	0.80	0.79	0.77	0.74	0.74	0.79	0.80	0.77	0.80
A6	0.83	0.80	0.79	0.75	0.75	0.76	0.76	0.78	0.80
A16	0.17	0.17	0.17	0.17	0.17	0.17	0.16	0.17	0.20
A17	0.45	0.45	0.48	0.46	0.47	0.50	0.50	0.47	0.48
A18	0.84	0.83	0.75	0.67	0.59	0.74	0.79	0.74	0.68
A19	0.93	0.97	0.94	0.80	0.80	0.81	0.90	0.88	0.87
A20	1.03	1.03	1.01	0.91	0.79	0.92	1.00	0.96	1.04
A21	1.02	1.03	0.93	0.84	0.79	0.97	1.03	0.94	1.12
A22	0.21	0.20	0.21	0.21	0.20	0.20	0.20	0.20	0.22
A23	0.56	0.55	0.54	0.52	0.53	0.55	0.55	0.54	0.56

Table B.10.a (continued)

Expt. No.	Observed Values of D in ft. 0°	30°	60°	90°	120°	150°	180°	Ave.	$D_{cal.}$
A24	0.56	0.56	0.56	0.55	0.55	0.57	0.58	0.56	0.59
A25	0.51	0.51	0.50	0.50	0.51	0.51	0.50	0.50	0.47
A26	0.43	0.43	0.42	0.42	0.42	0.43	0.44	0.42	0.41

Table B.10.b

Observed Values and Calculated Ones of D

for $r/R_\theta = 2/3$

$$D = (D_m - h) (1 - r^2/R_\theta^2)$$

Expt. No.	Observed Values of D in ft. 0°	30°	60°	90°	120°	150°	180°	Ave.	$D_{cal.}$
A1	0.05	0.05	0.06	0.08	0.10	0.12	0.13	0.09	0.14
A2	0.19	0.21	0.21	0.18	0.18	0.22	0.21	0.21	0.26
A3	0.50	0.48	0.52	0.40	0.36	0.37	0.46	0.44	0.50
A4	0.46	0.45	0.42	0.42	0.42	0.45	0.51	0.45	0.44
A5	0.50	0.51	0.51	0.38	0.34	0.42	0.51	0.45	0.50
A6	0.14	0.14	0.11	0.11	0.11	0.11	0.09	0.11	0.13
A16	0.14	0.14	0.11	0.11	0.09	0.10	0.08	0.10	0.14
A17	0.17	0.12	0.35	0.32	0.25	0.29	0.33	0.25	0.18
A18	0.55	0.50	0.46	0.40	0.29	0.29	0.50	0.43	0.43
A19	0.50	0.50	0.50	0.45	0.39	0.40	0.38	0.45	0.54
A20	0.74	0.71	0.75	0.54	0.31	0.42	0.54	0.57	0.64
A21	0.64	0.75	0.67	0.55	0.39	0.46	0.67	0.59	0.71
A22	0.17	0.17	0.18	0.17	0.14	0.14	0.14	0.16	0.14
A23	0.41	0.40	0.38	0.31	0.31	0.36	0.37	0.36	0.35
A24	0.39	0.37	0.37	0.38	0.34	0.34	0.44	0.38	0.37

Table B.10.b (continued)

Expt. No.	Observed Values of D in ft.								$D_{cal.}$
	0^o	30^o	60^o	90^o	120^o	150^o	180^o	Ave.	
A25	0.35	0.31	0.29	0.28	0.28	0.30	0.36	0.31	0.29
A26	0.29	0.27	0.26	0.23	0.23	0.23	0.27	0.25	0.26

Table B.10.c

Observed and Calculated Values of D

for $r/R_\theta = 3/4$

$$D_{cal.} = (D_m - h) (1 - r^2/R_\theta^2)$$

Expt. No.	Observed Values of D in in. 0°	30°	60°	90°	120°	150°	180°	Ave. ft.	$D_{cal.}$ ft.
A7	2.25	2.25	2.50	2.50	2.75	2.75	2.50	0.21	0.25
A8	3.25	3.00	3.25	3.00	3.00	3.00	3.50	0.27	0.35
A9	5.00	5.00	5.00	5.00	5.00	5.00	6.00	0.43	0.43
A10	2.50	4.00	4.00	4.00	4.00	3.00	3.75	0.27	0.41
A11	6.25	7.00	4.00	4.00	2.75	3.80	7.00	0.44	0.56
A12	1.00	1.83	2.00	2.00	1.83	1.00	1.50	0.14	0.25
A13	2.00	1.50	4.00	4.00	4.00	3.00	3.00	0.28	0.37
A14	4.00	5.00	4.00	4.00	3.00	2.00	2.00	0.31	0.45
A15	6.00	4.00	6.00	3.50	3.00	3.00	4.00	0.38	0.49
A27	1.88	3.38	4.63	2.88	2.88	2.38	2.38	0.25	0.23
A28	3.00	3.00	2.00	2.50	3.00	2.25	2.25	0.24	0.31
A29	2.80	4.00	3.00	3.00	4.50	4.00	4.00	0.31	0.36
A30	2.25	2.50	3.00	2.50	3.00	3.00	3.00	0.24	0.41
A31	5.25	7.50	6.25	6.50	6.75	5.75	5.25	0.49	0.57
A32	0.75	2.25	4.25	2.25	2.75	3.25	4.00	0.26	0.32

Table B.10.c (continued)

Expt. No.	Observed Values of D in inches 0°	30°	60°	90°	120°	150°	180°	Ave.ft.	$D_{ca.}$ ft.
A33	5.50	5.00	4.50	3.00	2.50	2.50	2.50	0.30	0.47
A34	4.00	5.00	4.00	2.75	2.75	4.00	3.25	0.33	0.51
A35	5.00	5.00	4.00	3.00	3.00	3.00	4.75	0.35	0.59

Table B.10.d

Observed and Calculated Values of D

for $r/R_\theta = 1/4$

$$D_{cal} = (D_m - h) (1 - r^2/R_\theta^2)$$

Expt. No.	Observed Values of D in inches 0°	30°	60°	90°	120°	150°	180°	$D_{ave.}$ ft	$D_{cal.}$ ft
A7	2.25	2.25	2.50	2.50	2.75	2.75	2.50	0.21	0.25
A8	3.25	3.00	3.25	3.00	3.00	3.00	3.50	0.27	0.35
A9	5.00	5.00	5.00	5.00	5.00	6.00	5.00	0.43	0.43
A10	12.50	12.50	12.50	12.25	12.00	12.00	13.25	1.03	1.08
A11	14.75	15.00	14.50	12.75	12.75	13.50	15.75	1.15	1.21
A12	3.50	3.50	3.50	3.50	3.50	3.50	3.50	0.29	0.43
A13	10.00	9.50	10.00	10.00	9.50	9.50	9.00	0.73	0.84
A14	11.00	11.00	11.00	10.00	10.00	10.00	10.00	0.87	0.98
A15	12.00	12.00	12.00	11.00	10.00	11.00	11.50	0.96	1.06
A16	4.88	5.88	6.13	5.88	5.88	6.13	6.13	0.49	0.48
A28	5.00	7.00	7.00	7.00	7.00	6.50	6.50	0.56	0.68
A29	7.50	7.50	8.50	8.50	8.50	7.50	7.50	0.65	0.76
A30	10.00	9.75	9.75	10.00	9.50	9.50	9.50	0.77	0.93
A32	8.75	9.25	9.25	8.75	8.75	9.25	9.25	0.76	0.68
A33	12.00	11.50	10.50	10.00	9.50	9.50	8.50	0.87	1.01

Table B.10.d (continued)

Expt. No.	Observed Values of D in inches							$D_{ave.}$ ft.	$D_{cal.}$ ft.
	0°	30°	60°	90°	120°	150°	180°		
A34	12.00	12.00	11.00	10.75	10.25	10.50	11.00	0.94	1.16
A35	12.50	12.50	12.00	10.00	10.00	11.50	11.30	0.98	1.18

Table B.11

Data and Calculation of Jet Trajectory Length

$$V_o = (2 g H_a)^{1/2}$$

$$L = L_a + L_w$$

$$L_a = \frac{V_o^2 \cos^2 \alpha}{g} \left(\tan \alpha + \sqrt{\tan^2 \alpha + \frac{2 D_t g}{V_o^2 \cos^2 \alpha}} \right)$$

$$L_w = \frac{D_m}{\frac{g L_a}{V_o^2 \cos^2 \alpha} - \tan \alpha}$$

B.A. : Bucket Angle

Expt. No.	B.A. deg.	D_T ft	D_m ft	H_a ft	L_a ft	L_w ft	L ft	$L_{obs.}$ ft
A1	15	1.82	1.41	1.17	3.15	1.02	4.17	3.88
A2	15	1.76	1.74	1.27	3.39	1.29	4.68	4.41
A3	15	1.68	2.26	1.41	3.65	1.81	5.46	5.31
A4	15	1.62	2.18	1.54	3.80	1.78	5.58	5.25
A5	15	1.56	2.36	1.64	3.85	2.14	5.99	5.40
A6	15	1.67	2.26	1.42	1.99	1.82	5.81	5.32
A7	30	1.30	0.77	1.45	3.23	0.45	3.68	3.39

Table B.11 (continued)

B.A. : Bucket Angle

Expt. No.	B.A. deg.	D_t ft.	D_m ft.	H_a ft.	L_a ft.	L_w ft.	L ft.	$L_{obs.}$ ft.
A8	30	1.03	1.27	1.62	3.59	0.75	4.34	4.14
A9	30	0.78	1.64	1.64	3.78	1.32	5.10	5.21
A10	30	0.50	2.01	1.79	3.95	1.49	5.44	5.62
A11	30	1.01	2.27	1.87	4.03	1.58	5.61	5.70
A12	30	2.61	0.85	0.77	3.20	0.39	3.59	3.40
A13	30	2.33	1.85	0.92	3.46	0.96	4.42	4.28
A14	30	2.16	2.08	1.05	3.67	1.19	4.86	4.80
A15	30	1.89	2.29	1.19	3.83	1.47	5.30	5.37
A16	45	1.97	1.40	0.95	3.01	0.51	3.52	3.29
A17	45	1.73	2.04	1.09	3.31	0.99	4.30	4.13
A18	45	1.87	2.28	0.96	3.09	1.03	4.12	4.41
A19	45	1.84	2.39	1.18	3.57	1.18	4.75	4.61
A20	45	1.82	2.48	1.24	3.70	1.25	4.95	5.00
A21	45	1.76	2.54	1.29	3.78	1.32	5.10	5.00
A22	60	2.06	1.28	0.93	2.42	0.43	2.85	3.01
A23	60	1.98	1.95	1.05	2.64	0.60	3.24	3.61
A24	60	1.93	2.03	1.67	2.82	0.66	3.48	3.71
A25	60	1.83	1.99	1.27	2.99	0.78	3.77	4.09
A26	60	1.76	1.90	1.35	3.23	0.79	4.02	4.31
A27	30	1.44	0.88	1.51	2.78	0.58	3.36	3.45
A28	30	1.42	1.02	1.54	2.85	0.76	3.61	3.76

Table B.11 (continued)

B.A. : Bucket Angle

Expt. No.	B.A. deg.	D_T ft.	D_m ft.	H_a ft.	L_a ft.	L_w ft.	L ft.	$L_{obs.}$ ft.
A29	30	1.25	1.24	1.63	2.94	0.93	3.87	4.18
A30	30	1.22	1.54	1.70	3.13	1.28	4.41	4.81
A31	30	1.00	2.19	1.81	4.02	1.83	5.25	5.63
A32	30	2.45	1.65	1.01	3.72	0.86	4.58	4.32
A33	30	2.32	2.00	1.08	3.82	1.11	4.93	4.81
A34	30	2.10	2.23	1.22	4.01	1.17	5.18	5.16
A35	30	1.92	2.42	1.30	3.92	1.55	5.47	5.40

APPENDIX C

REFERENCES

1. Ackerman,N.L. and Undan,R., Forces from Submerged Jets, J. of Hydraulic Div.,A.S.C.E., Nov. 1970.

2. Ahmad, N., Mechanism of Erosion below Hydraulic Works, Proc. of I.N.C., Minneapolis, Minnesota, Sep.1953, pp.133-143.

3. Albertson,M.L., Dai,Y.B., Jenson,R.A., and Rouse,H., Diffusion of Submerged Jets, Trans.A.S.C.E.,Vol. 115, 1950, pp. 639-664.

4. Bakke,P., An experimental Investigation of a Wall Jet, J. of Fluid Mechanics, Vol. 2, 1957.

5. Ballofet, A., Pressures on Spillway Flip Buckets, Proc. of A.S.C.E., Vol. 87, Hy 5, Paper No. 2930, Sept. 1961.

6. Birkhoff,G., and Zarantonello, E.H., Jets, Wakes, and Cavities, Academic Press Inc., N.Y., 1957.

7. Blaisdell, E.A., Equation of the Free-falling Nappe , Proc. of A.S.C.E., Vol. 80, Aug. 1954.

8. Blench, T., Mobile Bed Fluiviology, Dept. of Tech. Services, Univ. of Alberta, Canada.

9. Bradshaw, P., and Gee.M.T., Turbulent Wall Jets with and without an External Stream, A.R.C. 22008, F.M. 2971, 1960.

10. Burkov,F.G., Gunko,A.F., Rubinstein,G.L., and Yudisty, G.A., Research on the Hydraulic Regime and Local Scour of River bed below Spillways, 11 th Congress, I.A.H.R., Vol. 1, 1965.

11. Carstens, R.H., Similarity Laws for Localized Scour, J. of Hydraulic Div., A.S.C.E., Vol. 92, May 1966, pp. 72-84.

12. Charles, A.D., Straight Drop Spillways Stilling Basins, J. of Hydraulic Div., A.S.C.E., Vol. 91, May 1965, p.101.

APPENDIX C (continued)

13. Chee,S.P., and Kung,T., Stable Profiles of Plunge Basins, J. of American Water Resources, April 1971.

14. Chee,S.P., and Padiyar,P.V., Erosion at the Base of Flip Buckets, The Engineering Journal, Vol. 52, Nov. 1971.

15. Chee, S.P., Strelchuk, D.L., and Kung, T., Configurations of Water Basin for Energy Dissipation, 86 th Annual Congress of Engineering Inst. of Canada, Saskatoon, Oct. 1972.

16. Chee, S.P., Payne, H.G., and Kung, T., Incipient Motion of Bed Material, Proc. of Symposium of River Mechanics, I.A.H.R., Bangkok, Thailand, Jan. 1973.

17. Chow, V.T., Open Channel Hydraulics, Mc Graw-Hill Book Co. N.Y., 1959, pp. 168-180.

18. Dept. of Army, Hydraulic Design of Reservoir Outlet Structures, Engineer Manual, Aug. 1958.

19. Doddish, D., and Albertson, M.L., and Thomas, R.A., Scour from Jets, Proc. of Minnesota International Hydraulics Convention, Sept. 1953.

20. Elevatorski, E.A., Trajectory Bucket Type Energy Dissipators, J. of Irrigation, Pipeline, and Power Div., A.S.C.E., Vol. 84, 1957.

21. Eskinazi, S., and Kruka, V., Mixing of a Turbulent Wall Jets into a Free Stream, Trans. of A.S.C.E., Vol. 128, Pt. 1, 1963.

22. Forthmann, E., Turbulent Jet Expansion, N.A.C.A., Tm 789, 1934.

23. Glauert, M.B., The Wall Jet, J. of Fluid Mechanics, Vol. 1, 1956, pp. 625-643.

24. Gurevich, M.I., Thoery of Jets in Ideal Fluids, Academic Press Inc., N.Y., 1965.

25. Harris, G.L., The Turbulent Wall Jet on Plane and Curved Surfaces beneath an External Stream, Tech. Note 27, von Karman Inst. for Fluid Dynamics, Aug. 1965.

APPENDIX C (continued)

26. Henderson, F.M., Open Channel Flow, Mac Millan Co., N.Y., 1966.

27. Hilbebrand, F.B., Introduction to Numerical Analysis, McGraw-Hill Book Co., N.Y., 1956.

28. Hinds, J., Creager, W.P., and Justin, J.D., Engineering for Dams, John Wiley and Sons, Inc., N.Y., 1945, Vol. 2, pp. 358-361.

29. Hinze, J.D., Turbulence, McGraw-Hill Book Co., 1959.

30. Husian, S.A., Stability of Blooks below Flip Buckets, Master Thesis, Univ. of Windsor, Canada, 1970.

31. Iamandi, C., and Rouse, H., Jet induced Circulation and Diffusion, J. of Hydraulic Div., A.S.C.E., March 1969.

32. Jain, S.H., and Gupta, S.N., Ski-jump Energy Dissipator for Rihand Spillway, 11 th Congress, I.A.H.R., Vol. 1, 1965.

33. Kennedy, J.B., and Neville, A.M., Basic Statistical Method for Engineers and Scientists, International Textbook Co., Scranton, Penn.

34. Khosla, A.N., Bose, N.K., and Taylor, E., Design of Weirs on Permeable Foundation, Publication No. 12, Central Board of Irrigation, India, 1964.

35. Lacey, G., Flow in Alluvial Channels with Sandy Mobile Beds, Proc. of Inst. of Civil Engineers, (U.K.), Vol. 9, 1958.

36. Leliavsky, S., Design of Dams for Perolation and Erosion, Design Textbook in Civil Engineering, Vol. 1, 1965.

37. Mathien, J., Contribution to the Aerothermic Study of a Flat Jet Evoling in the Pressure of a Wall, NASA-TT-9088, 1964.

38. McPherson, M.B., and Karr, M.H., Study of Bucket-type Energy Dissipator Characteristics, J. of Hydraulic Div., A.S.C.E., June 1957, pp. 1-18.

39. Meyer, A.A., Discussion on Hydro Models, J.of Hydraulic Div., A.S.C.E., June 1957.

40. Myers, G.E., Schauer, J.J., and Eustis, R.H., Plane Turbulent Wall Jet Flow Development and Friction Factor, Trans. A.S.M.E., J. of Basic Engineering, March 1963, pp. 47-54.

41. Padiyar. P.V., Erosion below Flip Buckets, Master thesis, Univ. of Windsor, Canada, 1969

42. Payne, H.G., Incipient Motion of Bed Materials, Master Thesis, Univ. of Windsor, Canada, 1971.

43. Peterka, A.J., Improved Tunnel Spillway Flip Buckets, Hydraulic Design of Stilling Basin and Energy Dissipators, Water Resources Technical Publication, Engineering Monograph No. 25, U.S.B.R., 1964.

44. Poreh, M., and Cermark, J.E., Flow Characteristics of of Circular Submerged Jet Impinging Normally on a Smooth Boundary, Proc. 6 th Midwest Conference on Fluid Mechanics, Univ. of Texas, Austin, Texas.

45. Poreh, M., Tsuei, Y.G., and Cermark, J.E., Investigation of a Turbulent Radial Wall Jet, Proc. A.S.M.E., J. of Applied Mechanics, June 1967, pp. 457-63.

46. Rajaratnam, N., The Hydraulic jump as a Wall Jet, J. of Hydr. Div., A.S.C.E., Sept. 1965, pp. 107-132.

47. Rajaratnam, N., and Subramanya, K., Plane Turbulent Reattached Wall Jets, J. of Hydr. Div., A.S.C.E., Jan. 1968.

48. Rajaratnam, N., and Subramanya, K., Diffusion of Rectangular Wall Jets in Wider Channels, J. of Hydraulic Research, 1967, pp. 281-294.

49. Ralston, A. and Wilf, H.S., Mathematical Method for Digital Computors, John Wiley and Sons, N.Y., 1960.

50. Rhone, T,J., and Peterka, A.J., Improved Tunnel-Spillway Flip Buckets, Trans. A.S.C.E., Vol. 126, 1961.

51. Rouse, H., Engineering Hydraulics, John Wiley and Sons, Inc., N.Y., 1958, pp. 496-588.

52. Russel, H., The Contra Costa Energy Dissipator, J. of Hydr. Div., A.S.C.E., Vol. 88, March 1962.

53. Schlichting, H., Boundary Layer Theory, Mcgraw-Hill Book Co., N.Y., 1968.

54. Schoklitsch, A., Prevention of Scour and Energy Dissipation, Translated by U.S.B.R., Denver, Colo., 1935.

55. Shen, H.W., Sedimentation (Einstein), Colorado State Univ., Ft. Collins, Colo., 1972.

56. Shield, A., Application of Similarity Principles and Turbulent Research to Bed-load Movement, 1936, Available from Calif. Inst. of Tech., Pasadena, Calif.

57. Sigalla, A., Experimental Data on Turbulent Wall Jet, Aircraft Engineering, Vol. 30, May 1958, pp. 131-133.

58. Sigalla, A., Measurements of Skin Friction in a Pl ne Turbulent Wall Jet, J. of Royal Aeronautical Society, Vol. 62, pp.873-877, London, 1958.

59. Starr, J.B., An Experimental Investigation of a Cylindrical Turbulent Wall Jet, Ph. D, Thesis, Univ. of Minnesota, U.S.A., June 1966.

60. Smith, C.D., and Strang, D.K., Scour in Stone Beds, 12th Congress, I.A.H.R., Vol. 3, Colorado State Univ., Sept. 1967.

61. Strelchuk, D.L., Scour at the Base of Spillway Buckets, Master Thesis, Univ. of Windsor, Canada, 1969.

62. Schwarz, W.H., and Cosart, W.P., The Two Dimensional Turbulent Wall Jet, J. of Fluid Mechanics, Vol. 10, 1961 pp. 481-485.

63. Sridhar, K., and Tu, P.K.C., Effect of an Initial Gap on the Flow in a Turbulent Wall Jet, Technical Note, J. of Roy. Aero. Society, Vol. 70, June 1966.

64. Task Force, Energy Dissipation for Spillways and Outlet Works, J. of Hydr. Div., A.S.C.E., Vol. 90, Jan. 1964, p.121.

65. Tsuchiya, Y., Basic Studies on the Criterion for Scour Resulting from Flows Downstream of an Outlet, Tech. Bull. No. 65, Kyoto Univ., Japan, 1963.

66. Thorn, R.B., River Engineering and Water Conservation Works, Butterworths, London, 1966.

67. U.S.B.R., Studies of Crests for Overfall Dams, Boulder Canyon Project Final Reports, Pt. VI, Hydraulic Investigations, Bulletin 3, 1948

68. U.S.B.R., Design of Small Dams, U.S. Dept. of Interior, 1965, Chap. VIII.

69. Vanon, V.A., Brooks, N.H., and Kennedy, J.F., Lecture Notes on Sediment Transportation and Channel Stability, Calif. Inst. of Tech., 1960.

70. Varga, L., and Laushey, L.M., Application of the Wall Jet theory to Erosion at the Outlet of Hydraulic Structures, 12 th Congress, I.A.H.R., Colo. State Univ., Vol. 3, 1967.

71. White, C.M., Equilibrium of Grains on the Bed of a Stream, Proc. of Roy. Soc. (London), Vol. 174, 1940, P.322.

72. Zerbe, J., and Selna, J., An Empirical Equation for the Coefficient of Heat Transfer to a Flat Surface from a Plane Heated Air Jet, N.A.C.A., Tn No. 1070, Feb. 1946.

APPENDIX D

NOMENCLATURE

A	Dimensionless term, V_m^2/gd
A_c	Area of cross-section
a	Area of influence of particle
B	Dimensionless term. $(S_s - 1)^{-1}$
B_o	Jet thickness at flip bucket lip
B_1	Jet thickness at the point when jet strikes the tail-water
B_2	Thickness of initial wall jet
B_s	Surface water width
b	Exponent constant used in the wall jet theory
C	Dimensionless term, $(1+ z/d)^{-1}$
C_v	Velocity coefficient
$C_1 \cdots C_8$	Constants
C_f	Friction factor, $2 \tau_w / \rho U^2$
C_L	Lift constant
c	Exponent constant used in wall jet theory
C_s	Single constant used in submerged diffusion jet
D	Intermediate depth of scour
D_m	Maximum depth of scour
D_T	Vertical distance from the edge of bucket to tailwater
d	Size of bed material
d_{35}	Grain size of which 35% by weight of the bed material is finer

E	u/u_m in inner layer of wall jet
F	u/u_m in outer layer of wall jet
g	Acceleration due to gravity
H	Difference in evelation between upstream and tailwater levels
H_a	Difference in elevation between upstream level and bucket lip
F_d	Drag force on each prominent grain
F_R	Resistant force of a particle
F_s	Entrainment function
F_1	V_1^2/gh
f	Silt factor, $8d^{1/2}$ in.
H_o	Total head - velocity head
h	Tailwater depth
Δh	Difference in elevation between bucket lip and bucket invert
I	$\dfrac{D_m/d}{B^{0.35} C^{0.83} \beta^{0.87}}$
J	$\dfrac{D_m/d}{C^{0.83} \beta^{0.87}}$
K_t	Tractive force ratio
$K_1 \cdots K_8$	Constants
L	Total length of jet trajectory
L_a	Horizontal distance from the lip of bucket to the position where jet enters the tailwater

L_w	Horizontal distance from the point where jet enters the tailwater to the position of maximum scour
M	Momentum flux
n	Constant used in Prandtl's hypothesis
P	Wetted perimeter
P^*	Increased average load
P^*_{ult}	Ultimate value of increased average load
Q	Discharge
q	Unit discharge of spillway
R	Length of radius vector measured to the rim of the scour hole
R_b	Radius of bucket
R_e	Reynolds number
R_e^*	Particle Reynolds number
R_h	Hydraulic Radius
R_o	Reference radius vector pointing in the downstream direction where the rim of scour is closest to the origin
R_θ	Length of radius vector at the angle θ_b measured to the rim of the scour hole
R_{90}	Value of R_θ when $\theta_b = 90^o$
r	Distance at any point along a radius vector
r_p	Packing factor
S_e	Engergy slope
S	$D_m/\text{Sin}\,\beta$
S_s	Specific gravity of bed material

T^*	Tearing load
t	U_m/U
U	Initial velocity of wall jet
u	Velocity component in x direction
U_m	Maximum velocity of u in the cross-section
U_{35}	Velocity measured at a distance equal to 0.35 d_{35}
V_{max}	Maximum velocity of the submerged jet at any cross section
V_m	Velocity of submerged jet at the center of the block or of the bed material
V_x	Longitudinal component of velocity
V_o	Jet velocity at the bucket lip
V_1	Velocity at the position where the jet enters the tail-water
V^*	Shear velocity,
v	Velocity component in y direction
y_o	Vertical distance from the original bed to the maximum scour point
W_s	Weight of particle of bed material
z	Height of the obstruction to the bed material
x_s	Distance travelled by the jet relative to the free stream
u_s	Free-stream velocity
W_w	Weight of water
W_1	0.85 R_{90}
α	Exit angle of flip bucket
β	Angle between tailwater and jet projectile

γ	Specific weight of water
γ_s	Specific weight of bed material
σ	Standard deviation
ρ	Density of fluid
δ	Thickness of boundary layer
δ_m	Thickness of boundary layer when $u=u_m$
δ_1	Boundary layer thickness when $u=1/2\ u_m$
ν	Kinematic viscosity
τ	Shear stress
τ_w	Shear stress of wall jet
τ_3	Unit tractive force on the side of channel
τ_L	Lift stress
τ_b	Unit tractive force on the bottom of the scour hole
θ	Angle of repose of material
θ_b	Angle in radians measured clockwise and anticlockwise from the reference radius vector
ϕ	The side slope of channel, or the angle between the tangent of scour profile and the horizontal level
η	y/δ_m
ζ	$(y - \delta_m) / (\delta - \delta_m)$

VITA AUCTORIS

1941 Born on August 1, 1941, in Chuang-King, China.

1964 Graduated from the Cheng Kung University, Taiwan, with a Bachelor of Science degree.

1969 Graduated from the Asian Institute of Technology, Bangkok, Thailand, with a Master of Engineering degree.

1969 Accepted as a candidate for Doctor of Philosophy Degree at the University of Windsor.